NAVAL AIR WARFARE CENTER AIRCRAFT DIVISION
PATUXENT RIVER, MARYLAND

REPORT OF TEST RESULTS

REPORT NO: NAWCADPAX/RTR-2000/114

AV-8B –408 EXTERNAL ENVIRONMENT OUTWASH FLOW SPEED AND TEMPERATURE SURVEY

by

Robert Lake
Kevin McCarthy
Robert Nantz
Hugo Gonzalez

29 August 2000

Approved for public release; distribution is unlimited.

DEPARTMENT OF THE NAVY
NAVAL AIR WARFARE CENTER AIRCRAFT DIVISION
PATUXENT RIVER, MARYLAND

NAWCADPAX/RTR-2000/114
29 August 2000

AV-8B –408 EXTERNAL ENVIRONMENT OUTWASH FLOW SPEED AND TEMPERATURE SURVEY

by

Robert Lake
Kevin McCarthy
Robert Nantz
Hugo Gonzalez

RELEASED BY:

29 Aug 2000

J. R. VACHALEK / 4.11C4 / DATE
By direction of the Head,
Test and Evaluation Engineering Department
Research and Engineering Group

REPORT DOCUMENTATION PAGE

Form Approved
OMB No. 0704-0188

1. REPORT DATE	2. REPORT TYPE	3. DATES COVERED
29 August 2000	Report of Test Results	

4. TITLE AND SUBTITLE

AV-8B -408 External Environment Outwash Flow Speed and Temperature Survey

5a. CONTRACT NUMBER

5b. GRANT NUMBER

6. AUTHOR(S)

Robert Lake
Kevin McCarthy
Robert Nantz
Hugo Gonzalez

5d. PROJECT NUMBER

5e. TASK NUMBER

5f. WORK UNIT NUMBER

7. PERFORMING ORGANIZATION NAME(S) AND ADDRESS(ES)

Naval Air Warfare Center Aircraft Division
22347 Cedar Point Road, Unit #6
Patuxent River, Maryland 20670-1161

8. PERFORMING ORGANIZATION REPORT NUMBER

NAWCADPAX/RTR-2000/114

9. SPONSORING/MONITORING AGENCY NAME(S) AND ADDRESS(ES)

Naval Air Systems Command
47123 Buse Road Unit IPT
Patuxent River, Maryland 20670-1547

10. SPONSOR/MONITOR'S ACRONYM(S)

11. SPONSOR/MONITOR'S REPORT NUMBER(S)

12. DISTRIBUTION/AVAILABILITY STATEMENT

Approved for public release; distribution is unlimited.

13. SUPPLEMENTARY NOTES

14. ABSTRACT

The outwash flow field around a hovering AV-8B aircraft with –408 engine was measured during two separate phases of testing. The aircraft gross weight varied between 16,100 to 19,600 lb. Testing consisted of taking velocity and temperature measurements at heights above the ground from 3 in. to 10 ft at 20 deg increments primarily about the aircraft's port side and at radial distances between 30 and 100 ft from the aircraft's hover center. Testing concentrated on 50 ft-AGL hovers although tests included, vertical takeoff, vertical landing, hover height variations from 30 to 125 ft-AGL (radar height) and gross weight changes of approximately 2,000 lb. The outwash flow field was analyzed in the areas of flow field velocity, direction, and temperature in addition to velocity dynamics, temperature extremes, aerodynamic forces, and personnel hazards and limitations.

15. SUBJECT TERMS

AV-8B Environment Jet Outwash Velocity Pressure Temperature Flow Field

16. SECURITY CLASSIFICATION OF:			17. LIMITATION OF ABSTRACT	18. NUMBER OF PAGES	19a. NAME OF RESPONSIBLE PERSON
a. REPORT	b. ABSTRACT	c. THIS PAGE			19b. TELEPHONE NUMBER (include area code)
Unclassified	Unclassified	Unclassified	SAR	115	Robert Lake (301) 342-8401

Standard Form 298 (Rev. 8-98)
Prescribed by ANSI Std. Z39-18

SUMMARY

The outwash flow field around a hovering AV-8B aircraft with –408 engine was measured during two separate phases of testing. The aircraft gross weight varied between 16,100 to 19,600 lb. Testing consisted of taking velocity and temperature measurements at heights above the ground from 3 in. to 10 ft at 20 deg increments primarily about the aircraft's port side and at radial distances between 30 and 100 ft from the aircraft's hover center. Testing concentrated on 50 ft-AGL hovers although tests included, vertical takeoff, vertical landing, hover height variations from 30 to 125 ft-AGL (radar height) and gross weight changes of approximately 2,000 lb. The outwash flow field was analyzed in the areas of flow field velocity, direction, and temperature in addition to velocity dynamics, temperature extremes, aerodynamic forces, and personnel hazards and limitations.

New instrumentation was designed and fabricated to allow outwash surveys in the relatively harsh thermal environment of a jet lift aircraft. The instrumentation and test techniques developed allowed accurate and efficient flow field measurement. Test data determined that the outwash flow field was similar in character to rotary wing aircraft. Therefore, personnel working in the AV-8B flow field must react to mean windspeed in addition to high magnitude, low frequency wind oscillations (gusts). Wind gusts generally oscillated at a frequency below 3 Hz.

Flow emanated primarily radially away from the aircraft and in a direction parallel to the ground plane. Flow off the 0-180 deg (relative to the aircraft nose) stagnation line contained peak velocities lower than what was found in the nonstagnation region flow; however, the existence of uniform (with height), moderately high velocities produced high aerodynamic forces (derived). The largest force was found in excess of 190 lb, located 32 ft from center of the 180 deg test azimuth. However, forces at all test azimuths quickly decayed to very workable levels beyond the current NATOPS 50 ft radius hazard zone. Outwash strength was a moderate function of hover height and a weak function of gross weight (as tested). Outwash strength was found to be very sensitive to aircraft position. Due to the cooler bypass flow from the forward nozzles and the hotter core flow from the aft nozzles, higher temperatures were found aft of center and did not cool to ambient values even at the furthest test distances. Flow field temperatures and velocities were loaded into a model representing the burn properties of the human skin. The burn model results show the AV-8B outwash (as tested) presents no short-term exposure threat to personnel pain or injury due to excessive heat.

Contents

INTRODUCTION

BACKGROUND

1. Ground or ship deck personnel working in close proximity to an operating vertical or short takeoff or landing (V/STOL) aircraft must perform mission duties while working in a hot, high velocity, gusting wind environment. This wind, commonly referred to as jet outwash, is generated when high velocity/high temperature exhaust exits the nozzles, travels downward until impingement with the ground, changes direction by 90 deg, and then spreads radially outward along the ground plane. A generic illustration of the mechanisms of a V/STOL (fan in wing) outwash flow field is presented in figure 1. This figure illustrates the mixing of ambient flow entrained by the higher velocity jet flow. This mixed flow turns after impacting the ground to create the outwash flow field, also known as the wall jet. The velocity and temperature measurements collected during this test were obtained from this wall jet region. Figure 1 also illustrates the formation of a "fountain" between the jets, which is created by the interaction between the multiple jets. The testing documented in this report was conducted typically out of ground effect. This minimizes the strength of the fountain, which results in a more stable hover with fewer control inputs. Figure 2 is a pictorial representation of the interaction of the four exhaust nozzles for the AV-8B Harrier in a low-level hover. Note that there are two intersecting surfaces of symmetry labeled A-A and B-B, typically referred as stagnation lines or reinforcement zones. Created from the interaction of the jets, these regions are typically characterized by higher velocity, thicker outwash flows and are the reason that multiple jet configurations do not have a symmetric footprint. The forward cant in the stagnation lines illustrated in figure 2 was not derived empirically; however, the general shape is consistent with the results of this test.

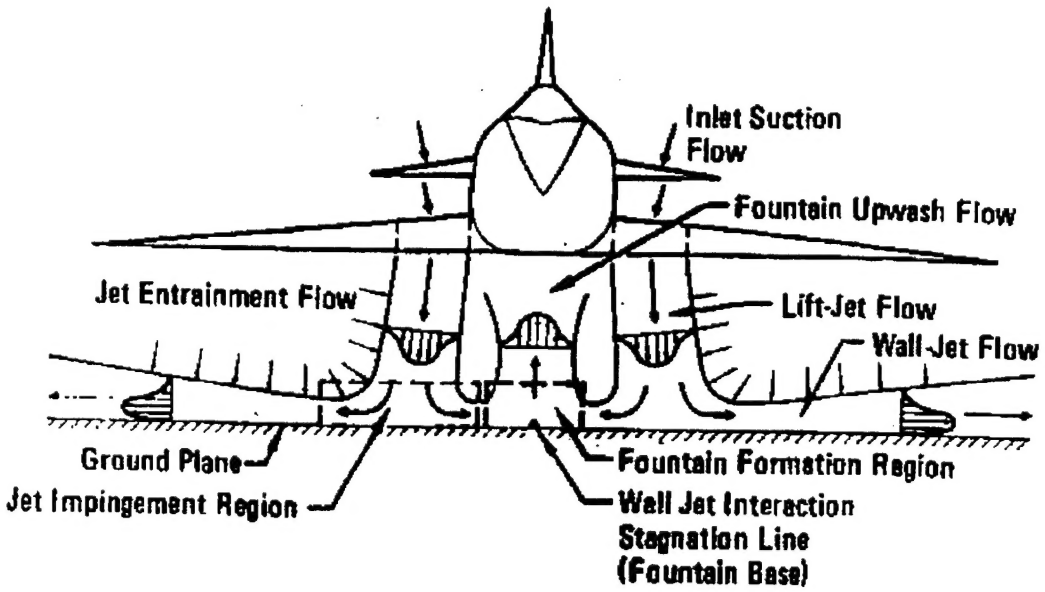

Figure 1: Artist Conceptual Drawing of a Typical (Fan in Wing Type) V/STOL Aircraft Outwash Flow

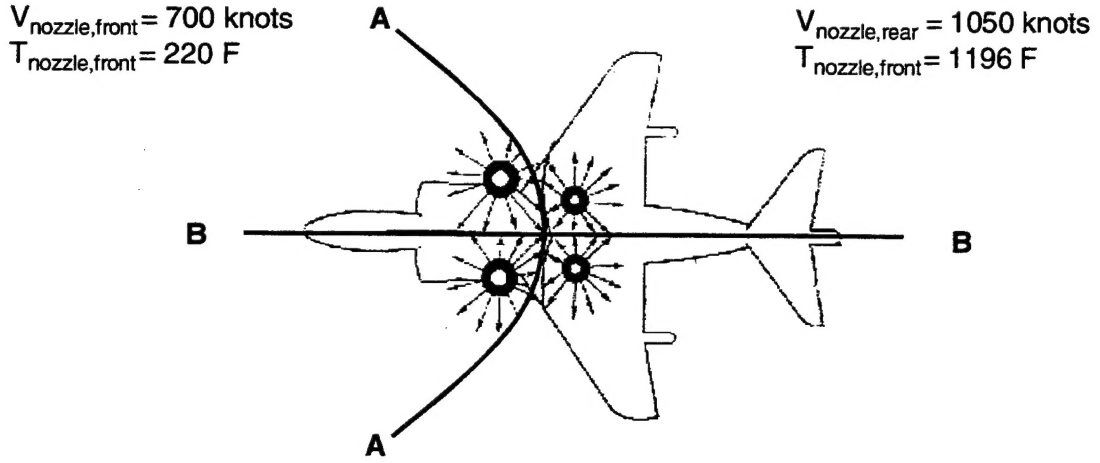

Figure 2: Nozzle Exhaust Patterns Showing Stagnation Lines (Nozzle Velocity and Temperature Data are for an Earlier Version of the Pegasus Engine)

2. NAWCAD Patuxent River was tasked by the Joint Strike Fighter (JSF) Program Office to: 1) design and fabricate an outwash measurement system suitable for use in the outwash flow field of JSF class Short Takeoff and Vertical Landing (STOVL) aircraft and 2) quantify the outwash flow field of the AV-8B –408 Harrier to be used as a comparison with future JSF candidate aircraft. The testing described in this report is a compilation of two test phases: Phase 0 was a risk reduction test to determine optimum instrumentation techniques and provide a limited outwash data set. Phase 1 tests featured a new instrumentation system based on lessons learned from Phase 0 testing and data complimentary to Phase 0. The primary focus of this report is to present Phase 1 results and analysis; however, a complete data base of both phases are contained in the AV-8B External Environment Survey data release 0 and 1, references 1 and 2, respectively. Specific test photos, site layout, and other Phase 0 pertinent information are included in appendix A.

PURPOSE

3. The purpose of this test was to quantitatively measure the AV-8B outwash flow field pressures, temperatures, and velocities in addition to analyzing the potential effects the flow field has on ground personnel. A complementary purpose of this test was to develop outwash test methods, data acquisition, and analysis procedures in conjunction with JSF Air Vehicle Analysis and Integration and Systems Test personnel. The results from this test will be used for future JSF specific STOVL testing.

DESCRIPTION OF TEST AIRCRAFT

4. The AV-8B Harrier is a subsonic, single cockpit, single engine, jet propelled day/night tactical fighter built by Boeing and BAE Systems. The aircraft is powered by Rolls Royce axial flow, twin spool turbo fan engines. The four engine nozzles can be vectored from about 105 deg (15 deg forward of vertical) as necessary for V/STOL, transition, and up-and-away operations. A complete description of the AV-8B aircraft may be found in the AV-8B NATOPS Flight Manual, reference 3. The test aircraft for this survey was AV-8B BuNo 163854/modex 85

equipped with a F402-RR-408A engine from NAWCWD, China Lake, Naval Weapons Test Squadron and was considered production representative for the purpose of these tests. The aircraft was configured with deep strake lift improvement devices (LID's). The F402-RR-408A engines have the capability of providing 22,200 lb thrust (without water injection) under optimum conditions.

SCOPE OF TESTS

TESTS AND TEST CONDITIONS

5. Both phases of AV-8B outwash testing were conducted at the NAS Patuxent River centerfield vertical takeoff and landing (VTOL) pad. Phase 0 testing was conducted during the week of 7 July 1997 and Phase 1 testing was conducted during the week of 20 September 1998. A pictorial representation of the airfield layout is shown in figure 3. Aircraft gross weight (GW) ranged from 15,500 to 18,700 lb for Phase 0 testing and 16,100 to 19,600 lb during Phase 1 tests. Test data presented in the main body of this report were acquired during periods of calm ambient winds (generally less than 5 kt) although some data were acquired during higher ambient winds. The data releases contained in references 1 and 2 provide both low and high ambient wind condition outwash data.

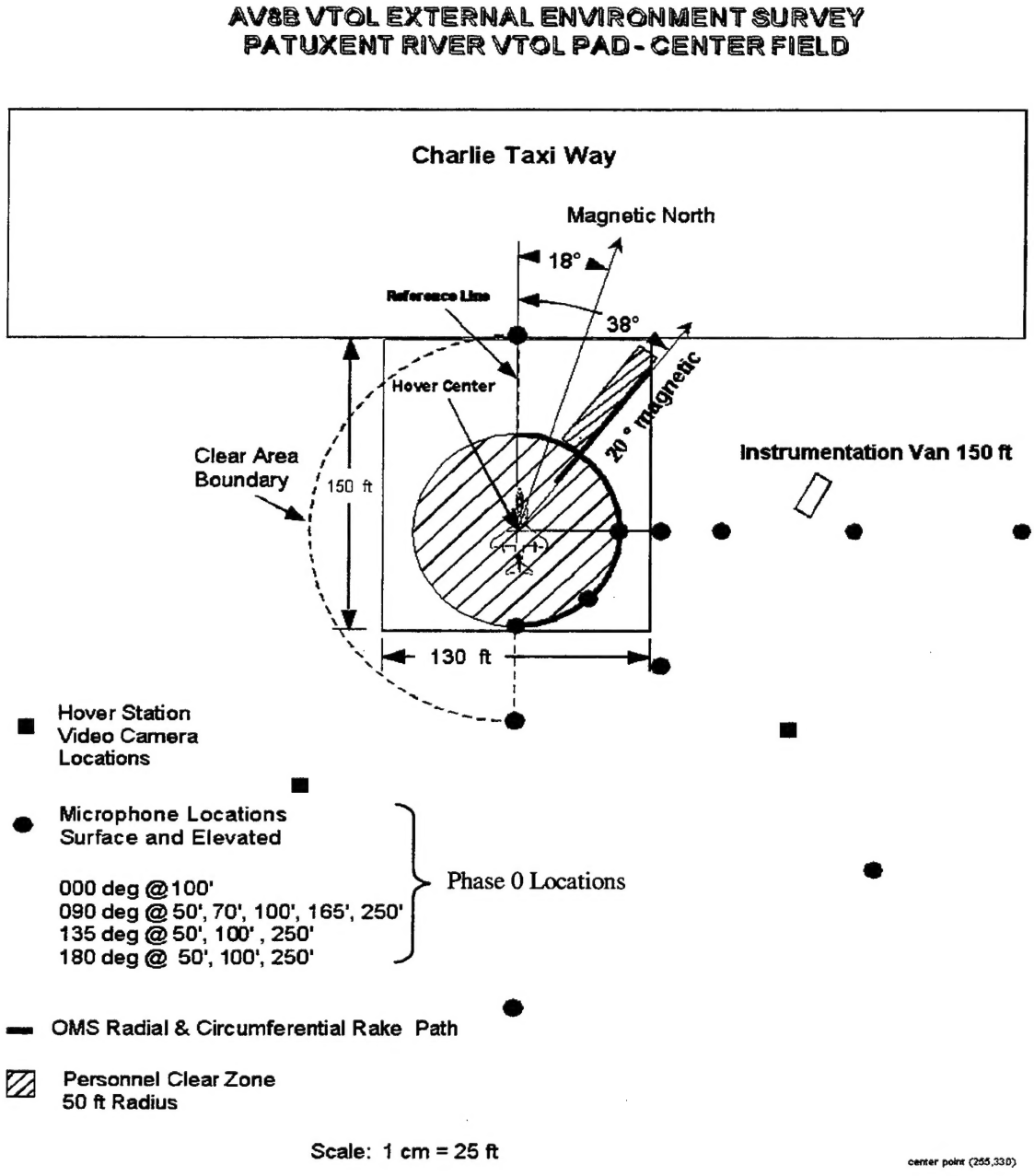

Figure 3: AV-8B External Environment Test Layout
(Note: Circumferential rake path not used, microphones showed at Phase 0 locations)

6. Phase 1 outwash data were obtained on each of the test azimuths listed in table 1. Aircraft center was defined as the centroid of the four nozzles and hover height was collected by radar altimeter. All aircraft hover height data presented in this report is referred to in feet above ground level (ft-AGL) as measured by radar altimeter and the reader shall be aware that actual 0 ft-AGL wheel height was indicated as 12 ft-AGL by radar altimeter. Data were taken at radial distances of 32, 40, 50, 60, 75, and 100 ft from aircraft center. While the majority of the data was collected during 50 ft-AGL steady hovers, measurements were also conducted at 30, 50, 80, 100, and 125 ft-AGL hover heights. Several azimuths were repeated with varied aircraft GW's, with differences between low and high GW configurations of 1,300 to 3,300 lb. In addition, full power wheels on the ground "No-Go VTO" maneuvers were conducted.

Table 1: Phase I Outwash Data Syllabus (Low Ambient Wind Conditions)

	Measurement Azimuth (degrees off aircraft nose)									
	0	20	40	60	80	100	120	140	160	180
30 ft hover		x			x					
50 ft hover	x	x(1)	x	x(1)	x(1)	x	x	x	x(1)	x
80 ft hover		x			x					
100 ft hover		x			x					
125 ft hover		x			x					
VTO(2)	x			x	x		x		x	x

NOTES: (1) Repeated for high and low GW conditions.
(2) Vertical takeoff.

TEST METHODS AND PROCEDURES

7. The typical aircraft test cycle consisted of a VTO, several 2- sec hover dwells at constant heading (with pedal turn to change heading between dwells), and a vertical landing. Prior to the VTO, the pilot taxied the aircraft into position over center using deck handler signals. After acceleration checks were performed, the pilot pushed the nozzle control lever to hover stop, applied full power, and initiated a VTO - ascending to the test hover height as monitored by radar altimeter. During hover, the pilot maintained position over hover center using alignment pole pairs. A comprehensive discussion of precision hover with the use of pole positioning is presented in reference 4 and appendix B. The throttle setting associated with each hover dwell was required to maintain hover at the target altitude. Control adjustments to maintain position were typically made during "data-off" conditions. Upon completion of a data record, and pending satisfactory fuel status, the alignment poles were reset and a pedal turn was initiated to proceed to the next test heading. Upon completion of the steady hover dwells, the pilot performed a vertical landing, taxied off hover center, and allowed for reaction control system cool-down in accordance with NATOPS procedures. Given the ambient conditions and aircraft performance level, several test cycles were typically completed before taxiing to the hot pits to refuel.

8. A remotely controlled, battery operated, tracked, instrumentation cart was used to collect the outwash data at various radial distances from the hover center, as shown in figure 4. The cart was approximately 10 ft wide by 10 ft long and contained a pressure probe instrumented rake, signal conditioners, power supplies, and telemetry transmitters. Cart power was supplied by eight 12 VDC deep cycle batteries of which six were used for drive power and the remaining two batteries were used for instrumentation power. All of the batteries were located inside a foam lined, twin walled box to insulate them from high temperatures. High temperature wheels allowed for sustained operation on deck containing temperatures to 260°F. For additional high temperature protection, critical instrumentation, circuitry, and wiring were located above 5 ft-AGL to avoid the high temperature wall-jet flow that is usually found below 4 ft-AGL. The cart remained aligned on test azimuth by an 80 ft long, 1 in. by 4 in. aluminum u-channel and forward/reverse movement was remotely controlled by an RF servo that operated the motor's relay switch. A "dead-man" switch and low profile ramped barriers prevented any "run-away" cart hazards.

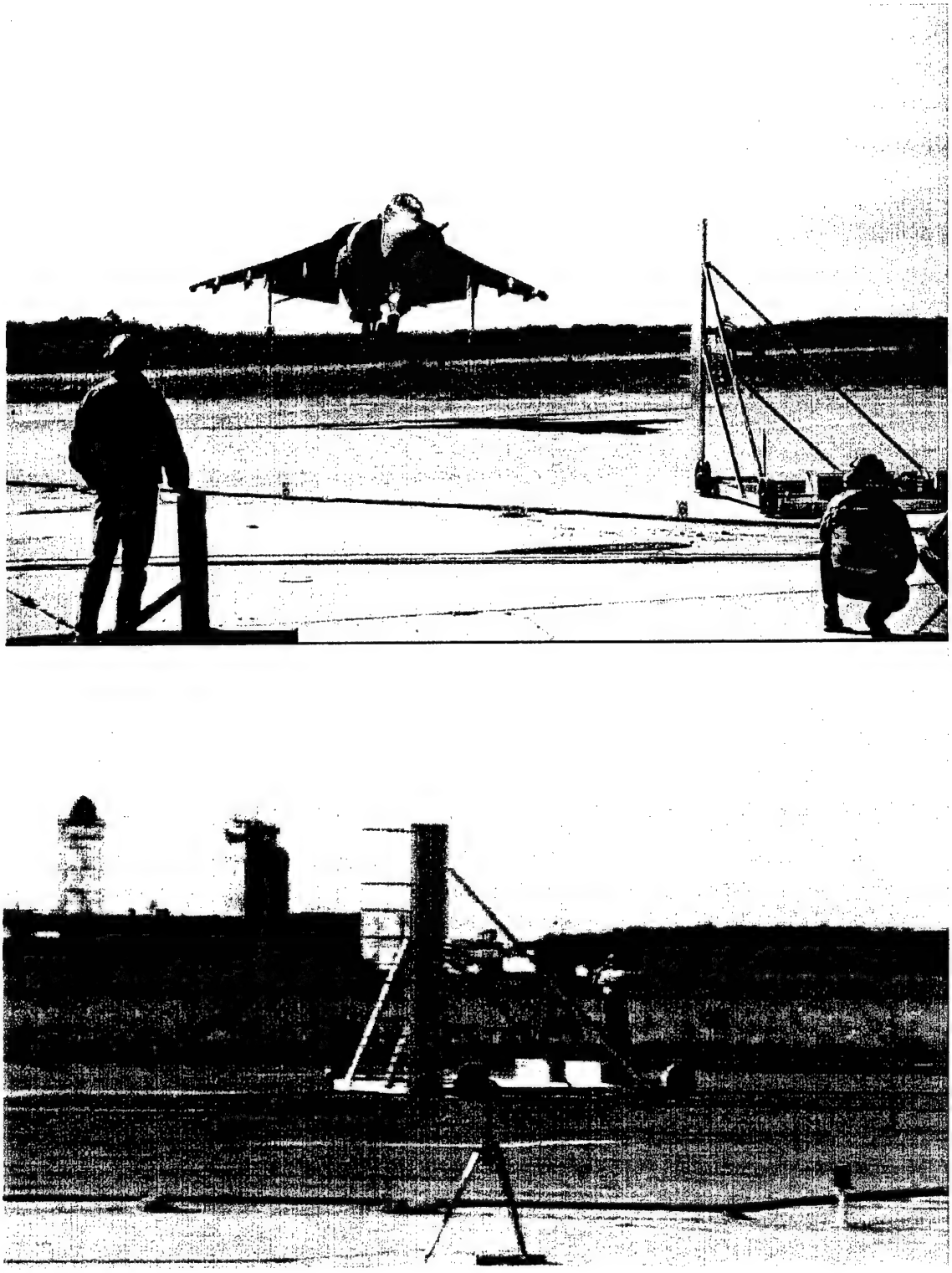

Figure 4: Outwash Instrumentation Cart during Test Operations

9. The cart contained a pressure probe rake capable of making velocity and temperature measurements from 3 in.-AGL to 120 in.-AGL, as shown in figure 5. The rake contained both five-tube and pitot-static type pressure probes. The five-tube probes were chosen for their ability to measure wind velocity magnitude and direction; whereas, the pitot-static probe was capable of only measuring velocity magnitude. The hemispherical tips for both type probes are illustrated in figure 6. Velocity is calculated from the pressure differential between the total pressures (hole #1) and static pressures (hole #2). This pressure differential is commonly referred to as the dynamic pressure. Wind tunnel calibrations on both probes demonstrated the five-tube probe allowed accurate wind velocity and direction measurement within a 45 deg cone of incidence. The pitot-static probes were accurate in velocity with a 25 deg cone of incidence. Each pressure transducer was ported (referenced) to a rake-mounted (internal) barometer. SensoTech, Inc. manufactured the pressure transducers and the barometer. All of the pressure transducers had a 3000 Hz frequency response, temperature compensated to 200°F, and accurate to 0.1% full-scale. Table C-2 lists the specific transducer ranges, as they corresponded to their location above ground. A corresponding type-J thermocouple temperature probe was mounted 1 in. below each pressure probe to determine temperature profiles and to allow accurate temperature compensated velocity calculation. The pressure probes angularity specifications and constants were determined 3 weeks before testing using the methods described in reference 5. Pressure transducers were calibrated using standard NIST traceable practices 1 week using before the test and rebiased (rezeroed) several times during the test day.

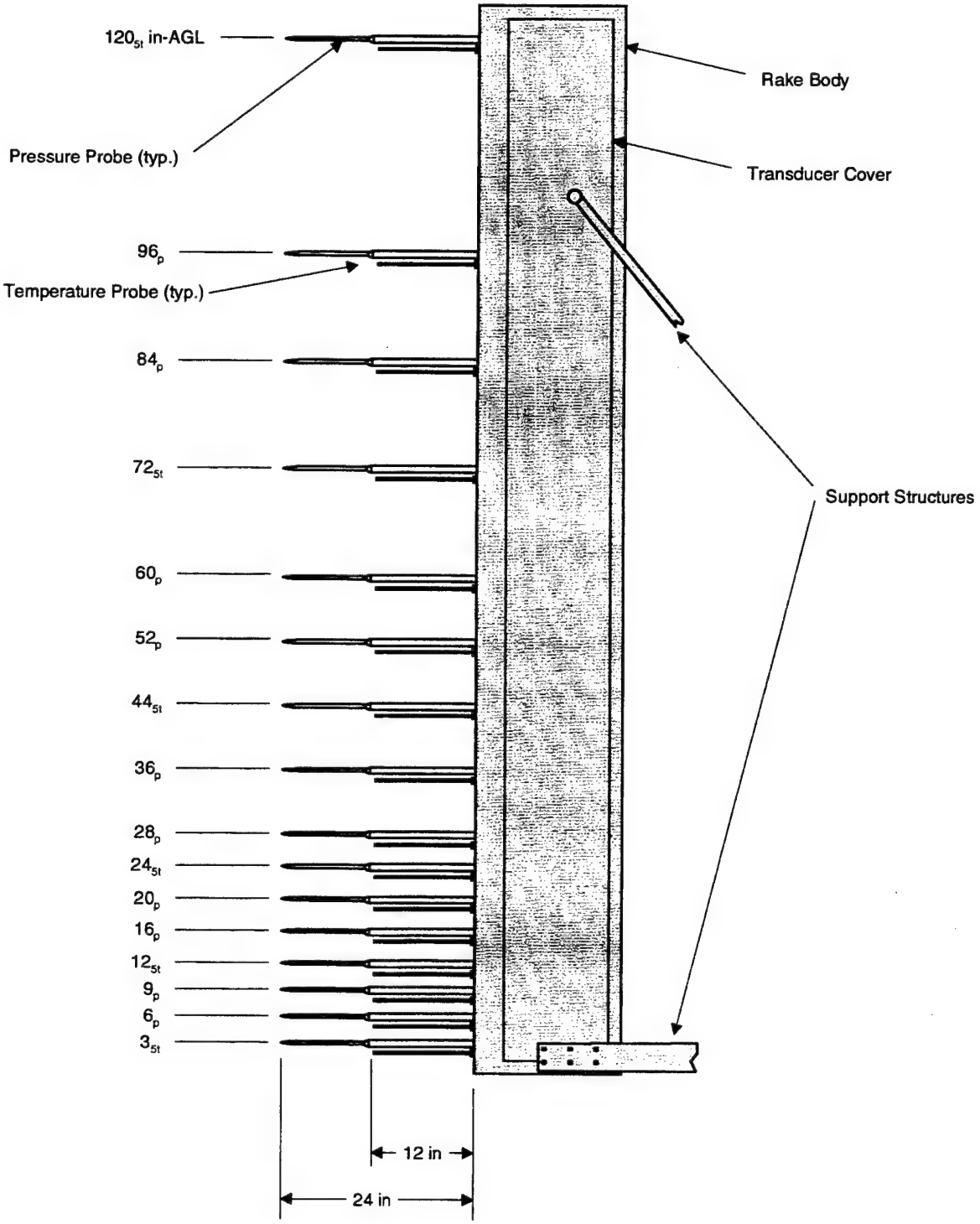

Figure 5: Outwash Pressure Probe Rake
(Subscripting denotes probe type: 5t = 5-tube, p = pitot-static)

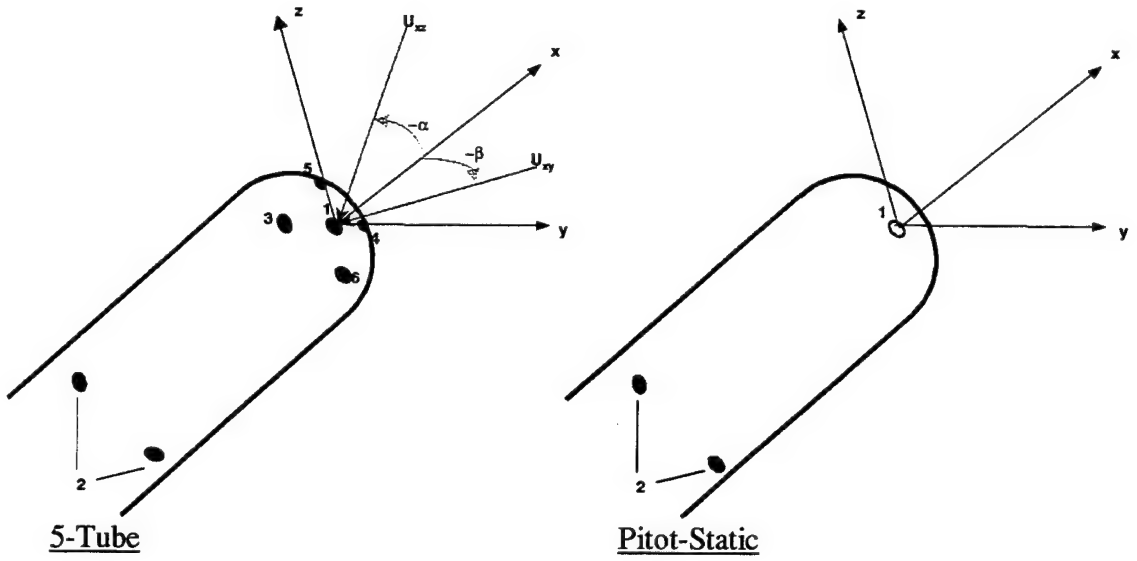

Figure 6: Five-tube and Pitot-Static Pressure Hemispherical Probe Tips

10. During data acquisition, pressure transducer voltage data were filtered with a two-pole, 50 Hz filter to prevent unwanted data distortion caused by aliasing. Temperature data were not filtered as aliasing distortion was prevented by the thermocouple's naturally slow response time. Temperature and filtered pressure data were converted from analog to digital through a Nicolet Technologies 16-bit MicroPro analog/digital data acquisition system. A digital data stream (PCM RS-232 format) was transmitted real-time via Digital Wireless, Inc. 1.2 GHz spread spectrum RF link to a laptop computer. The computer acquired a 10 sec data sample from the digital data stream and further processed by discretely filtering to four-pole, 10 Hz (type: Butterworth) to estimate the human body's response to wind gusts and to provide an accurate statistical analysis. Computer time was linked to global positioning system (GPS) time prior to each test.

11. A cart "health" system was used to monitor cart temperatures and battery voltages. Analog data from separate (from the rake) type-J thermocouples and DC voltages were digitized through a National Instruments FieldPoint data acquisition system and transmitted via Digital Wireless, Inc. 1.2 GHz spread spectrum RF link to a dedicated (separate from Nicolet) laptop computer. The computer provided real-time display of critical parameters and displayed warning flags if temperatures or voltage levels exceeded recommended values. A list of health system parameters is listed in figure B-1.

12. A portable weather system monitored ambient windspeed, wind direction, barometric pressure, temperature, and humidity during the test. This portable system was located approximately 350 ft from hover center. Data from the weather transducers were real-time transmitted via a FreeWave, Inc. 900 MHz spread spectrum RF link to a dedicated laptop computer. Prior to each test, weather computer time was time linked to GPS time.

RESULTS AND EVALUATION

OUTWASH FLOW FIELD CHARACTERISTICS

13. Personnel engulfed in a V/STOL aircraft outwash flow field must respond to mean windspeed, semi-periodic flow oscillations (gusts). It has been shown (reference 6) that personnel instabilities are primarily caused by insufficient reaction to these large amplitude flow oscillations. Figure 7 shows a typical oscillating waveform that contains a 10-sec time history from the 9 in.-AGL pitot-static probe and its associated power spectrum is presented in figure 8. The AV-8B outwash signal is very similar, temporally and spectrally, to that of signals acquired from helicopter downwash tests, in that the peak levels may be 50% higher than the mean and majority of the energy resides at frequencies below 5 Hz. Also, review of power spectrums indicates every spectrum is unique in appearance, concluding that although the flow has periodic components, the overall nature of the outwash flow field remains a very random event. To put into perspective, this randomness will make personnel unable to anticipate when some large magnitude gusts are about to strike them. For the above-mentioned reasons, NAWCAD Patuxent River feels it is applicable to use previous helicopter downwash test results and stability criteria when used in comparison to the AV-8B flow field.

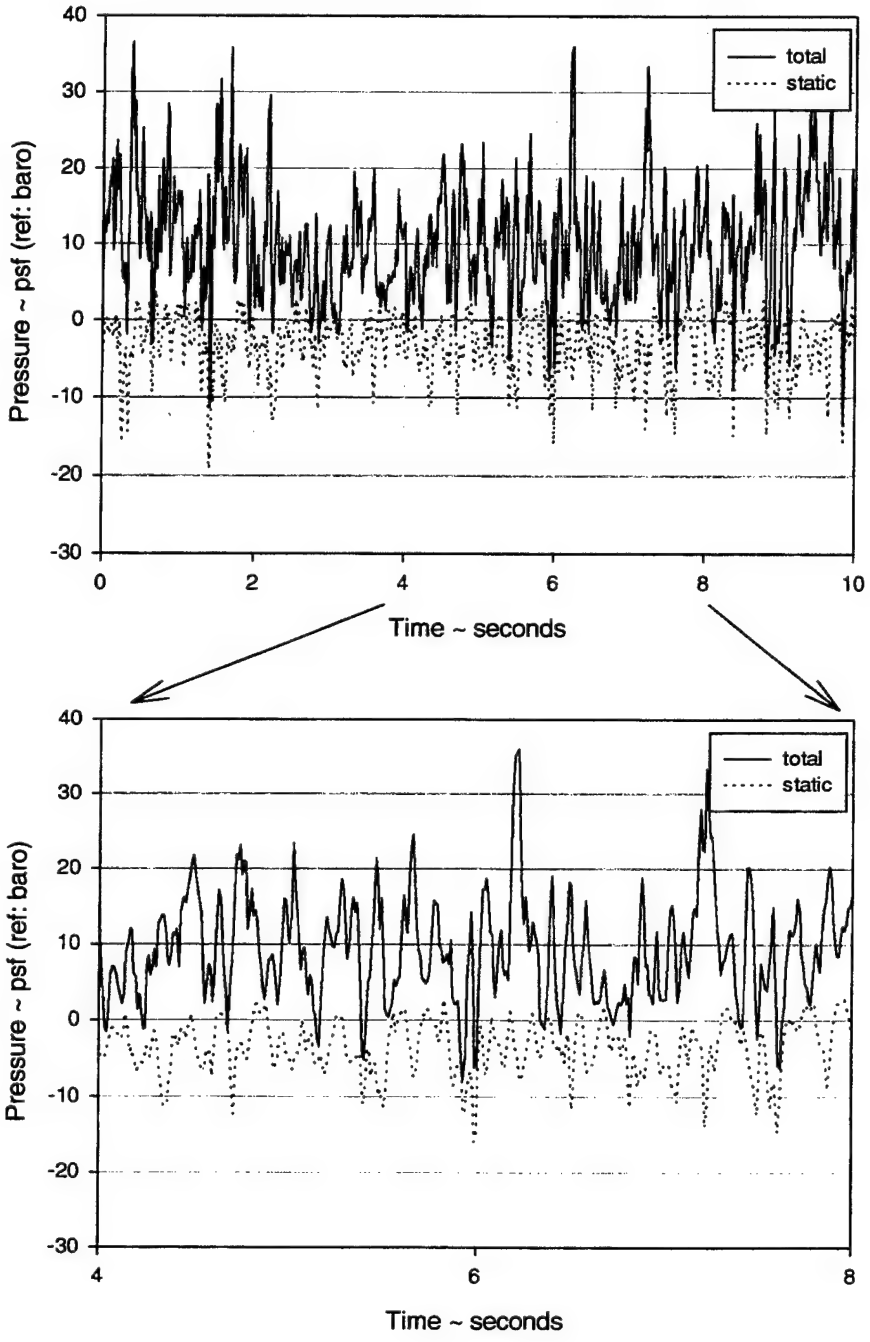

Figure 7: 10-sec Time History of the AV-8B Outwash Total and Static Pressures as Measured by the 9 in.-AGL Pitot-Static Probe (with 2 sec magnification included for clarity)

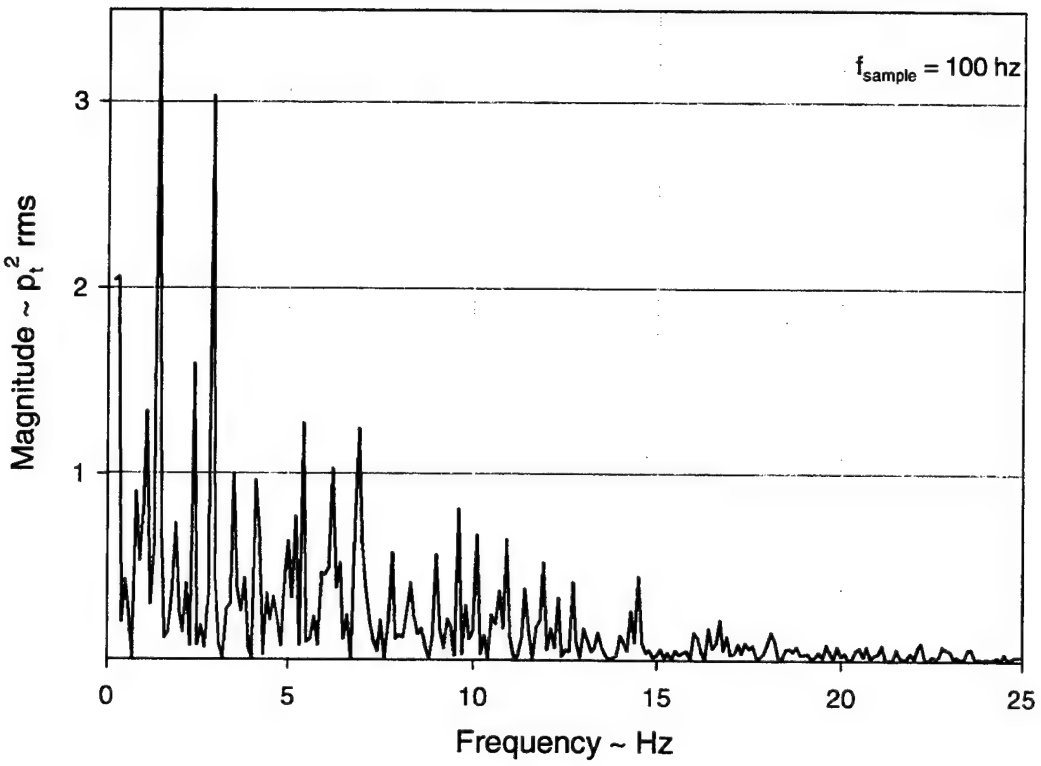

Figure 8: Power Spectrum of Total Pressure Time History
(Data presented has not had 10 Hz filtering applied)

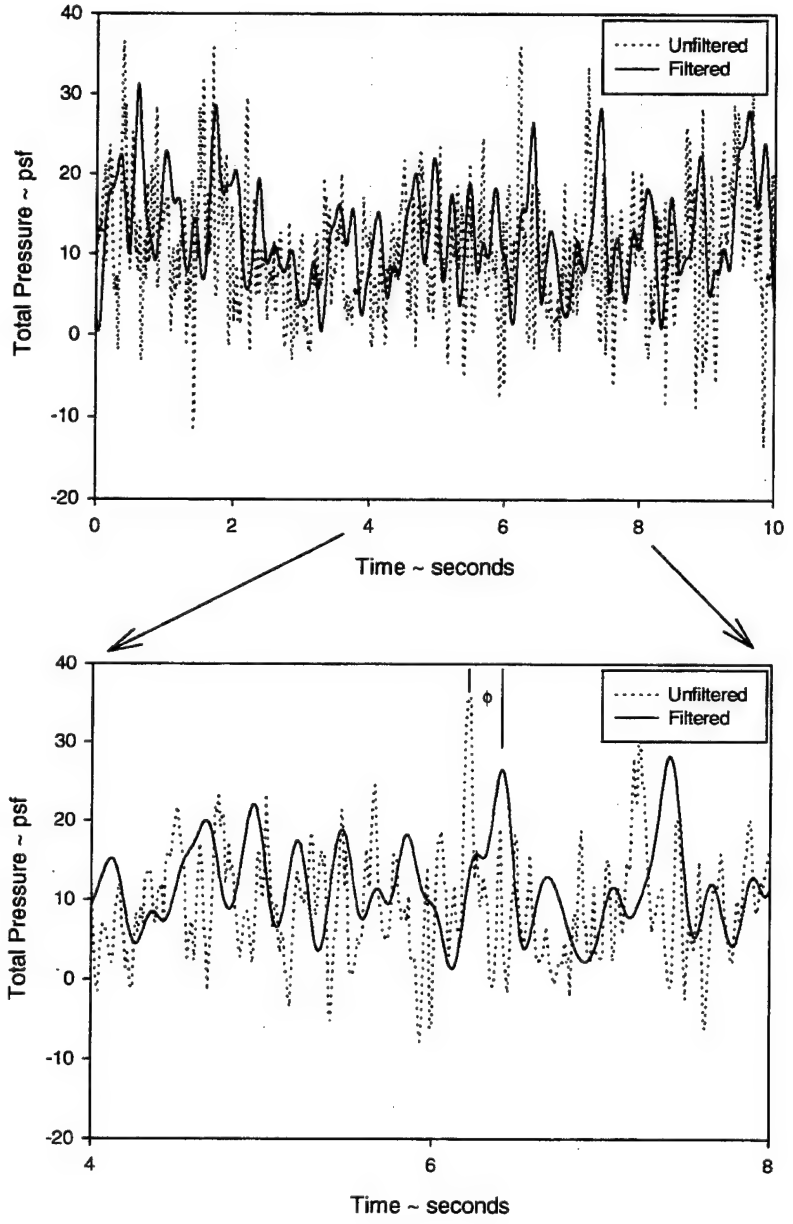

Figure 9: The Effects of Filtering on the 9 in.-AGL Total Pressure Waveform

DATA ANALYSIS

14. To provide an accurate statistic solution, mean dynamic pressure ($q = 1/2\ \rho V^2$) was determined by the difference in mean static and mean total pressure, averaged over the entire sample period. Peak dynamic pressure was determined by the between peak total pressures and mean static pressures. This process is shown in the upper graph of figure 9. An axial, uniform flow field with small flow angles is the optimum medium for pressure probes. Generally, this is the flow field found in AV-8B outwash; however, some flow rotation/angularity is inevitably present. Flow angularity is detected when the roles of the probe's total and static ports become somewhat reversed due to flow becoming incident on the sides of the probe, as shown in figure 10. This condition is shown in the lower graph in figure 9 where the difference between total and static pressure falls below zero resulting in a negative dynamic pressure and an undefined velocity solution. Flow angularity admittedly causes measurement errors but occurred for very small times and appeared at the higher (lower velocity) measurement locations where wall jet flow becomes entrained with the local environment. Furthermore, this error primarily affects the mean velocity calculation, which negligibly affects the outwash personnel stability criterion (as based only on the analysis of peak velocity).

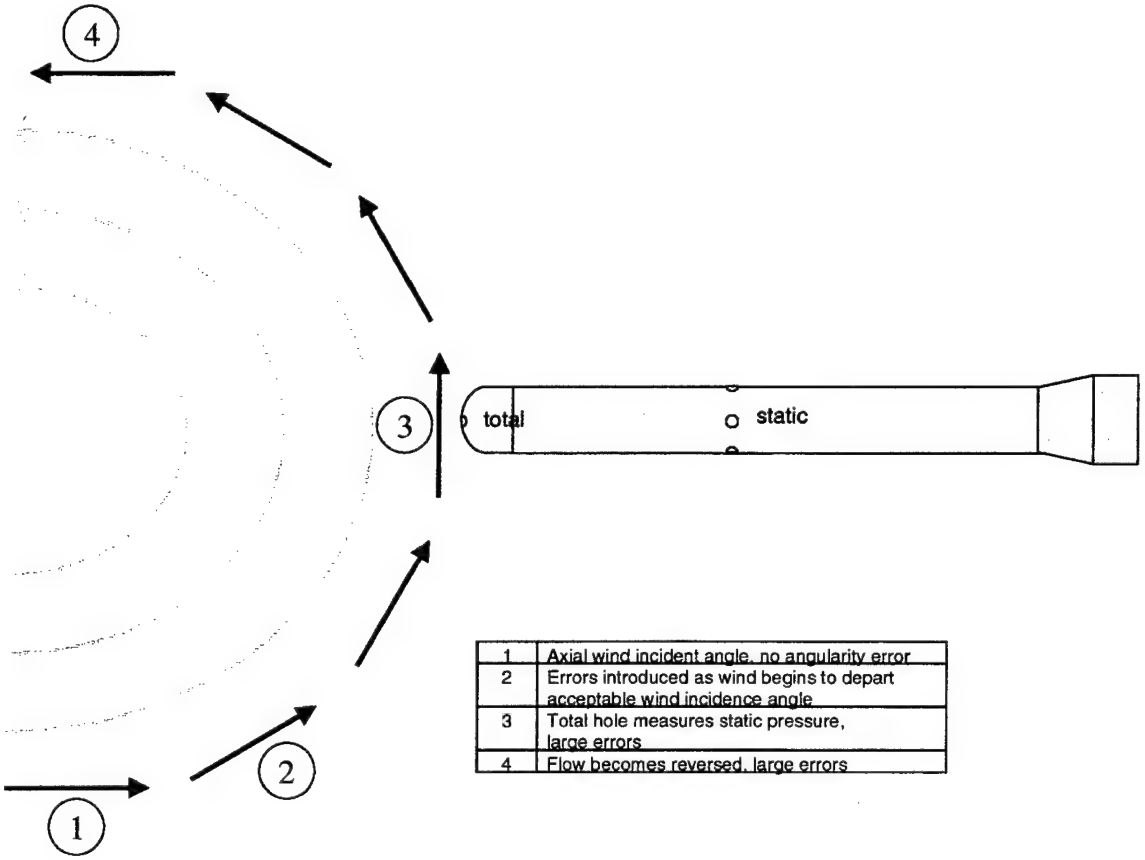

Figure 10: Angularity/Rotational Effects on Total and Static Ports

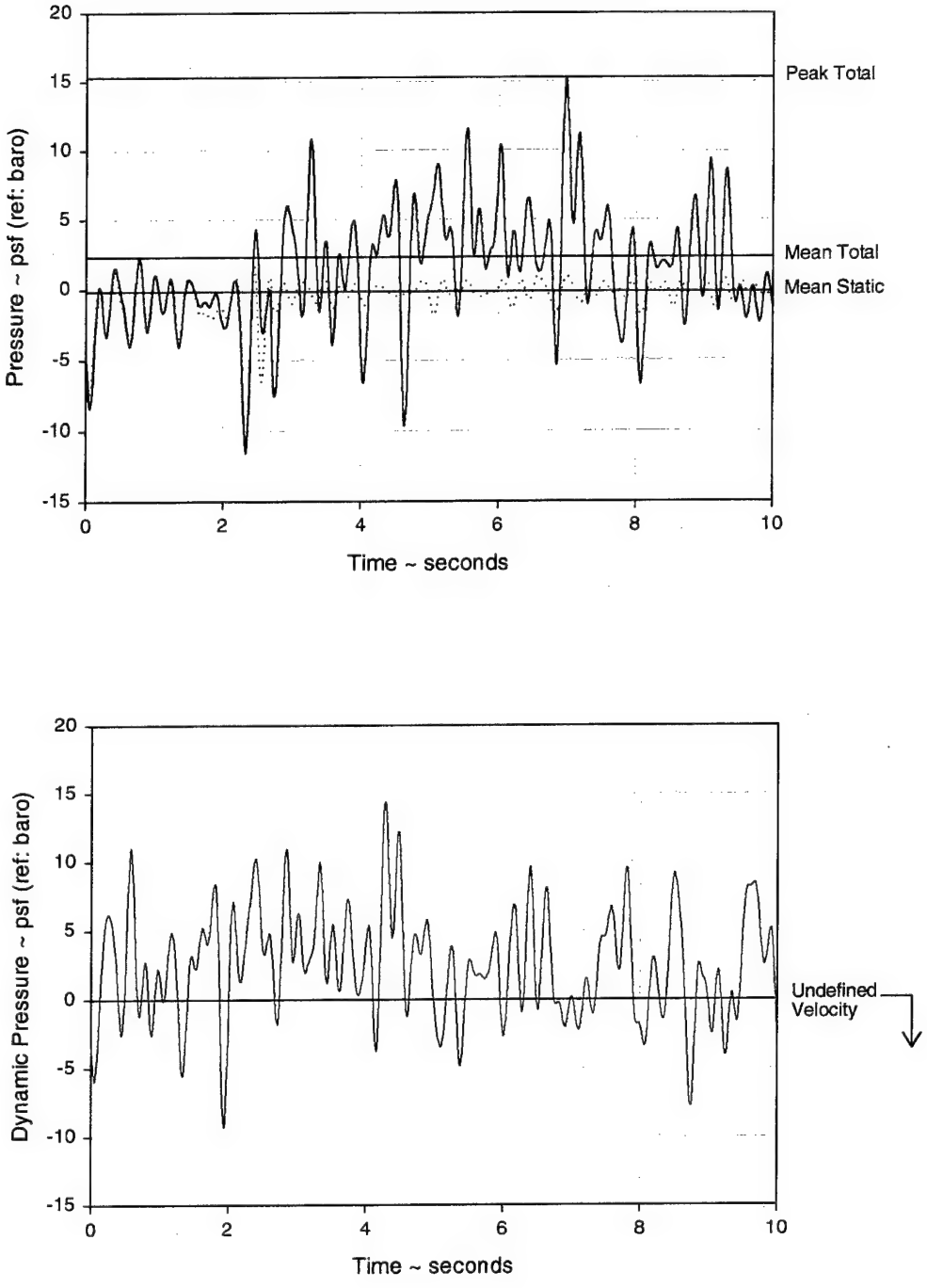

Figure 11: Statistical Processing and an Example of Undefined Velocity Due to Negative (Indicated) Dynamic Pressure

15. The relationship of flow field pressures, mean velocity, and peak velocity with respect to measurement height above ground are described in the velocity-height profile, constructed in figure 12. The mean and peak dynamic pressures yielded mean and peak velocities that use the calibration constants and algorithms included in appendix C. Although the figure 12 velocity-height profile represents a specific test condition, most velocity-height profiles had the same general shape with the higher velocities remaining close to ground plane and a minimal velocity at 120 in.-AGL. This effect decreased when the measurements were taken in the stagnation regions or at locations farther away from hover center. The velocity-height profile in figure 12 shows an anomaly at the 52 in.-AGL and 72 in.-AGL measurement locations that was caused by condensation in the pressure tubing. This anomaly disappeared later in the test day as the heated flow field dried the tubing. A complete collection of the velocity-height profiles for all test conditions is contained in appendix D. Wind direction in horizontal and vertical plane was provided as an algorithm output from the mean pressure data obtained from the five-tube probes. A complete collection of the direction data for all test conditions is contained in appendix E.

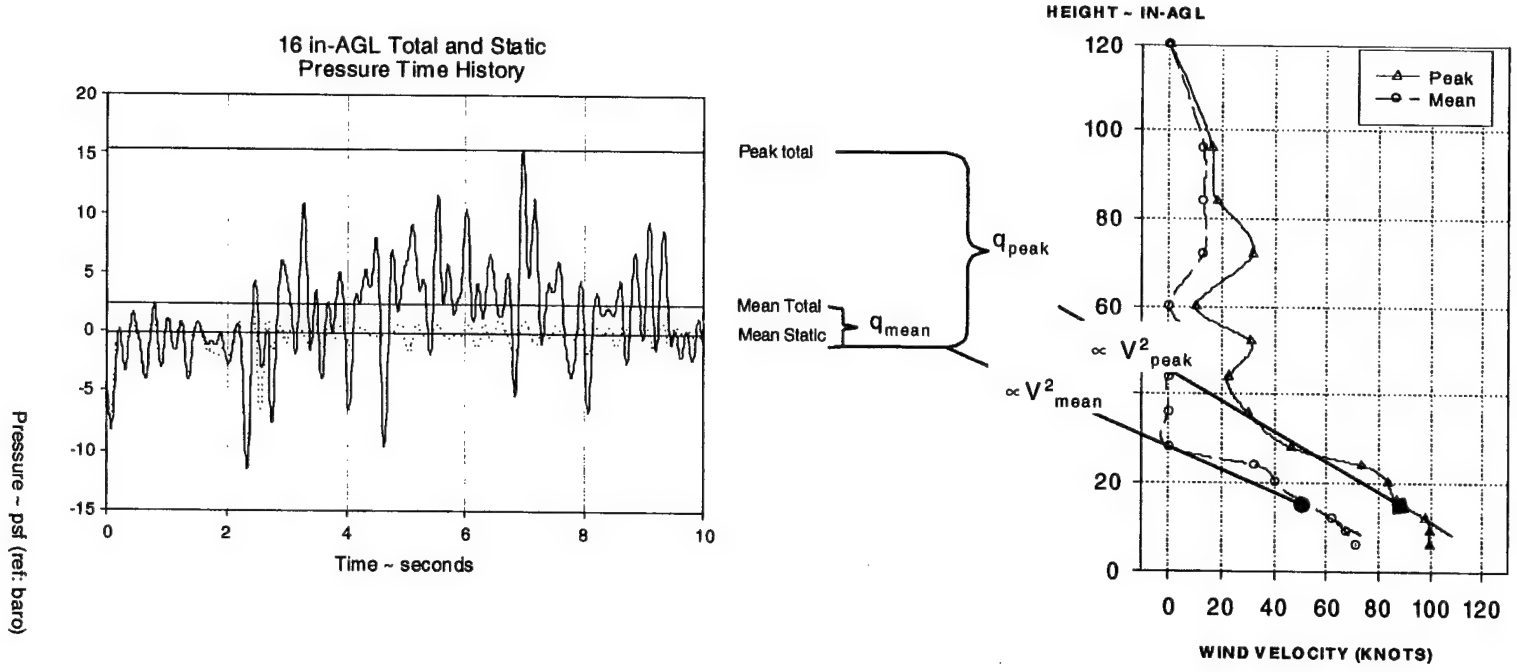

Figure 12: Construction of the Velocity-Height Profile
(Shown 50 ft-AGL Hover, 140 deg Test Azimuth as Measured 32 ft from Hover Center)

16. Temperature-height profiles were constructed in a similar manner as velocity-height profiles; however, only mean temperatures were analyzed due to the steady behavior of the temperature time histories, shown in figure 13. Analysis also required significantly less processing due to the calibration and linearization real-time processed by the Nicolet data system. Additionally, the total temperature probes were relatively insensitive to flow angles due to their slower (relative to the pressure transducers) time response, thus alleviating angularity errors in flow field temperatures. A complete collection of the temperature-height profiles for all test conditions is contained in appendix F.

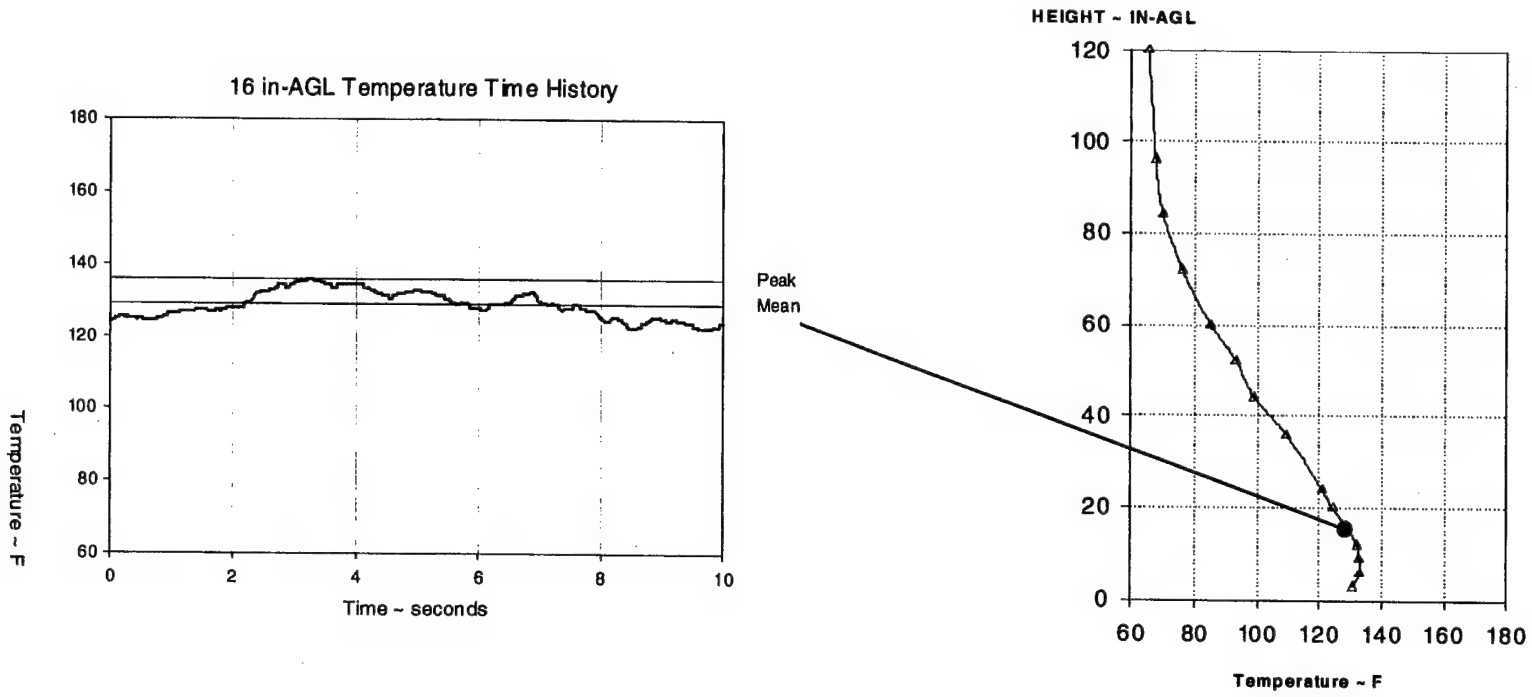

Figure 13: Construction of the Temperature-Height Profile
(Shown 50 ft-AGL Hover, 140 deg Test Azimuth as Measured 32 ft from Hover Center)

FLOW FIELD DIRECTION

17. Flow field direction was measured and analyzed to determine the AV-8B flow field patterns. Figure 14 shows vertical plane flow direction during a 50 ft-AGL hover on the 0 deg azimuth. Figure 14 represents the typical flow field pattern in that the lower, high-velocity flow aligns with the ground plane and the reduced velocity flow contains a small upwash component as the flow expands radially and upward. Horizontal plane wind direction is illustrated in figure 15 as measured by the 6 in.-AGL five-tube probe. On the whole, flow emanates radially away from hover center and closely aligns with the test azimuth. However, at the closer test positions (32 and 40 ft from hover center), it is apparent that the flow tends to expand outward from the for/aft stagnation region, (the 0 and 180 azimuths (refer to figure 2, section B-B)). The interaction between for/aft nozzles (along the lateral stagnation line, figure 2, section A-A) was not apparent in horizontal plane direction data.

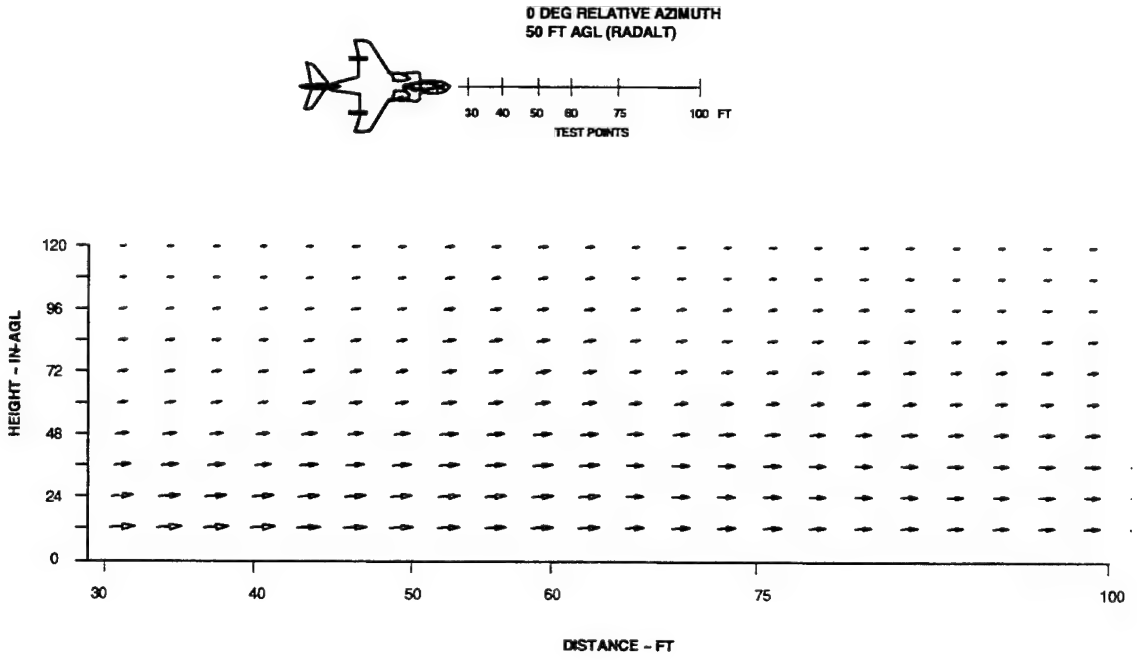

Figure 14: Vertical Plane Flow Direction
(Shown for 50 ft-AGL Hover, 0 deg Test Azimuth,
Figure Includes Interpolated Vectors for Clarity)

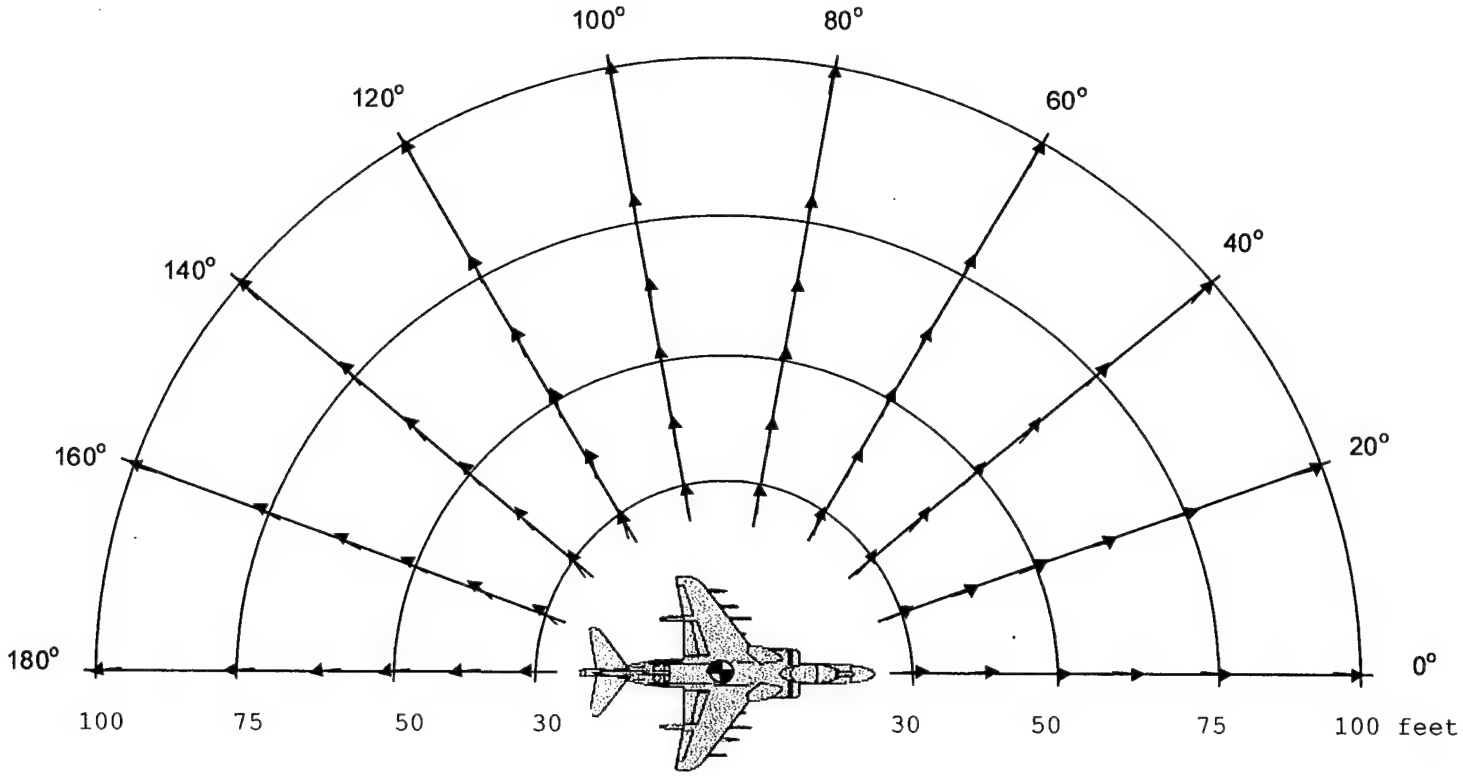

Figure 15: Horizontal Plane Wind Direction
(Shown for 50 ft-AGL Hover, as Measured 12 in.-AGL)

FLOW FIELD VELOCITY

18. The outwash velocity field was measured to assess the local environment to which personnel and equipment are subjected. Although personnel are affected by primarily the horizontal component of velocity, all data presented and discussed in this report are based on the total velocity vector, as the vertical velocity component was negligibly small (as shown in figure 14). Additionally, the mean and peak velocity magnitudes of these flow fields are presented to illustrate the dynamic range of the outwash winds. This analysis method permits an accurate representation of AV-8B outwash flow field and allows comparison to past NAWCAD Patuxent River V/STOL aircraft outwash test results.

19. A typical plot of mean and peak wind velocities as a function of transducer height above ground is shown in figure 16, during a 50 ft-AGL hover on the 60 deg test azimuth. The flow field begins (at 32 ft) as a rather narrow sheet approximately 30 in. high where peak velocities tend to be relatively high, reaching near 140 kt (50 ft-AGL, 60 deg test azimuth). Velocities above the sheet tend to be smaller, only as generated by the entrained flow. At heights above 72 in.-AGL, velocities are minimal and appear generally independent of distance away from the aircraft. As the flow field is allowed to extend in distance, the sheet tends to expand and the lower height velocities decay and equal the higher height velocities, settling into a uniform flow field. This narrow sheet to uniform flow trend does not hold true along the 0-180 deg stagnation lines (ref: figure 2, B-B). Figure 17 shows the stagnation region flow for a 50 ft-AGL hover point on the 180 deg test azimuth. This type flow field produces a high velocity, uniform flow field, even at the closer distances such as 32 ft. Although the flow's peak velocities may be lower than what is found in nonstagnation regions, the existence of moderately high velocity flow at heights between 30 and 60 in.-AGL produce a very large amount of aerodynamic drag force on the torso region of personnel working in the flow field. Flow at these stagnation regions tends to decay (with respect to distance from the aircraft) at the same rates as that of the nonstagnation region flow, and tends to equalize when allowed to travel beyond 75 ft from center. This equalization effect of velocities in the wall jet is shown in the outer regions of the velocity contour of figure 18. A Phase 0 mean velocity contour (measures at 6 in.-AGL) is included for reference in appendix G. Data from the 60 deg stagnation region did not exhibit the uniformity found on the 0-180 stagnation region. It is probable that this uniformity (caused by combined mass flow and resulting expansion) occurs off the A-A stagnation line (ref: figure 2) but could not be confirmed given the data resolution (with respect to test azimuth) of this testing. Recommend for future testing that the instrumentation cart be capable of circumferential tracking to allow fine data resolution at the stagnation lines.

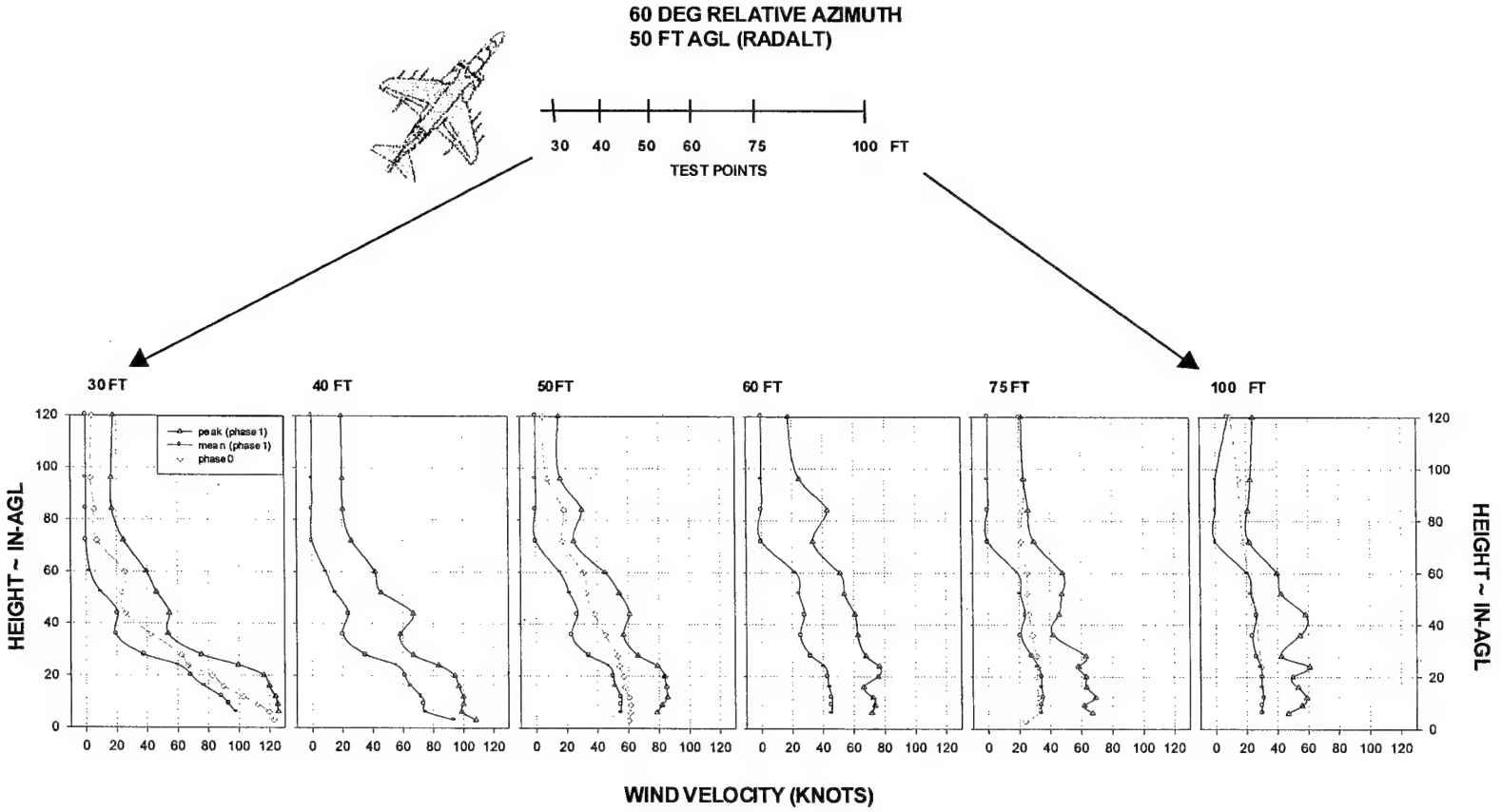

Figure 16: 60 deg Azimuth Velocity Height Profiles
(Shown for 50 ft-AGL Hover, 60 deg Test Azimuth, Red Plot Indicates Phase 0 Test Results)

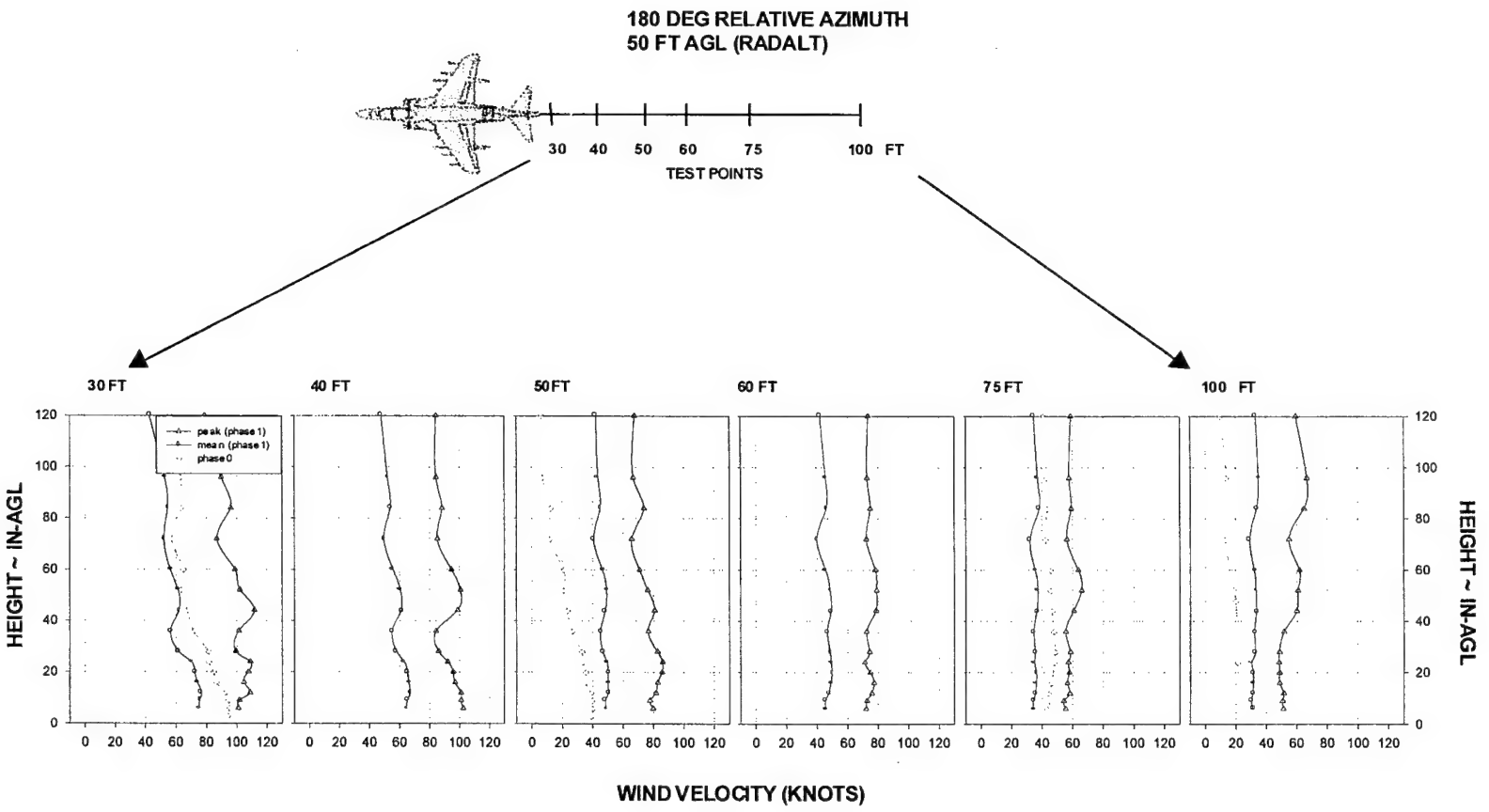

Figure 17: 180 deg Azimuth Velocity Height Profiles
(Shown for 50 ft-AGL Hover, Red Plot Indicates Phase 0 Test Results)

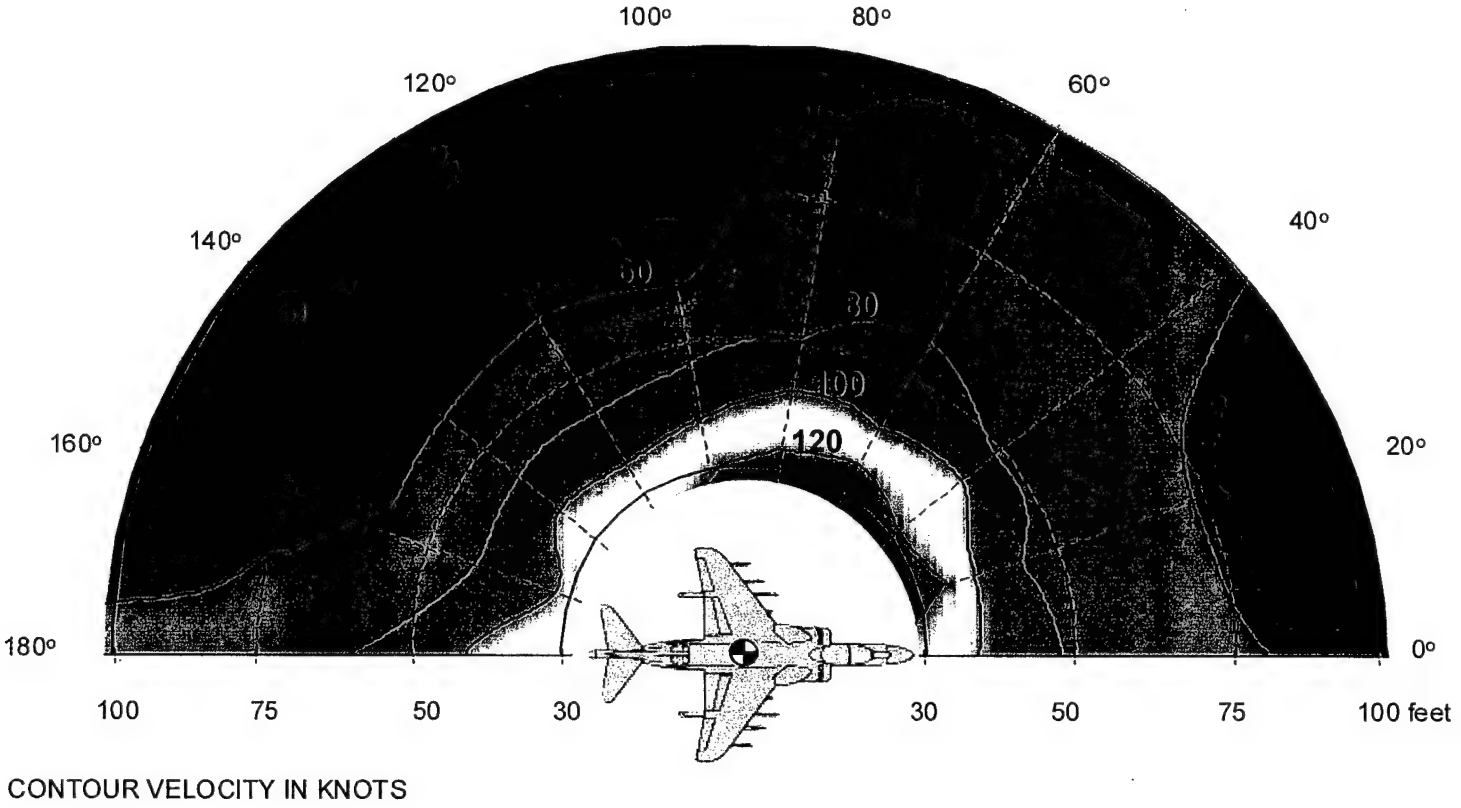

Figure 18: The 6 in.-AGL Ground Sheet Peak Velocity Contour during a 50 ft-AGL Hover
(Phase 1 Results, Velocity Contours are in kt)

20. The change of the velocity field with respect to aircraft hover height was measured at 30, 50, 80, 100, and 125 ft-AGL (radar altitude) on both the 0 and 60 deg test azimuths. The results of these tests are graphically presented in figure 19 for a cart position of 32 ft from aircraft center. It should be first noted that the 50 ft-AGL hover profile on the 0 deg azimuth has a significantly different velocity profile than the other hover points. This occurrence may be the result of the aircraft transitioning out of ground effect or the aircraft may have drifted out of test position. A 10 ft aircraft drift may be enough to misplace the rake outside the narrow 0 deg stagnation region. With this assumption in mind, data on the 0 deg azimuth at the 30 and 80 ft hover height tended to equal both in profile shape and velocity magnitudes. When heights increased from 50 ft-AGL on the 0 deg azimuth, peak velocity magnitudes tended to decay near 20 kt per each incremental change in hover height. Analysis of changing heights on the 60 deg azimuth show a less pronounced decay at height from 30 to 100 ft-AGL where peak velocities nominally remained steady between 100 and 123 kt. Decay to 80 kt was not attained until 125 ft-AGL, concluding that the outwash flow field on the 60 deg azimuth is moderately sensitive to changes in hover height, at least within the scope of these tests.

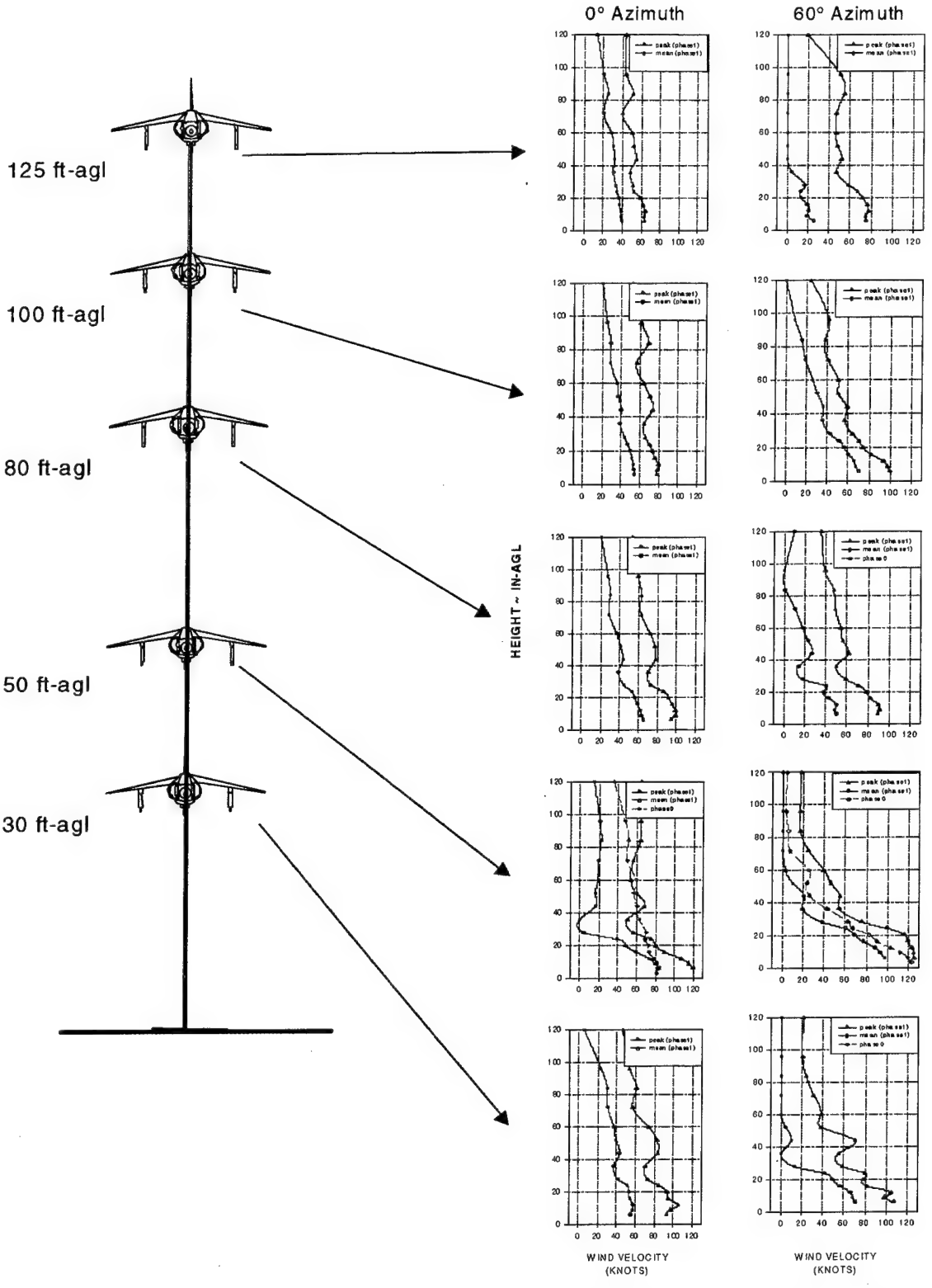

Figure 19: Velocity Height Profiles as a Function of Hover Height (Radar Altitude) (as Measured 32 ft from Hover Center on the 0 deg Test Azimuth)

TRANSIENT MANEUVER DATA

21. This report focuses primarily on outwash data from the aircraft while in a steady hover. However, Phase 0 tests captured transient maneuver data from vertical takeoffs, no-go VTO's, and vertical landings with a very limited time-accurate data system. Phase 1 testing attempted to expand the transient maneuver data base; however, the rapid time evolution between the completion of a transitional maneuver to a steady state hover (or vice versa) did not allow for complete data records. Recommended future outwash testing should allow the data system to capture both transient maneuvers and steady hover events on a single data record. The Phase 0 instrumentation was geared primarily for steady state mean velocity measurement; however, a smaller data system was provided to acquire four unsteady total pressure and temperature measurements. Static pressure measurements were not acquired although all pressure transducers were ported to local ambient conditions, under the assumption that static and barometric pressures were relatively equal. Figures 20 and 21 show the general behavior of the outwash flow field during a VTO and vertical landing, respectively. The temperature traces on figure 20 show the VTO's quickly heated the flow field, noted by a 2.5 sec time for the flow to achieve 63% steady state (or 1τ). It should be noted that the thermocouples were type J of 20 gage wire, resulting in a fast (1τ = 0.16 sec in 35 kt) convective heat transfer. The temperature trace of figure 21 shows the flow field also cooled to 63% ambient temperatures in approximately 2.5 sec. Once the hover was established, the pressure traces closely resemble the time histories, as shown in figure 7. Referring to the VTO transition of figure 20, the outwash velocity field tended to identify well with the 60 deg, 50 ft hover steady state event shown in figure 16 (32 ft), with the assumption that static and ambient pressures were relatively equal.

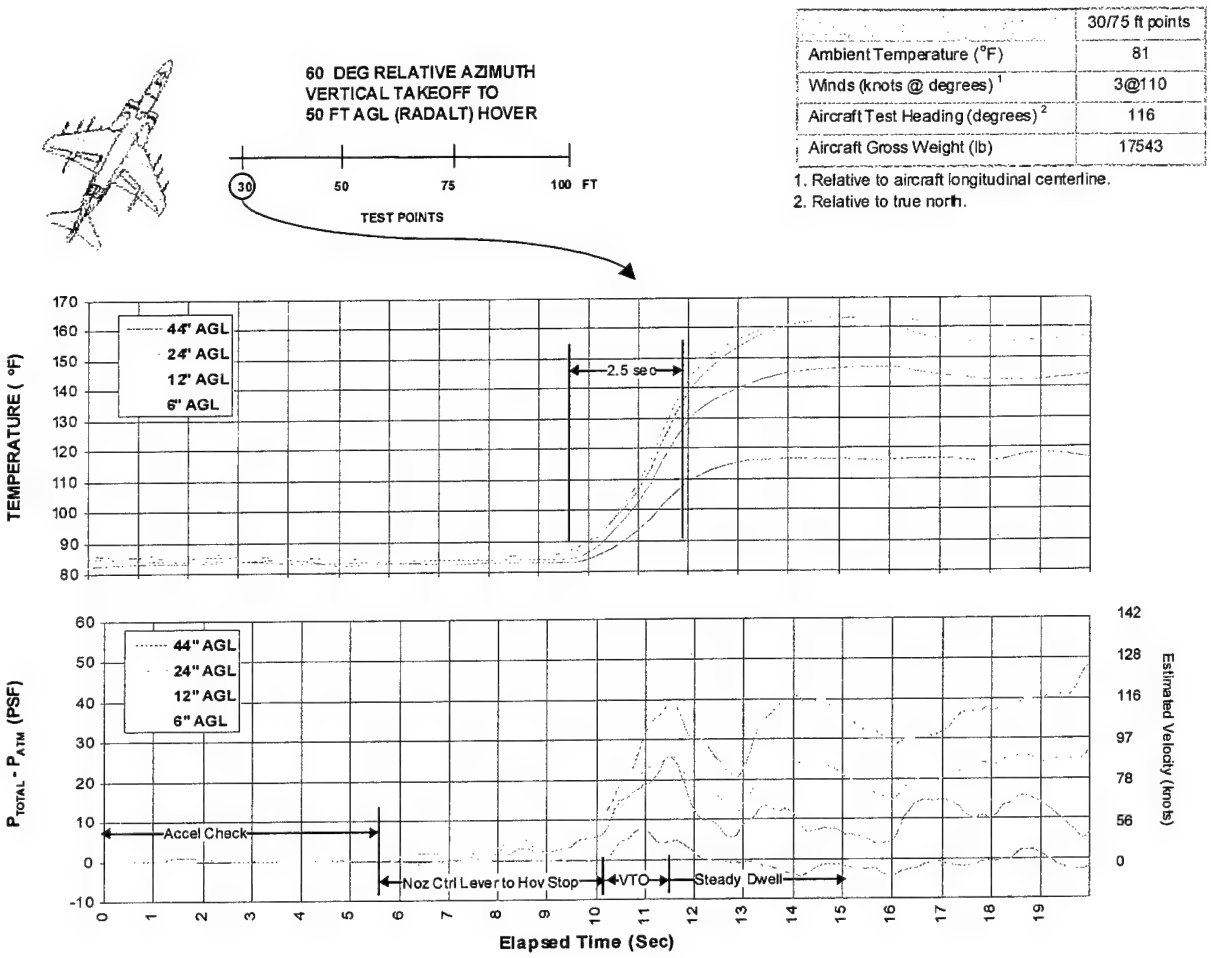

Figure 20: Temperature and Total Pressure Profiles during Transition from Vertical Takeoff to a Hover
(Phase 0 Results, Data Acquired 30 ft from Nozzle Centroid on the 60 deg Relative Azimuth)

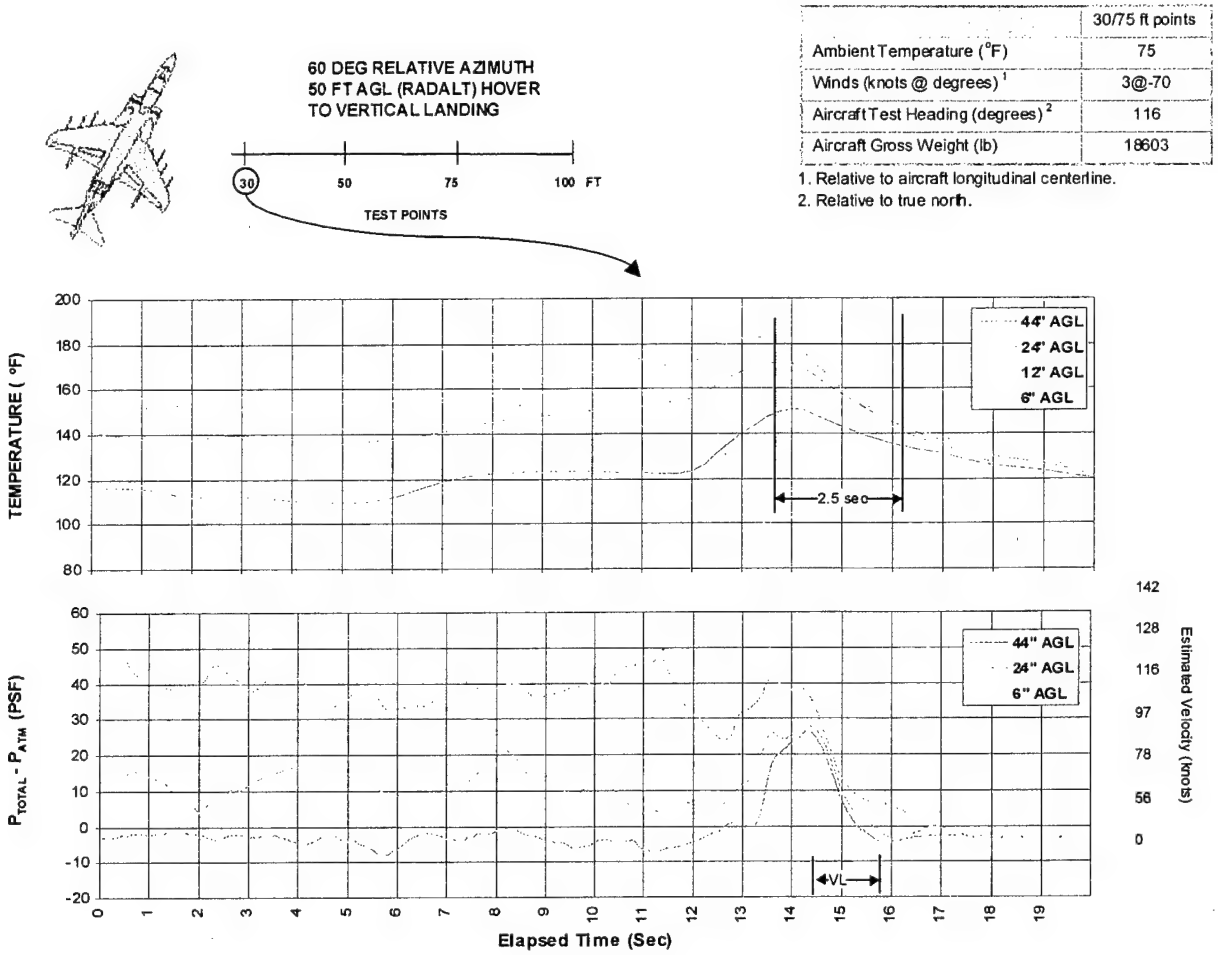

Figure 21: Temperature and Total Pressure Profiles during Transition from Hover to a Vertical Landing
(Phase 0 Data, Data Acquired 30 ft from Nozzle Centroid on the 60 deg Relative Azimuth)

FLOW FIELD TEMPERATURES

22. The temperature field was measured to obtain a general understanding of the AV-8B thermal characteristics of the outwash flow. Figures 22 and 23 show the temperature height profiles for the 60 and 180 deg azimuth, respectively, during a 50 ft-AGL hover. The temperature field follows the same basic trend as the velocity field by possessing a relatively narrow sheet (heights below 40 in.-AGL) at locations close to the aircraft and developing into a uniform temperature field when expanding away from the aircraft. For high thermal gradient profiles, maximum temperatures could reach as high as 150°F although the higher probe locations observe approximately ambient temperatures. As the flow field expands, temperatures in the ground sheet decay; however, there is a slight increase in temperature at the higher probe location as the flow field tries to stabilize at a uniform temperature. Large thermal gradients were absent at for/aft stagnation regions, such as on the 180 deg azimuth, shown in figure 23. For these positions, the relatively high temperatures found in the ground sheet are not attained and temperatures remain near constant throughout the profile, decaying at the same rate with respect to distance from the aircraft. The 6 in.-AGL temperature contour plot for a 50 ft-AGL hover is shown in figure 24. In general, the contour plot shows temperatures of 130°F at areas close to the aircraft decaying to slightly above ambient at 100 ft from the aircraft The hottest location recorded was found on the 80 deg azimuth, where temperatures exceeded 140°F. As could be expected from the difference between the aft hot nozzles and the front cool nozzles, temperatures in the fwd/aft stagnation region were slightly warmer in the aft and slightly cooler in the front.

23. The change of the temperature field with respect to aircraft hover height were analyzed at 30, 50, 80, 100, and 125 ft-AGL on both the 0 and 60 deg test azimuths. The results of these tests are graphically presented in figure 25 for a cart position of 32 ft from aircraft center. As with the velocity profiles, the temperature profile showed a significant difference on the 0 deg azimuth than the other hover points. With this exception in mind, the temperature field appeared to be moderately insensitive to hover height with the only noticeable change occurring at the 125 ft-AGL hover height, where temperatures, on both test azimuths, were reduced only by approximately 10°F to 15°F.

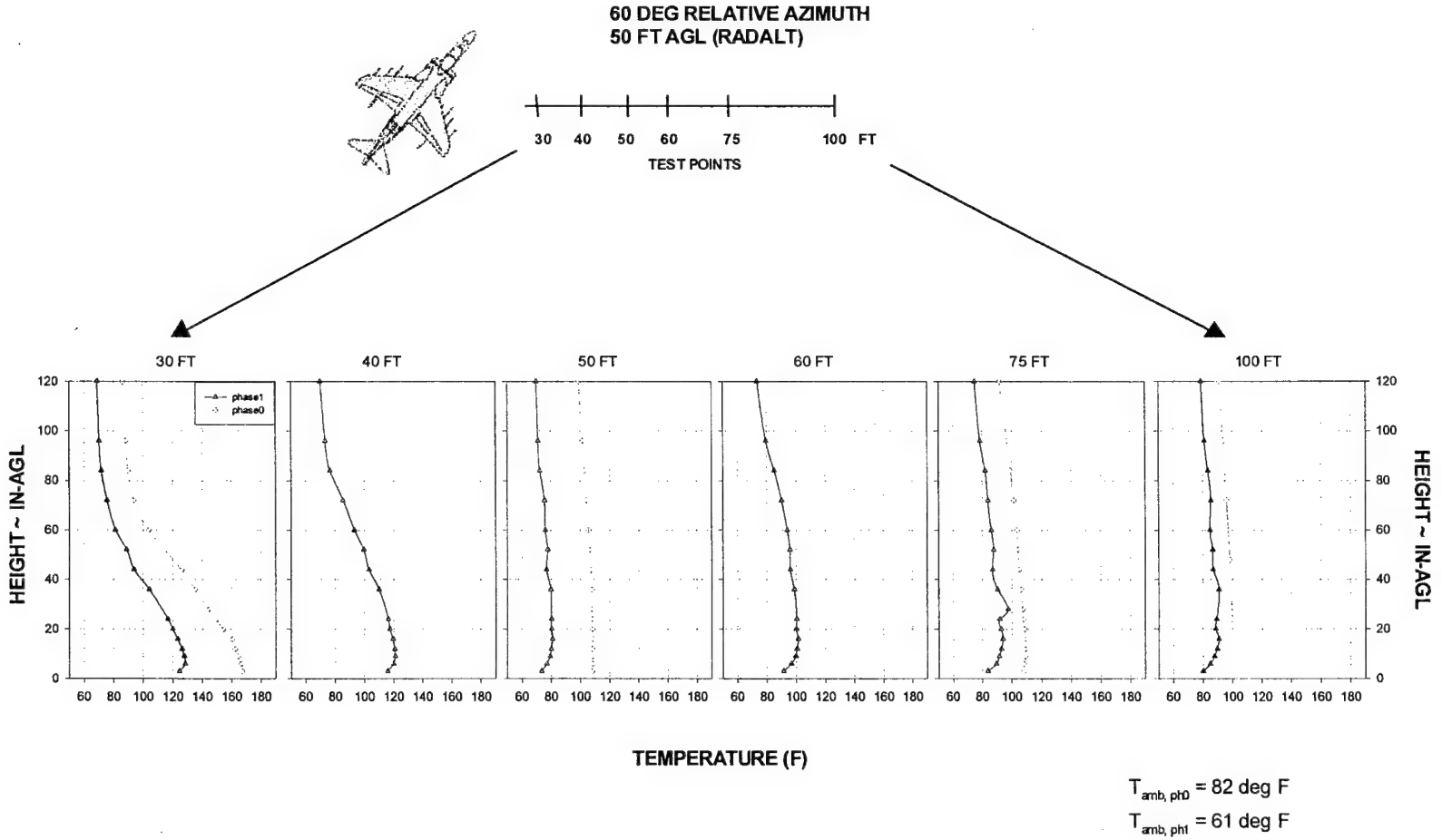

Figure 22: 60 deg Azimuth Temperature Height Profiles
(Shown for 50 ft-AGL Hover, Red Plot Indicates Phase 0 Test Results)

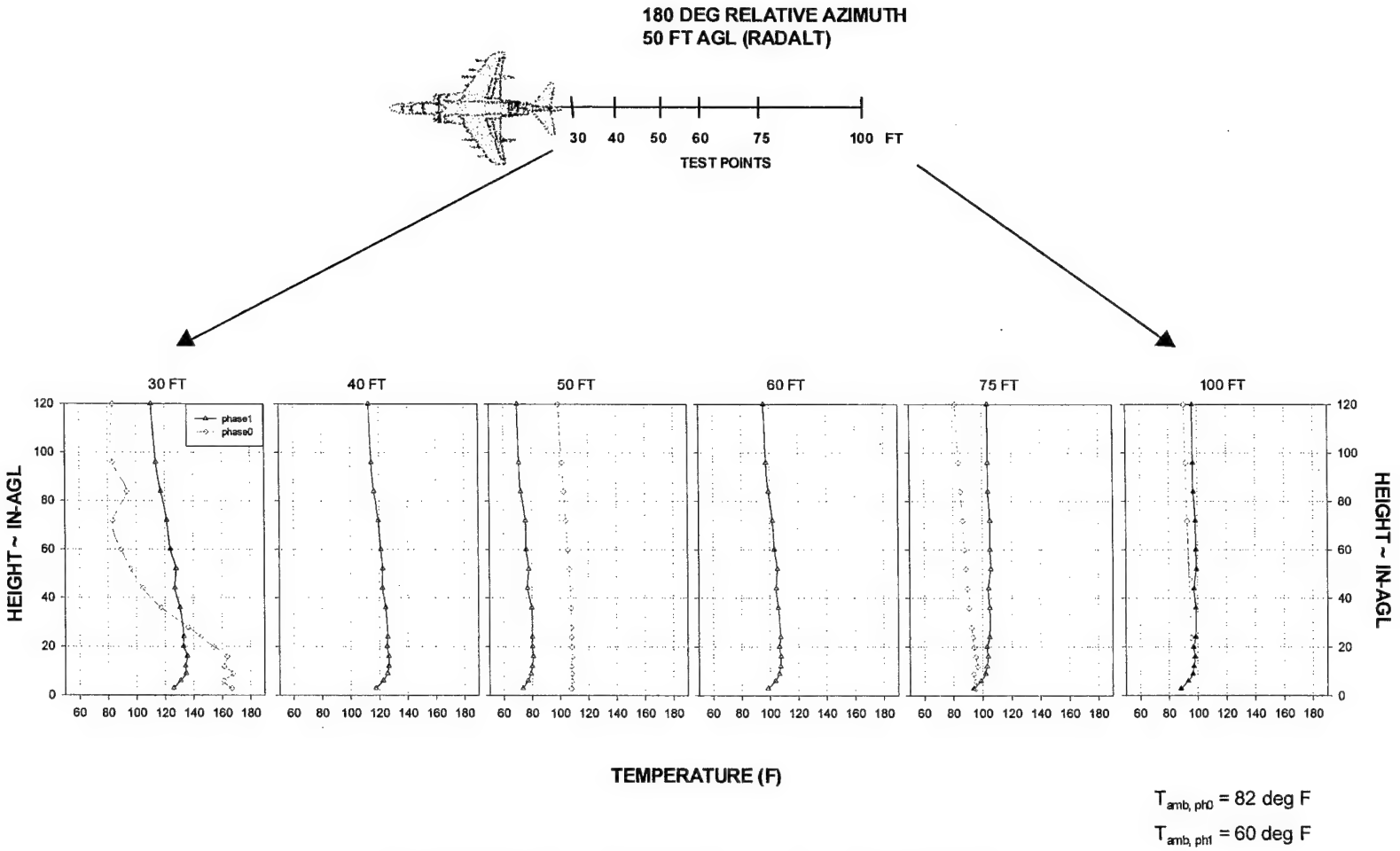

Figure 23: 180 deg Azimuth Temperature Height Profiles
(Shown for 50 ft-AGL Hover, Red Plot Indicates Phase 0 Test Results)

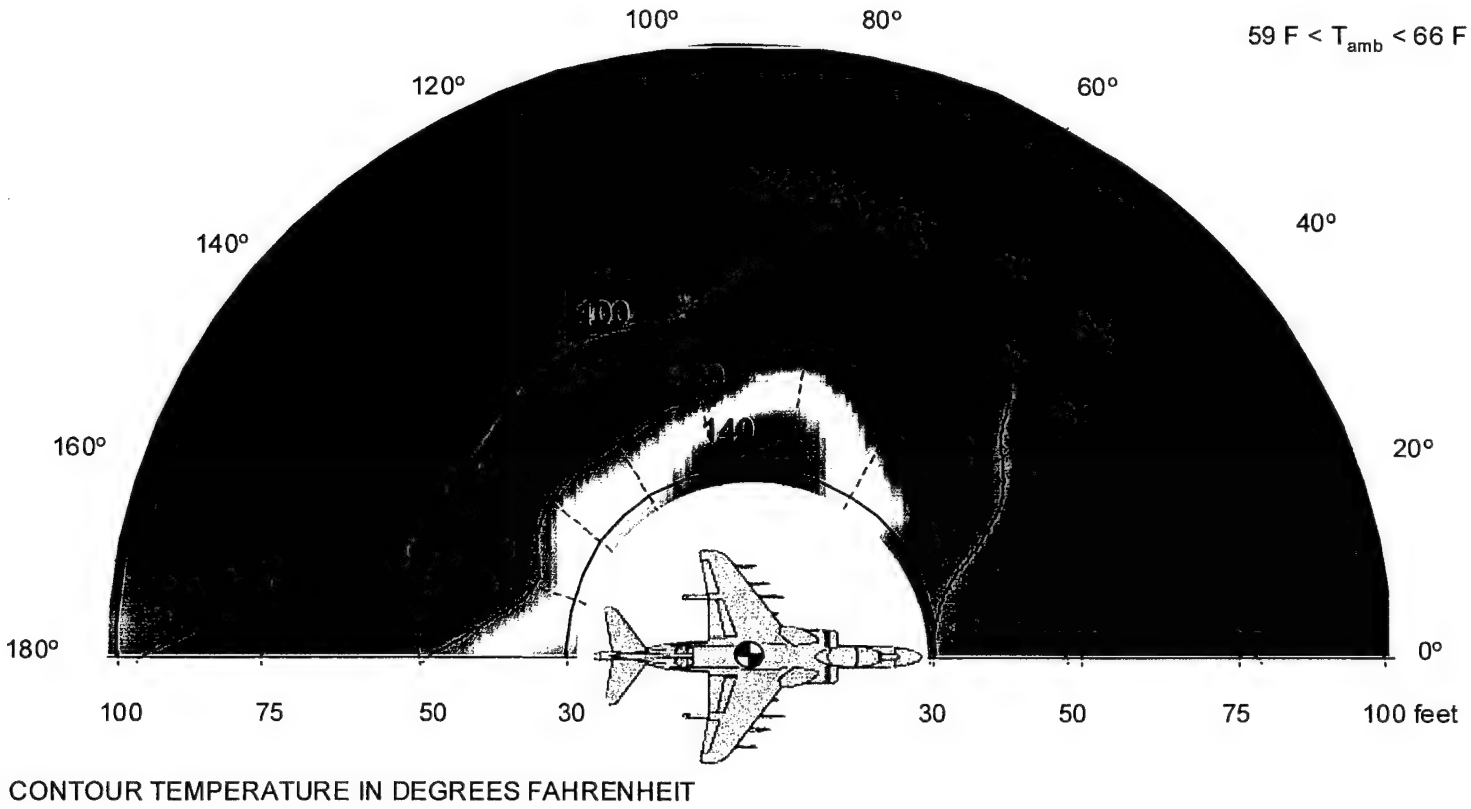

Figure 24: 6 in.-AGL Mean Temperature Contour during a 50 ft-AGL Hover
(Phase 1 Results, Temperature Contours are in deg Fahrenheit)

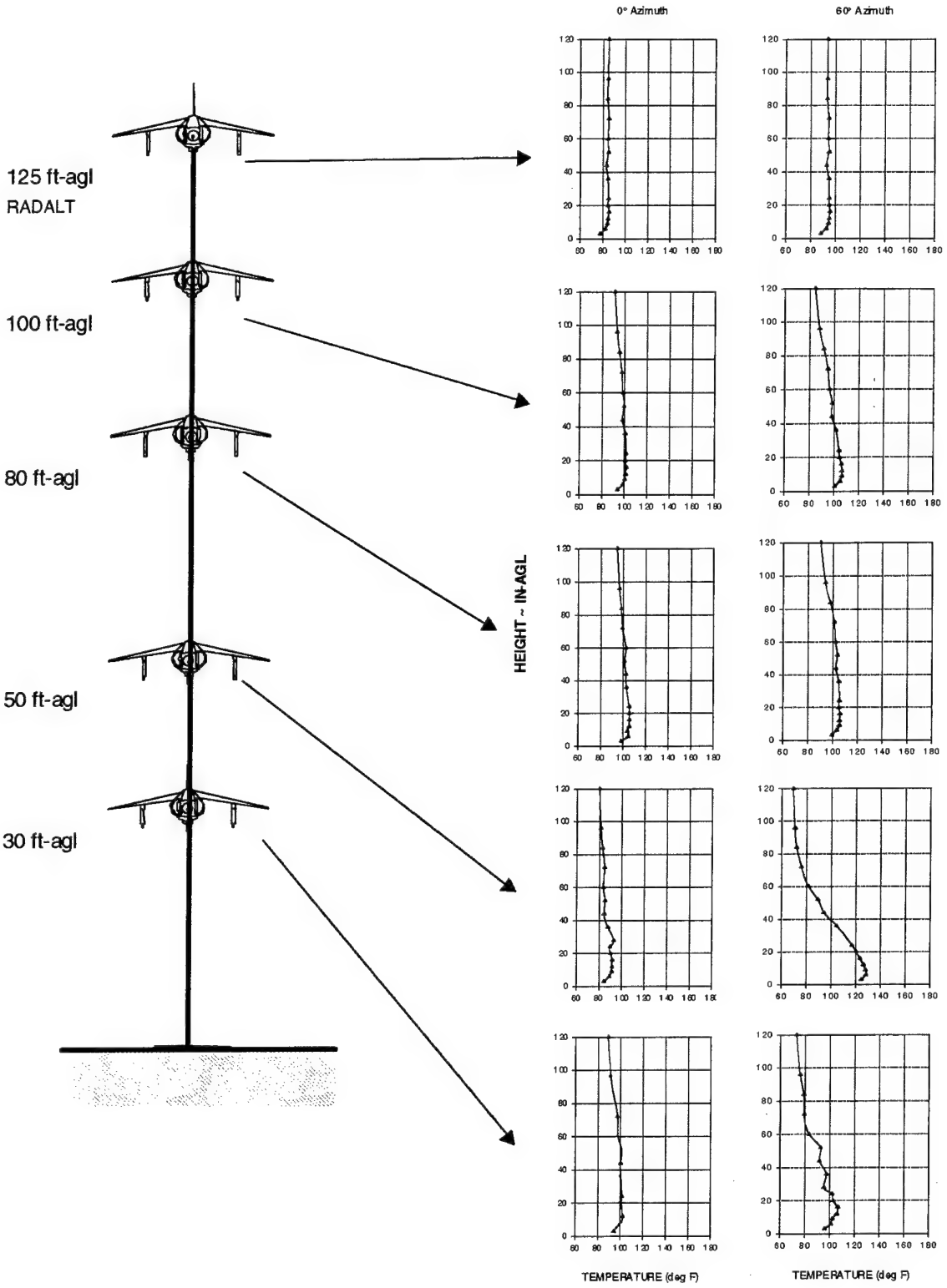

Figure 25: Temperature Height Profile as a Function of Hover Height
(as Measured 32 ft from Hover Center)

TEMPERATURE EXTREMES

24. NAWCAD Patuxent River and the Navy, in general, have a very limited qualitative data base on the effects hot jet exhaust has on personnel safety and performance. A Navy Safety Center data base search prior to these tests found no thermal injuries due to excessive Harrier exhaust temperatures; however, this data does not include the many nonreported performance/safety related occurrences not severe enough to be deemed a reportable "incident". The United States Air Force Wright Laboratories have researched this area extensively and have developed a burn simulation (BURNSIM) model as described in reference 7. Although the temperatures found in this AV-8B outwash test intuitively fall well below burn levels, the Wright Laboratory model determines the pain threshold. As shown in figure 26, thermal pain is defined by the amount of heat transfer necessary to elevate the skin temperature to 111.2°F (44°C) temperature at a depth 200 μm below the skin surface. This metric is particularly useful, as this is the thermal limit where personnel loose situational awareness, loose concentration, and begin to feel pain. For a general safety consideration, fleet personnel must remain focused on their sometimes-hazardous duties and any thermal exposure must remain below the pain threshold. To apply this method to AV-8B outwash data, the BURNSIM model inputted the highest amount convective heat transfer functions of air temperature, mean velocity, ambient conditions, present in the Phase 1 outwash test, particularly the 80 deg azimuth, 32 ft from aircraft center during a 50 ft-AGL hover. Results show that after a unit-step of heat is applied, the skin at a 200 μm depth heats to approximately 101.5°F, significantly lower than the pain threshold of 111.2°F. In fact, skin surface temperatures failed to reach over 102°F. This analysis concludes that within the scope of these tests and even at the hottest areas around aircraft, the AV-8B outwash flow should not cause any amount of thermal pain to personnel working close to the aircraft. However, thermal pain is not a sole indicator of a thermal problem. Ground or deck personnel exposed to continuous flight operations (launch/recovery cycles) in these elevated temperature fields may increase their susceptibility to heat exhaustion or heat stroke. Future analysis should be performed to determine the reduction of physiological performance of personnel working in these elevated temperature fields.

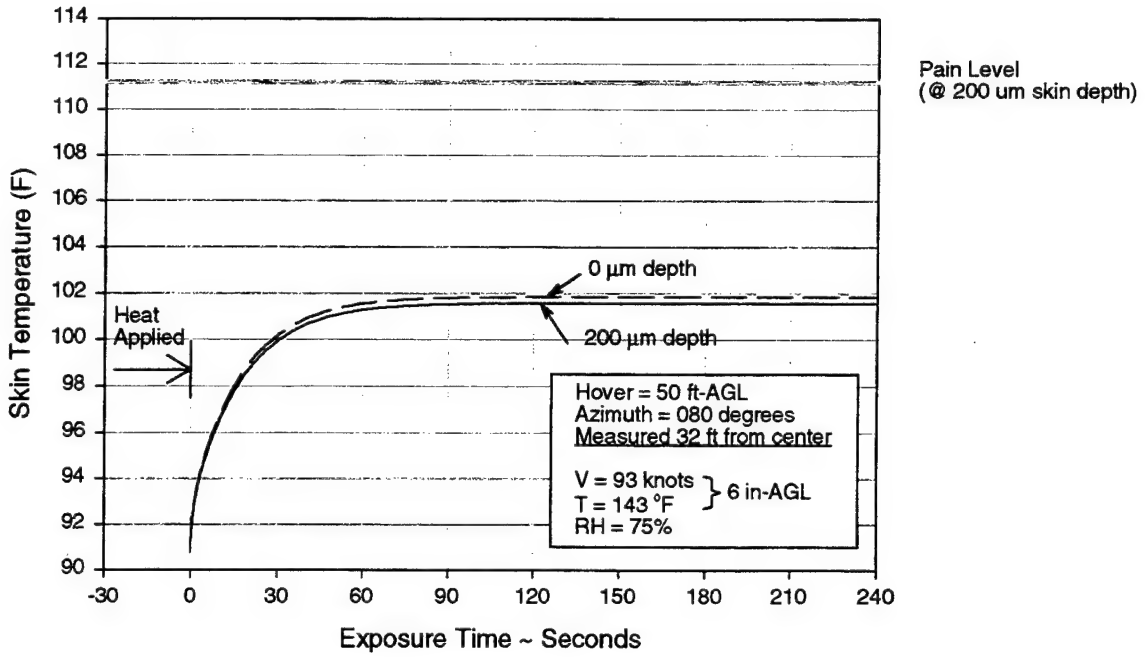

Figure 26: BURNSIM Model Results
(Shown for Time Step Outwash Inputs from a 50 ft-AGL Hover,
32 ft from the Aircraft on the 80 deg Test Azimuth)

OUTWASH FORCES ON PERSONNEL

25. Personnel engulfed in an outwash flow field experience postural instability by both being unable to withstand the high aerodynamic forces and also by being unable to properly react to high magnitude flow oscillations (gusts). A photograph of personnel engulfed in the AV-8B flow field is shown in figure 27. Past NAWCAD Patuxent River laboratory tests have shown that personnel of relatively large stature can withstand outwash forces to 115 lb. These laboratory tests also show personnel of smaller stature may be able to tolerate forces to 80 lb. Results of these laboratory tests are shown in figure 28 and the analytic methods are provided in appendix H. Although these laboratory tests provide a good yardstick, they may not be truly accurate because they do not account for an individual's uniqueness in situational awareness, personal strength, and flight operation experience. Flight deck personnel and helicopter support teams (of a wide range of personal statures) are accustomed to working near or under the CH-53E while subjected to outwash levels in excess of 115 lb without a significant injury incident (ref: appendix H, NAVSAFECEN data). Also, it has been demonstrated numerous times throughout the MV-22 DT/OT test phases that personnel (of average stature or greater) successfully ingress the MV-22 flow field where aerodynamic force levels can exceed 120 lb. This is not to underestimate the inherent hazards and stress associated with operating in these flow fields but more to keep these levels in operational perspective. Reaching these levels are essential for ground and flight deck personnel to perform their assigned duties and it must be understood that winds of these magnitudes can be physiologically strenuous and inherently dangerous. The mission of the AV-8B aircraft is very much different than that of large rotary wing aircraft in that personnel are not required to fully ingress into the outwash flow field and operate underneath the aircraft. Consequently, it stands to reason for general safety considerations, personnel of all weight percentiles should work near jet-borne V/STOL/STOVL aircraft at reduced outwash levels than that of large rotary wing aircraft. The Crew Systems, AEH laboratory, recommends that the **maximum allowable outwash level for personnel** shall be no greater than **90 lb peak force**. Figure 29 gives an illustration of the 90 lb peak force jet-borne V/STOL limit as compared to other NAWCAD Patuxent River rotary wing test results.

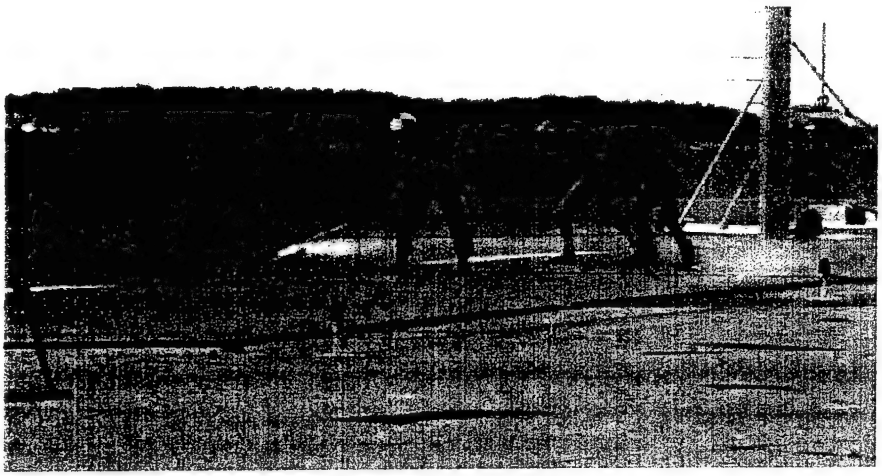

Figure 27: Test Personnel Engulfed in AV-8B Flow during a Smoke Visualization Study (Personnel Located Approximately 60 ft from Hover Center)

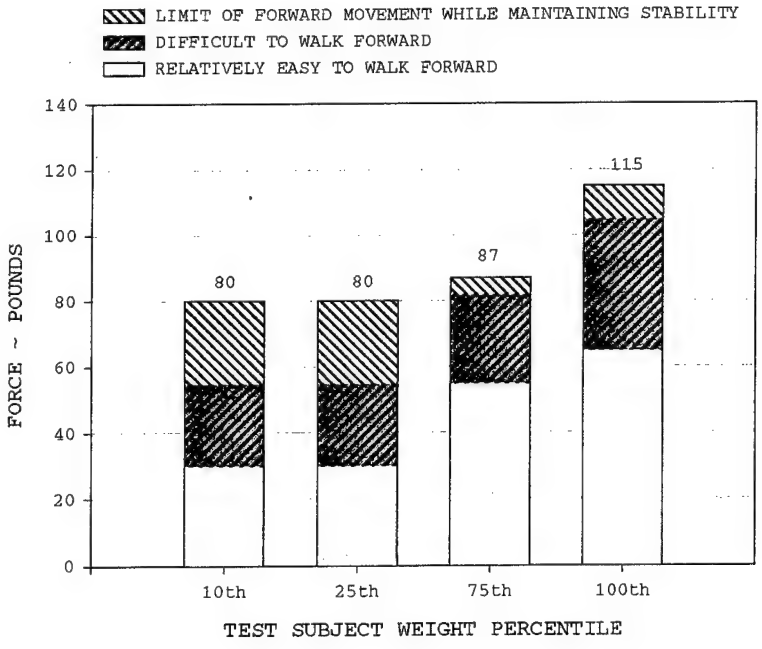

Figure 28: Ability of Various Test Subjects to Walk or Move Forward Under Various Amounts of Horizontal Restraint Loads Applied at a Position 3 ft-AGL

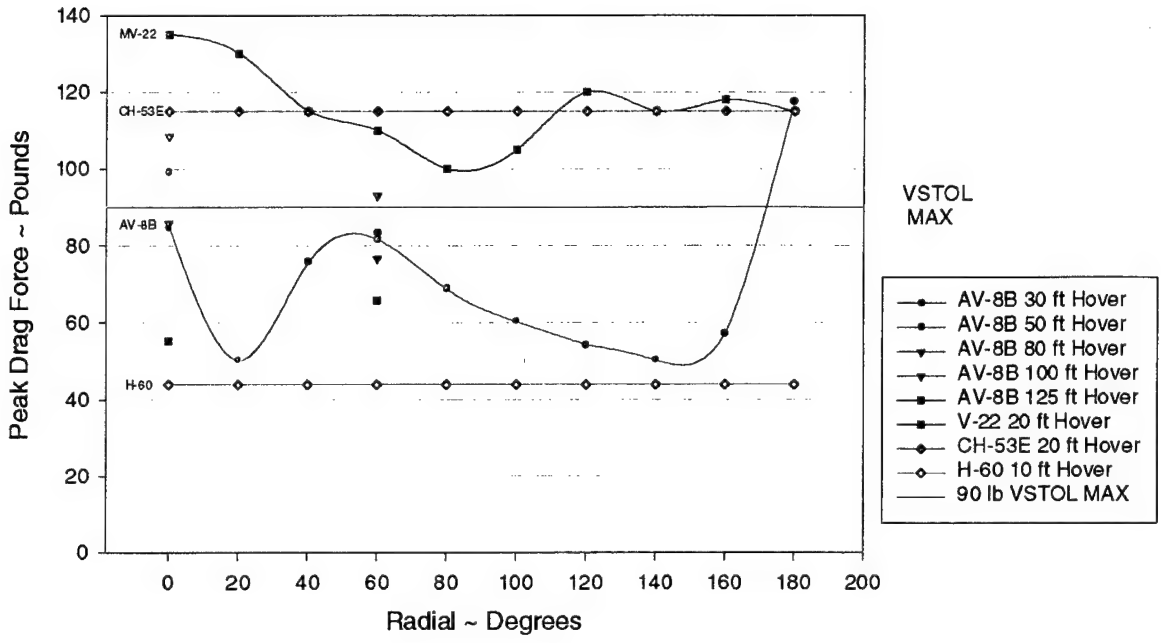

Figure 29: Outwash Peak Force Comparison between AV-8B, MV-22, CH-53E, and H-60 as Compared to the Maximum Allowable Outwash Level for Personnel Operating Near Jet-borne V/STOL Aircraft (All Data Referenced to NATOPS 50 ft Hazard Circle)

26. AV-8B velocity data were reduced to aerodynamic forces using the identical analytic methods derived from the CH-53E tests, contained in appendix H. Although this method for calculating forces was initially developed for rotary wing aircraft use, the temporal and spectral similarities between rotary wing and jet-borne V/STOL outwash signals allow confident adaptation. The aerodynamic drag values were calculated for all peak velocity-height profiles, for all test events. A contour of forces during a 50 ft-AGL hover is presented in figure 30. This contour shows large drag force levels are aligned off the 0, 60, and 180 deg stagnation lines with the highest forces in excess of 190 lb off the 180 deg azimuth. In the AV-8B NATOPS, defined hazard circle force levels rarely exceeded the 90 lb recommended limit although a 120 lb force level was found off the 180 deg azimuth. This force level does exceed a recommended limit and operations should restrict personnel from working in this area. Furthermore, during shipboard operations or during high local ambient wind conditions, downwind helicopter outwash velocities have been shown (reference 8) to strengthen significantly and become very hazardous.

27. The effects the variance in aircraft GW or hover height has on AV-8B outwash is most efficiently done by analyzing drag forces. Figure 31 compares the outwash force levels at different operational GW configurations. This figure shows very little relationship between operational GW and outwash forces but more accurately represents the test error band, which is not only sensitive to GW variances, but also changes in aircraft position, heading, and hover stability. Recommended for future testing that parameters of aircraft GW, heading, and position relative to the measuring system time be linked to the outwash data system. Figure 32 shows the effects hover height has on the outwash forces for the 0 and 60 deg test azimuths. Both graphs on figure 32 show that force levels at these test azimuths begin at relatively low magnitudes at the 30 ft-AGL hover height and increase as a 50 ft-AGL hover is reached. On the 0 deg azimuth, force levels continue to increase until the 80 ft-AGL hover is reached where forces gradually decay until a minimum is reached at 125 ft-AGL hover. On the 60 deg azimuth, outwash force levels begin to diminish upward of 50 ft-AGL and stabilize beyond an 80 ft-AGL hover.

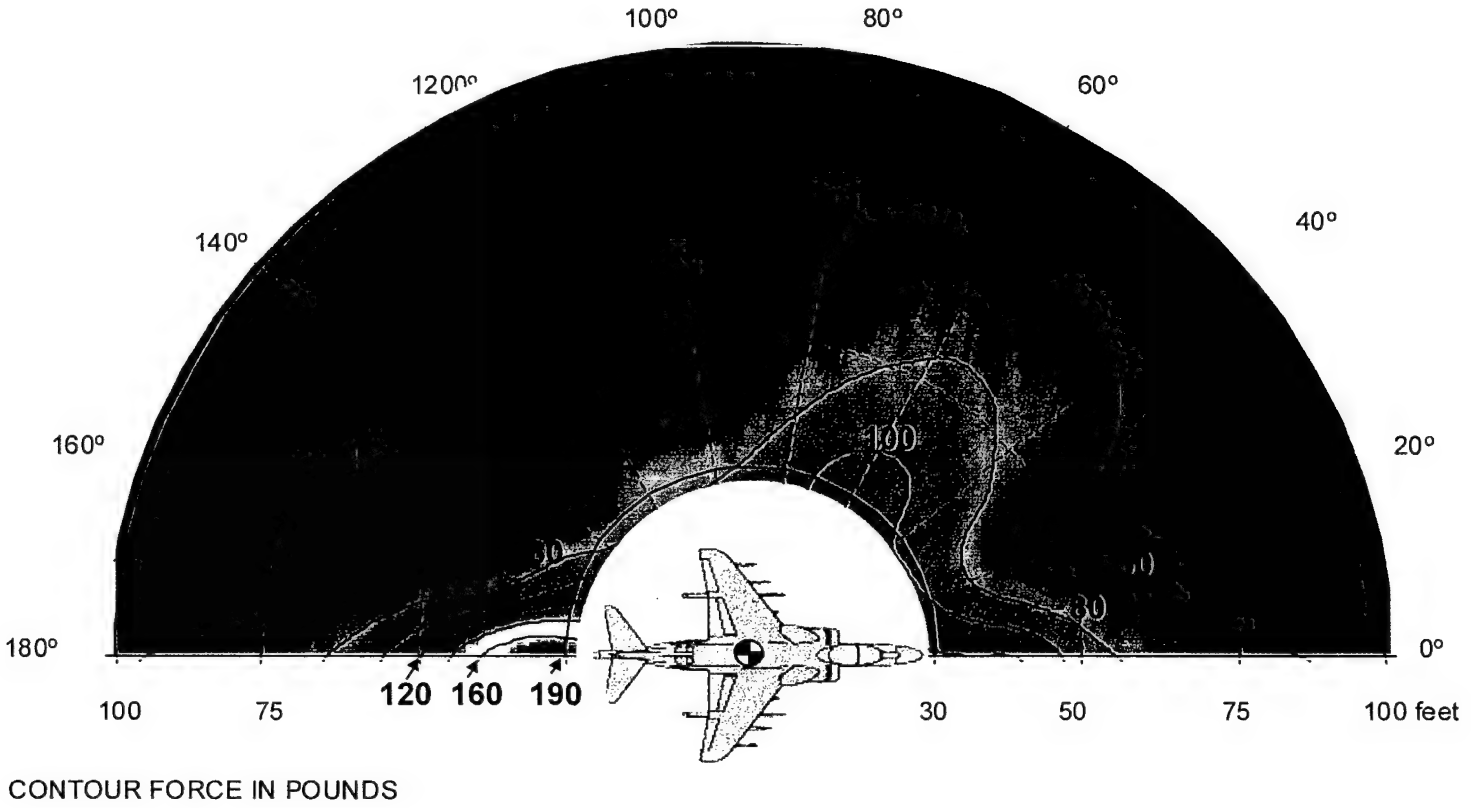

Figure 30: AV-8B Peak Aerodynamic Drag Force Contour during a 50 ft-AGL Hover

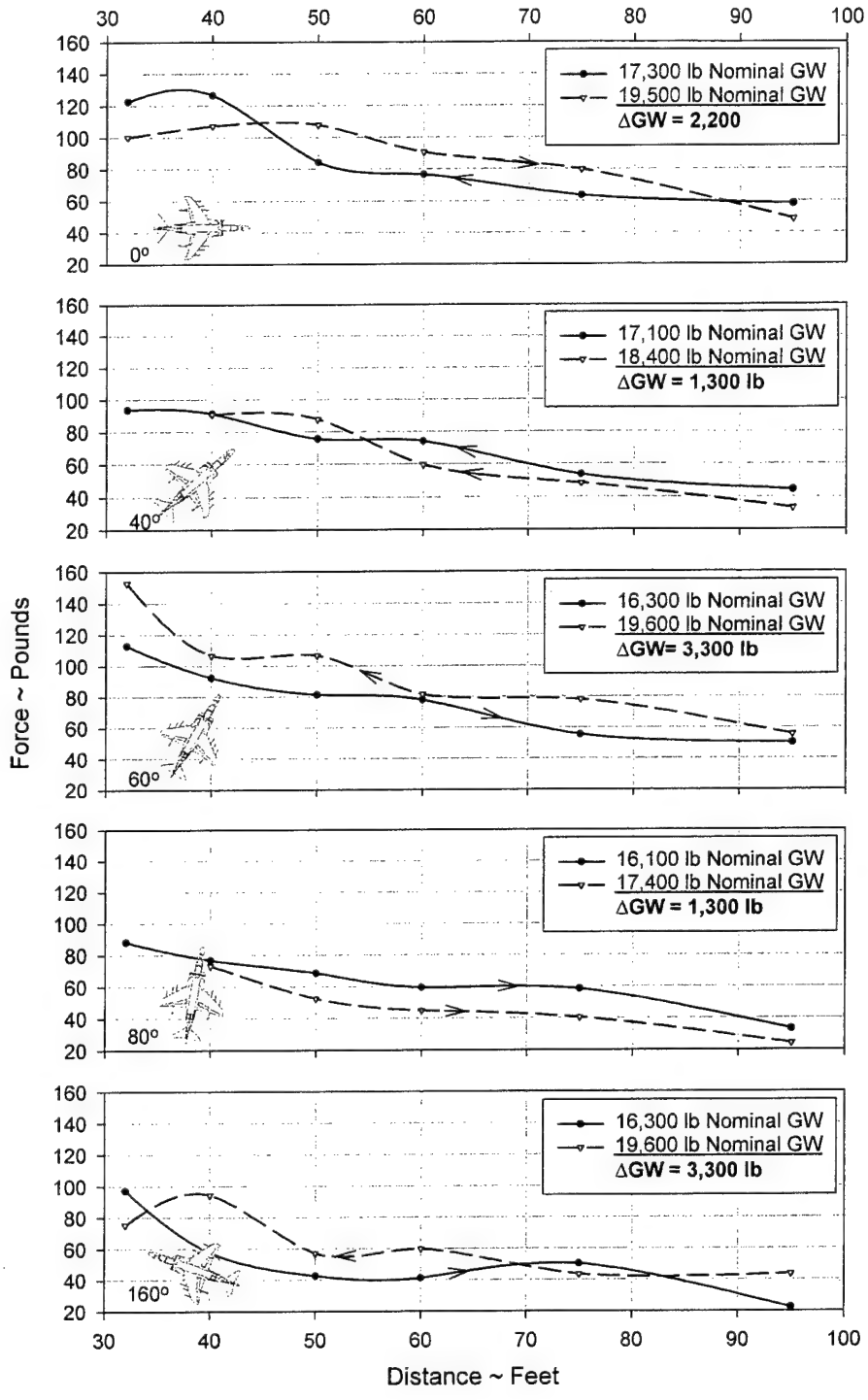

Figure 31: Varied Aircraft GW Effects on AV-8B Outwash Force Levels (Arrows direct fuel burn decrease with respect to distances, fuel burn was approximately 400 lb per complete azimuth, all data presented for a 50 ft-AGL hover)

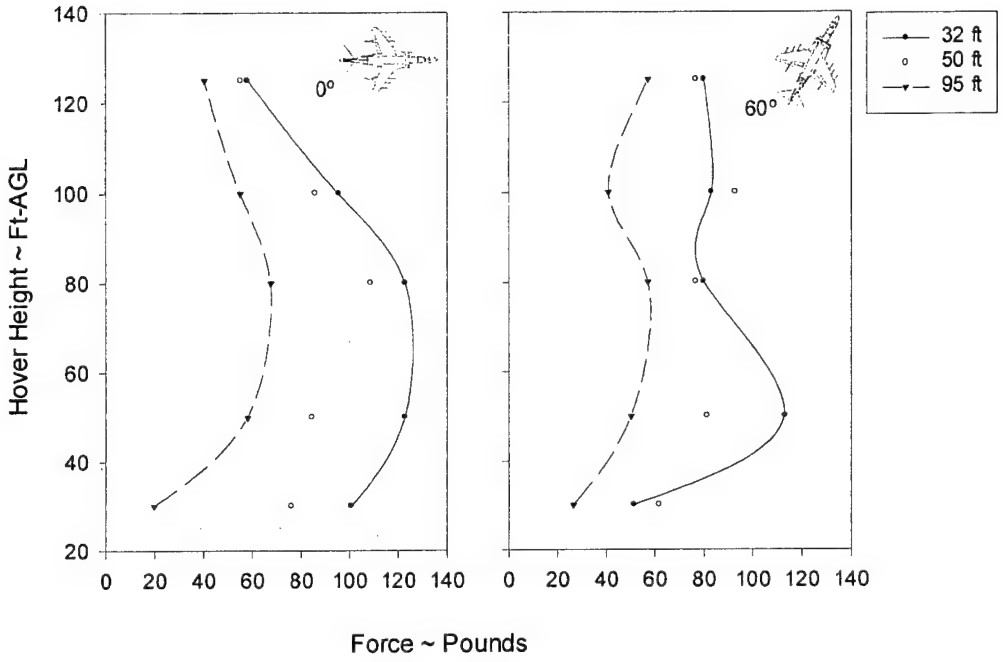

Figure 32: Varied Aircraft Hover Height Effects on AV-8B Outwash Force Levels on the 0 and 60 deg Test Azimuths (Measured 32, 50, and 95 ft from aircraft center)

COMPARISON TO OTHER AIRCRAFT

28. A comparison of aerodynamic forces between the AV-8B and other Navy aircraft are presented in figure 33. Due to outwash sensitivity to azimuth, AV-8B and V-22 forces are presented with the upper (AV-8B @ 180 deg, V-22 @ 0 deg) and lower (AV-8B @ 140 deg, V-22 @ 270 deg) force boundaries. The flow fields of the CH-53E and the H-60 are relatively independent on azimuth (except for very small changes due to the tail-rotor influence), and are represented only on one azimuth. Figure 33 shows the AV-8B outwash force levels significantly exceed that of any other naval aircraft. However, these high levels quickly diminish with increased distance to a much safer level. Force levels beyond 60 ft are considerably lower than CH-53E and V-22 levels. On the 140 deg azimuth, AV-8B outwash force levels are relatively low and comparable to H-60 winds. This data concludes that the AV-8B outwash will produce winds stronger than any rotary wing aircraft in the Navy inventory however they quickly diminish to very "workable" levels outside of the 50-ft hazard circle. This conclusion is subject to change as a dramatic transformation of outwash force magnitudes may occur due to elevated local ambient winds or shipboard wind-over-deck conditions.

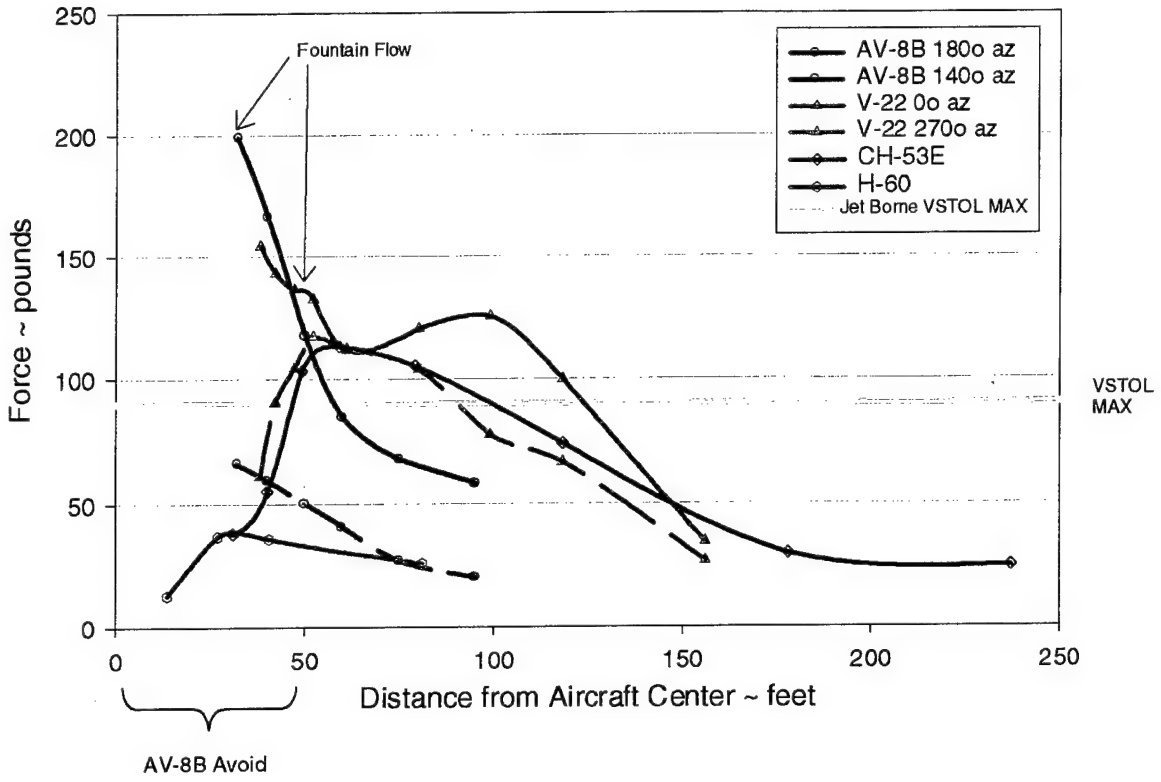

Figure 33: Aerodynamic Force Comparison between the AV-8B and Other Navy Aircraft (All test data presented at operational hover heights with the AV-8B at 50 ft-AGL and rotary wing aircraft at 20 ft-AGL, all aircraft tested at operationally representative GW's)

CONCLUSIONS

29. The AV-8B outwash signal is very similar, temporally and spectrally, to that of signals acquired from helicopter downwash tests, in that the peak levels may be 50% higher than the mean and majority of the energy resides at frequencies below 5 Hz (paragraph 13).

30. Flow angularity admittedly causes measurement errors but occurred for very small times and appeared at the higher (lower velocity) measurement locations where wall jet flow becomes entrained with the local environment (paragraph 14).

31. The total temperature probes were relatively insensitive to flow angles due to their slower time response, thus alleviating angularity errors in flow field temperatures (paragraph 16).

32. Flow emanates radially away from hover center and closely aligns with the test azimuth (paragraph 17).

33. Flow in the for/aft stagnation region contained velocities near the ground that are lower than that found in nonstagnation regions; however, the existence of moderately high velocity flow at heights between 30 and 60 in.-AGL produce a very large amount of aerodynamic drag force (paragraph 19).

34. The outwash flow field on the 60 deg azimuth is moderately sensitive to changes in hover height, at least within the scope of these tests (paragraph 20).

35. As could be expected from the difference between the aft hot nozzles and the front cool nozzles, temperatures in the fwd/aft stagnation region were slightly warmer in the aft and slightly cooler in the front (paragraph 22).

36. The temperature field appeared to be moderately insensitive to hover height with the only noticeable change occurring at the 125 ft-AGL hover height (paragraph 23).

37. Within the scope of these tests and even at the hottest areas around aircraft, the AV-8B outwash flow should not cause any amount of thermal pain to personnel working close to the aircraft. However, thermal pain is not a sole indicator of a thermal problem. Ground or deck personnel exposed to continuous flight operations (launch/recovery cycles) in these elevated temperature fields may increase their susceptibility to heat exhaustion or heat stroke (paragraph 24).

38. Personnel engulfed in an outwash flow field experience postural instability by both being unable to withstand the high aerodynamic forces and also by being unable to properly react to high magnitude flow oscillations (paragraph 25).

39. The largest drag force levels are aligned off the 0, 60, and 180 deg stagnation lines with the highest force in excess of 190 lb off the 180 deg azimuth (paragraph 26).

THIS PAGE INTENTIONALLY LEFT BLANK

RECOMMENDATIONS

40. Recommend the data used in this report not be used as a strict directive for development of ground personnel operational procedures. It should be used as a general guideline as increased ambient wind or wind-over-deck levels may significantly change the flow field patterns, resulting in localized high aerodynamic force regions. Flow forces may be somewhat higher during conventional and short takeoff operations. Future outwash testing should consider the use of an accurate method to determine aircraft position, as data may be very sensitive to actual aircraft location. A thorough analysis should be performed to determine the reduction of physiological performance of personnel working in these elevated temperature fields. Future tests should include a considerable effort to expose various test subjects to the flow field as to qualitatively validate the accuracy of the numerical representation of drag forces. Future instrumentation cart movement should allow circumferential tracking to allow accurate data capture of the stagnation regions. Test data systems should allow modification to capture an entire takeoff-hover-landing cycle to provide an increased insight on outwash transitional effects. An error analysis should be performed to quantify the affect flow angularity has on the accuracy of the measuring system. Personnel of all weight percentiles should work near jet-borne V/STOL/STOVL aircraft at reduced outwash levels than that of large rotary wing aircraft. The Crew Systems, AEH laboratory, recommends that the **maximum allowable outwash level for personnel** shall be no greater than **90 lb peak force**.

THIS PAGE INTENTIONALLY LEFT BLANK

REFERENCES

1. AV-8B External Environment Survey Phase 0 Data Release, Joint Strike Fighter Program Office, of Oct 1997.

2. AV-8B External Environment Survey Phase 1 Data Release, Joint Strike Fighter Program Office, of Apr 1999.

3. NATOPS Flight Manual, Navy Model AV-8B/TAV-8B 161573 and Up Aircraft, A1-AV8BB-NFM-000, of 1 Aug 1994.

4. AV-8B VTOL External Environment Survey-Overview, International Power Lift Conference, The Royal Aeronautical Society, of 2 Sep 1998.

5. Theoretical Derivation and Calibration Technique of a Hemispherical-Tipped Five Hole Probe, NASA Technical Memorandum 4047, of 1988.

6. NAVAIRTESTCEN Technical Report No. SY-89R-78, CH-53E Downwash Evaluation, of 1 Aug 1998.

7. Models for Aircrew Safety Assessment: Uses, Limitations, and Requirements, NATO RTO Proceeding 20, of Aug 1999.

8. NAVAIRWARCENACDIV Patuxent River Report of Test Results No. NAWCADPAX--99-87-RTR, Shipboard V-22 Rotor Downwash Survey, of Sep 1999.

THIS PAGE INTENTIONALLY LEFT BLANK

APPENDIX A
PHASE OF TEST METHODS

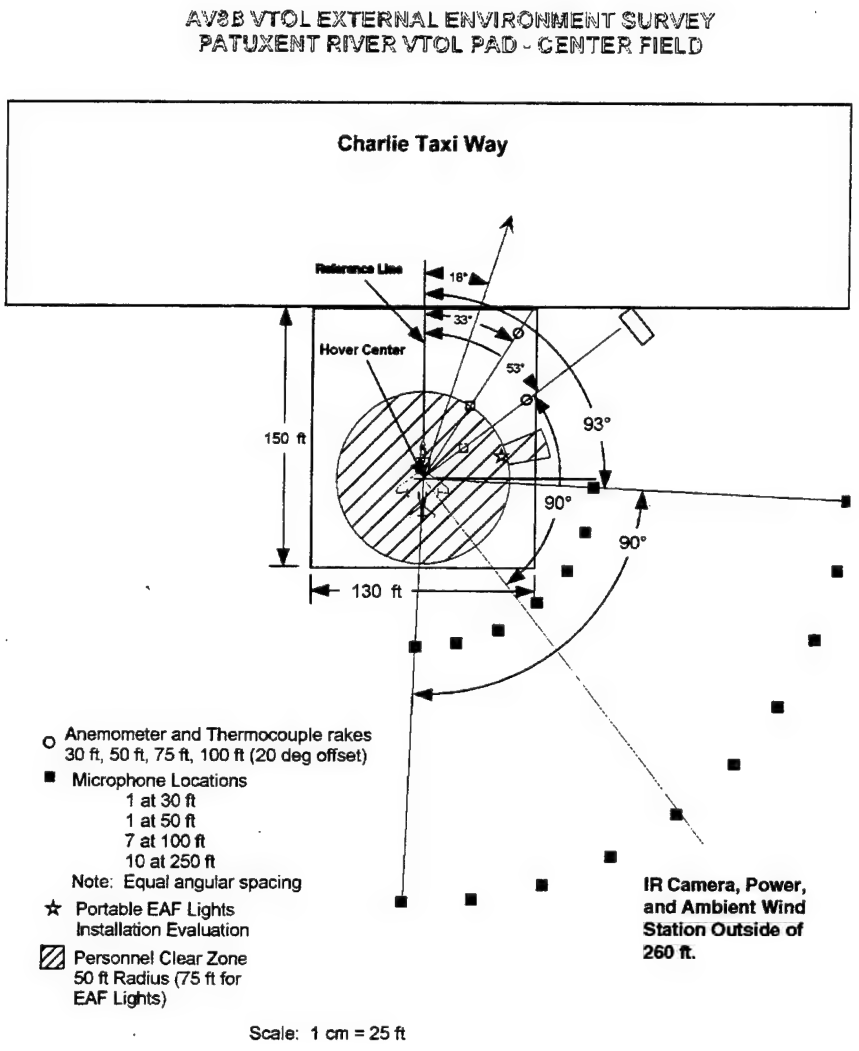

Figure A-1: AV-8B External Environment Survey Phase 0 Test Layout

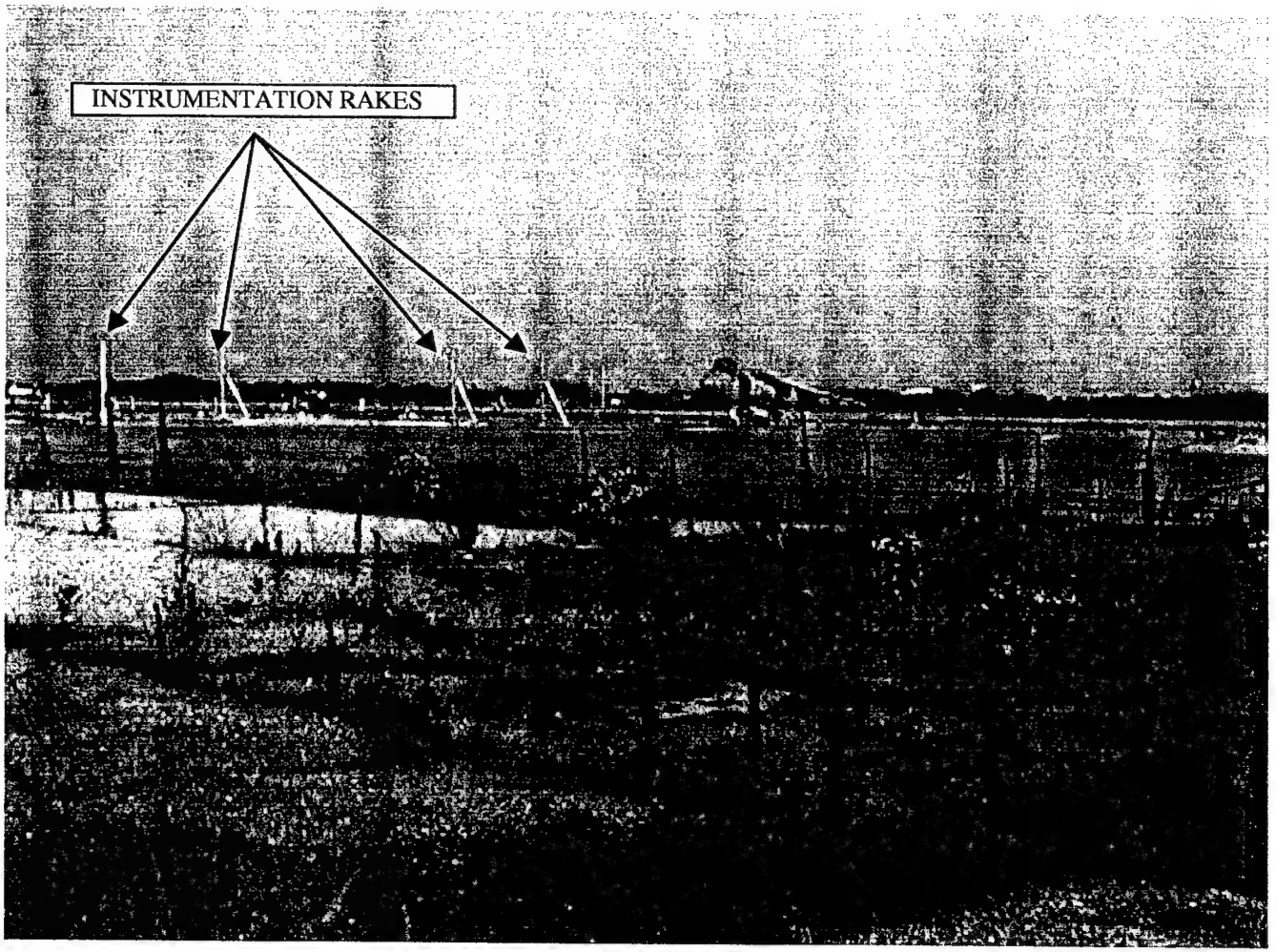

Figure A-2: Phase 0 Instrumentation Equipment

Angle Rake - Three angle rakes were used to measure the flow field velocities at the 30, 50, and 75 ft distances. The rake was composed of a combination of total, three-hole total and static pressure probes. A list of probe locations is shown in table A-1. The flow field dynamic pressure and hence velocity was obtained by the difference measured between total and static pressure probes. The three-hole total pressure probe was comprised of three total pressure probes oriented in a manner to resolve two vertical plane velocity components. The angle rake base plates were fastened to the interface plate to allow for easy removal at the end of a test day. The interface plate was fastened to the AM-2 mat via 1/4 in.-20 jacknuts supplied by NAWC Lakehurst. The angle rake was designed for past NASA Ames testing and its configuration and geometry was not specifically designed for this current test.

Table A-1: Instrumentation Pole Layout

Pole Distance (ft)	Measuring Height (in.-AGL)	Measuring Pressure	Pole Distance (ft)	Measuring Height (in.-AGL)	Measuring Pressure
30, 50, 75	120	3-hole [TC](1)	100	120	3-hole [TC]
	108	static		108	static
	96	total		96	total [TC]
	84	total		72	3-hole [TC]
	72	3-hole [TC]		48	total [TC]
	60	total		36	static
	52	3-hole		24	3-hole [TC]
	48	static			
	44	total [TC]			
	36	3-hole			
	28	total			
	24	total [TC]			
	20	total			
	16	3-hole [TC]			
	12	static			
	12	total [TC]			
	9	total [TC]			
	6	total [TC]			
	3	total [TC]			

NOTE: (1) TC = thermocouple location.

Long Rake - One long rake was used to measure the flow field velocities at the 100 ft distance. The rake was composed of a combination of total, three-hole total, and static pressure probes. The long rake base plates were fastened to the interface plate to allow for easy removal at the end of a test day. The interface plate was fastened to the concrete adjacent to the AM-2 mat via 3/8 in. lag screw system. The long rake was designed for past NASA Ames testing and its configuration and geometry was not specifically designed for this current test.

Pressure lines - Pressure lines transferred pressure readings from the probes to the probe data system. At each pole located at the 30, 50, and 75 ft location, 1/4 in. OD Teflon (high temperature) pressure lines were attached to the individual pressure probes (totals and statics). Pressure line bundles ran from the rake bases to transfer pressure data from the probe to the data system. These bundles were additionally protected from high temperatures by being inside of one of six 2.5 in. OD aluminum conduits running side by side to a temperature safe region, approximately 80 ft from hover site center. At a temperature safe location, the conduit terminated and the pressure line material changed (via Swagelok fittings) from Teflon to a standard vinyl. The 100 ft pole was equipped with standard vinyl pressure line only due to its location in a lower temperate region. All vinyl pressure lines terminated at the pressure scanning module located in the data van.

Pressure Transducers - Two types of pressure transducers were used in this evaluation:

a. Scanning Modules - A combination of 16, 32, and 48 multiplexing channel modules were used to scan all probes on the 3 angle rakes and the long rake for a total of 100 channels. The modules were capable of measuring wind speeds to 210 kt with a 1/2% overall accuracy. The scanning modules were controlled, receive power, and acquire data with the scanning module data system. The scanning modules were located in the data van.

b. Responsive Pressure Sensor - The responsive pressure sensors were used to measure the transitional characteristics of the flow field. For the angle rake, these sensors were tapped off the 12 and 48 in. probe's pressure lines, at a distance no greater than 6 ft from the probe (to prevent unwanted pneumatic damping). For the long rake, these sensors were tapped off the 24 in. and 48 in. probes pressure lines at a distance no greater than 6 ft from the probe. The responsive pressure sensors were capable of measuring winds to 210 kt with a 1/2% accuracy. They can operate continuously in 260°F temperature environment, and requires a 5 VDC excitation voltage. The sensor was mounted approximately 76 in. AGL to avoid the high temperature flow region. Sensor power was located in the data van.

Thermocouples - Exhaust gas temperatures were measured with 20 gauge, type J thermocouples, capable of measuring to 900°F with an accuracy of ±4°F or ±0.75% (whichever is greater). The thermocouple jacket was manufactured from Teflon to resist temperatures in excess of 400°F and provide a waterproof coating. The test required a quantity of 40 thermocouples at various lengths up to 140 ft.

Data Systems - Three data systems were used to collect steady state velocity, dynamic velocity, and temperature data:

a. Pressure Scanning Modules Data System - The pressure scanning modules data system was used to collect steady state velocity measurements from the 100 pressure probe lines. The scanning module data system consisted of a personal computer, scanner interface, vacuum pump, and nitrogen bottles. The computer controlled the scanning modules and performed data acquisition while the scanner interface supplied power and

provided signal conditioning to individual modules. The vacuum pump and nitrogen bottle allowed line purging and system calibration. Module data were sampled at 20 Hz for a maximum of 20 sec then time averaged to reflect steady state velocities. Data were stored on hard disk and a redundant file copied to floppy disk immediately after the scheduled event. Computer time was hand changed to reflect IRIG time (Patuxent River Range broadcasted) prior to aircraft arrival to the AM-2 pad. The pressure scanning module system was located in the data van.

b. Dynamic Measurement Data System - The dynamic measurement data system was used to collect transitional data received from the responsive pressure sensors and the directional sensors. This computer system was equipped with a input/output card allowing 32 channel analog voltage input. Data were sampled at 100 Hz, stored on hard disk, and a redundant file copied to a ZIP drive immediately after the scheduled event. Computer time was hand changed to reflect IRIG time (Patuxent River Range broadcasted) prior to aircraft arrival to the AM-2 pad. The dynamic measurement data system was located in the data van.

c. Temperature Measuring System - The temperature measuring system was used to collect thermocouple data. Thermocouple signals were conditioned and digitized with the TempScan/1100A manufactured by IoTech, Inc. The unit was a high-speed, compact instrument system capable of measuring 196 thermocouple inputs at a $\pm 0.9^{\circ}F$ accuracy. The system connected and transferred data to a personal computer through a RS-232/422 interface. Redundant data were stored on floppy disk immediately after the scheduled event. Computer time was hand changed to reflect IRIG time (Patuxent River Range broadcast) prior to aircraft arrival to the AM-2 pad. The temperature measuring system was located in the data van.

Ambient Wind System - A cup and vane anemometer, associated signal conditioners, and analog readout was used to monitor ambient wind conditions. The wind system had a maximum range of 50 kt with an accuracy of ± 1 kt. Data were hand tabulated with local Patuxent River time, wind speed, and wind direction at the beginning and end of each scheduled event. The ambient wind system was colocated with the infrared camera (and power generator) at a distance greater than 300 from hover center.

APPENDIX B
VISUAL CUES AND HOVER STATION KEEPING

Pilot Visual Cues and Hover Station Keeping Technique. Two pairs of brightly colored 12 ft vertical visual cue poles (VCP's) for each test azimuth were stationed nominally between 125 ft and 225 ft, relative to the hover center, to provide visual cues to the pilot for position keeping. The pole position varied with the target hover height. The pole pairs were positioned at ±35 deg relative to the design eye position. However, the radial distance, angular separation, and dimensions of the poles varied to optimize the cueing. The minimum radius of the inner pole will be 100 ft. The pilot used information provided in the head-up display to capture and maintain altitude and heading.

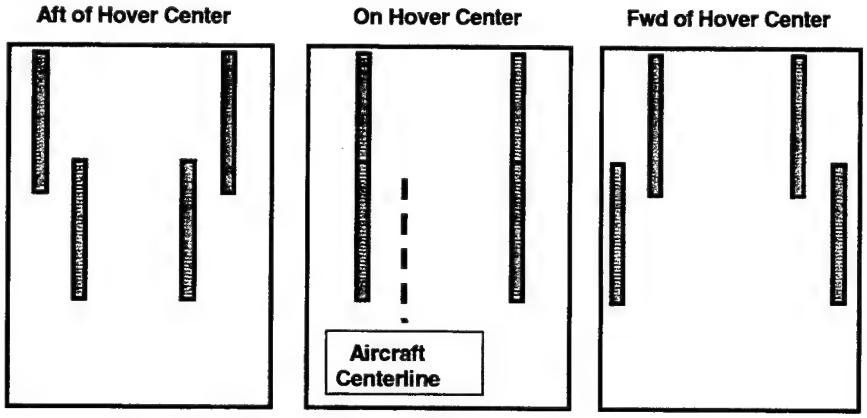

Figure B-1: Pilot View of Alignment Poles

THIS PAGE INTENTIONALLY LEFT BLANK

APPENDIX C
PROBE CONSTANTS AND CALIBRATION

Table C-1: Transducer Ranges

	1 (p_{total})	2 (p_{static})	3 (p_{left})	4 (p_{right})	5 (p_{up})	6 (p_{down})
Barometer	16-32 in. HgA					
120	±10 in. H_2OD	±10 in. H_2OD	±10 in. H_2OD	±10 in. H_2OD	±10 in. H_2OD	±10 in. H_2OD
96	±10 in. H_2OD	±10 in. H_2OD				
84	±10 in. H_2OD	±10 in. H_2OD				
72	±10 in. H_2OD	±10 in. H_2OD	±10 in. H_2OD	±10 in. H_2OD	±10 in. H_2OD	±10 in. H_2OD
60	±10 in. H_2OD	±10 in. H_2OD				
52	±10 in. H_2OD	±10 in. H_2OD				
44	±1 PSID	±10 in. H_2OD	±1 PSID	±1 PSID	±1 PSID	±1 PSID
36	±1 PSID	±10 in. H_2OD				
28	±1 PSID	±10 in. H_2OD				
24	±1 PSID	±10 in. H_2OD	±1 PSID	±1 PSID	±1 PSID	±1 PSID
20	±1 PSID	±10 in. H_2OD				
16	±1 PSID	±10 in. H_2OD				
12	±1 PSID	±10 in. H_2OD	±1 PSID	±1 PSID	±1 PSID	±1 PSID
9	±1 PSID	±10 in. H_2OD				
6	±1 PSID	±10 in. H_2OD				
3	±1 PSID	±10 in. H_2OD	±1 PSID	±1 PSID	±1 PSID	±1 PSID

Table C-2: Kjelgaard Subroutine for Five-Tube Velocity and Angularity Calculation

Listing of Five-Hole Probe Subroutine

This subroutine is used to convert the pressures measured by the yaw-pitch probe into flow velocity and angularity.

```
      SUBROUTINE FIVE-HOLE (PALPHA,BETATHETA,PHI,Q,PS,VEL-PREV)
C
C     FIVE-HOLE CONVERTS MEASURED PRESSURES INTO FLOW ANGLES
C     AND VELOCITY DATA USING THE CALIBRATION EQUATIONS DERIVED
C     IN APPENDIX A OF REFERENCE 2
C                        SUBROUTINE WRITTEN BY KJELGAARD IN AUGUST 1986
C   DESCRIPTION OF VARIABLES
C   INPUT
C     P - ARRAY CONTAINING PRESSURES MEASURED BY 5-HOLE PROBE
          C                    P(L) CONTAINS PRESSURE AT PORT I
          C                    P(2) CONTAINS PRESSURE AT PORT 2, ETC.
          C     OUTPUT
C     ALPHA - PITCH ANGLE MEASURED BY PROBE
C     BETA - YAW ANGLE MEASURED BY PROBE
C     THETA - TOTAL FLOW ANGLE MEASURED FROM PORT I TO STAGNATION
C        POINT
C     PHI - FLOW ROLL ANGLE MEASURED FROM LOWER ALPHA PORT TO
C     STAGNATION POINT
C     Q DYNAMIC PRESSURE OF THE FLOW AT THE PROBE TIP
C     PS STATIC PRESSURE MEASURED AT THE PROBE TIP
```

```
C       VEL-PREV - VELOCITY USED TO CALCULATE PROBE CONSTANTS
        REAL P(*)
        REAL ALPH(2),BET(2),THET(2),QT(2),PST(2.)
        REAL A(2),THETAO(2),PHIO(2),B(2),C(2),D(2),E(2),F(2),G(2)
        EXTERNAL POLY
        DPA=P(6)-P(5)
        DPB=P(3)-P(4)
        QP=P(I)-0.25*(P(3)+P(4)+P(5)+P(6))
        AI=SQRT(DPA**2+DPB**2)/QP
C-------------------------------------------------------------
C       PROBE CONSTANTS
C-------------------------------------------------------------
        A(1)=POLY(VEL_PREV,A(1,1),A(1,2),A(1,3),A(1,4))
        A(2)= POLY(VEL_PREV, A(2,1),A(2,2),A(2,3),A(2,4))
        THETA0(1)=POLY(VEL_PREV, THETA0 (2,1), THETA0 (2,2), THETA0 (2,3), THETA0
             (2,4))
        THETA0(2)=POLY(VEL_PREV, THETA0 (2,1), THETA0 (2,2), THETA0 (2,3), THETA0
             (2,4))
        B(1)=POLY(VEL_PREV,B(1,1),B(1,2),B(1,3),B(1,4))
        B(2)=POLY(VEL_PREV, B(2,1),B(2,2),B(2,3),B(2,4))
        PHIO(1)=POLY(VEL-PREV, PHIO (1,1), PHIO (1,2), PHIO (1,3), PHIO (1,4))
        PHIO(2)=POLY(VEL_PREV, PHIO (2,1), PHIO (2,2), PHIO (2,3), PHIO (2,4))
        C(1)=POLY(VEL-PREV,C(1,1),C(1,2),C(1,3),C(1,4))
        C(2)=POLY(VEL-PREV, C(2,1),C(2,2),C(2,3),C(2,4))
        D(1)=POLY(VEL-PREV,D(1,1),D(1,2),D(1,3),D(1,4)
        D(2)=POLY(VEL-PREV, D(2,1),D(2,2),D(2,3),D(2,4))

C       ITERATIVELY SOLVE FOR THETA

C
        DO 1 I=1,2
             THET(I)=O.
             THSTEP=10.
        C
        C       CALCULATE PHI
        C

 IF (DPA.EQ. 0)  DPA=.00001
             PHIM=ATAND(B(I)*DPB/DPA)
             IF (DPA.LT. 0) PHIM=180.+PHIM
             IF (PHIM.LT. 0) PHIM=PHIM+360.
             PHIT=PHIM-PHIO(I)
             A2=1
             DO 2000 ILOOP=1,50
               IF (ILOOP.EQ.50) THEN
                  WRITE(6,'(" TOO MANY ITERATIONS IN CALB")')
                  THET(I)=.5*ACOSD(A(I)*SIND(2.*THETAO(I))/AI+ COSD(2.*THETAO(I)
                  GO TO 3170
               END IF

               THET(I)=THET(I) + THSTEP
               A3=COSD(2.*THET(I))-COSD(2.*THETAO(I))

               IF (A3.EQ.0.0) THEN
                 WRITE(6,'(" PROBLEM IN CALIB")')
                 WRITE(6,'(4F10.5)') THET(I),THSTEP
```

```
            A3=lE-5
           END IF

           A2=A1-A(I)*SIND(2.*THET(I))/A3

           IF (A2 LT. 0) THEN
             THET(I)=THET(I)-THSTEP
             THSTEP=THSTEP*.5
             GO TO 3160
           ENDIF

           IF (A2 LE. .02) GO TO 3170

3160       CONTINUE
2000       CONTINUE
3170       ALPH(I)=ATAND(TAND(THET(I))*COSD(PHIT))
           BET(I)=ASIND(SIND(THET(I))*SIND(PHIT))
           QT(I)=QP/(C(I)*(COSD(2.*THET(I))-COSD(2.*THETAO(I)))+
           D(I)*(COSD(THET(I))-COSD(THETAO(I))))
           PST(I)=P(I)-QT(I)*(E(I)*COSD(2.*THET(I))+F(I)*COSD(THET(I)) +G (I))

1          CONTINUE

C          USE PHI FOR WEIGHTING FUNCTION FOR COMBINATION OF ALPHA

C          AND BETA CONSTANTS AND COMBINE

           WGHT=COSD(PHI)**2
           WGHT1=1-WGHT
           BETA=BET(l)*WGHT+BET(2)*WGHT1
           ALPHA=ALPH(l)*WGHT+ALPH(2)*WGHT1
           Q=QT(l)*WGHT+QT(2)*WGHT1
           PS=PST(l)*WGHT+PST(2)*WGHT1

C          USE THESE TO CALCULATE THETA AND PHI

           THETA=ACOSD(COSD(ALPHA)*COSD(BETA))
           IF (ALPHA EQ. 0) THEN
               PHI=SIGN(90.,BETA)
           ELSE
               PHI=ATAND(TAND(BETA)/SIND(ALPHA))
           END IF

           IF (ALPHA.LT. 0) PHI= PHI+180.
           IF (PHI LT. 0) PHI= PHI+360.
           RETURN
           END

           FUNCTION POLY(V,A,B,C,D)
           POLY = A + B*V + C*V*V + D*V*V*V
           RETURN
           END
```

Table C-3: Kjelgaard Subroutine Coefficients

	1	2	3	4
A(1)	3.18	0	0	0
A(2)	3.18	0	0	0
theta0(1)	55.25	0	0	0
theta0(1)	55.25	0	0	0
B(1)	0.918954	0.006815	-0.000104057	0.0000003
B(2)	-0.29997	0.022575	-0.000232593	0.0000007
phiO(1)	-1.20772	0.011003	-3.34E-05	5.23E-08
phiO(1)	-27.4001	0.75327	-0.007374613	2.19E-05
C(1)	0.474348	-0.00096	0.00000688	-1.45E-08
C(2)	1.172382	-0.01898	0.000103476	-0.000000178
D(1)	0.8	0	0	0
D(2)	-1.60495	0.062603	-0.000345478	0.00000061
E(1)	0.55			
E(2)	0.5			
F(1)	3			
F(2)	3.333			
G(1)	-2.55			
G(2)	-2.823			

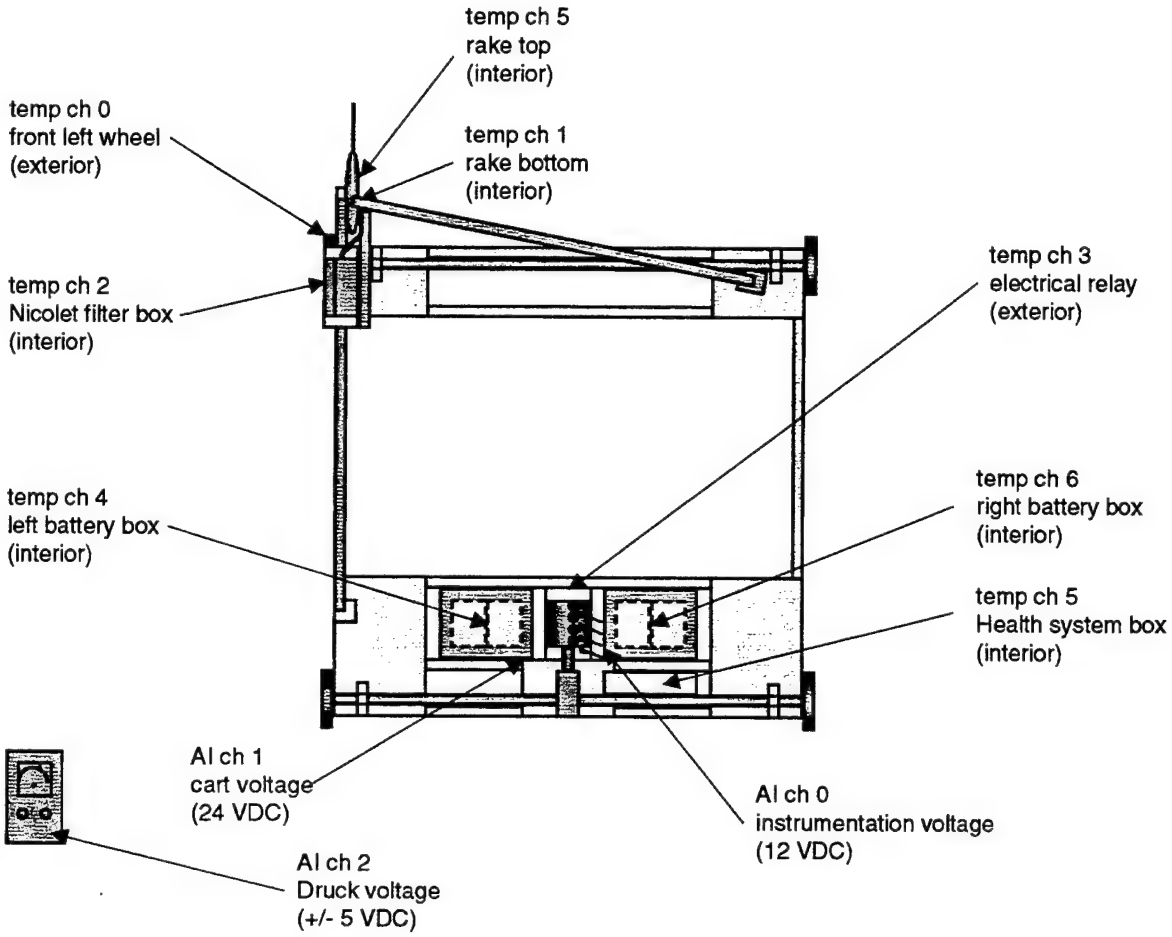

Figure C-1: Health System Parameters

THIS PAGE INTENTIONALLY LEFT BLANK

APPENDIX D
PHASE OF CONTOUR PLOTS

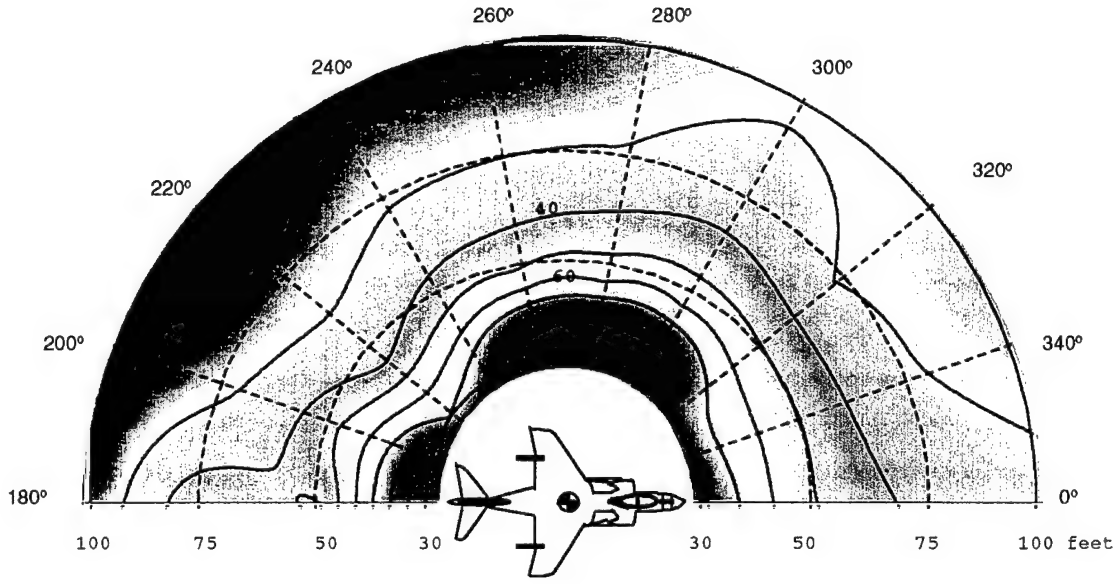

Figure D-1: 6 in.-AGL Mean Velocity Contour during a 50 ft-AGL Hover
(Phase 0 Results, Velocity Contours are in kt)

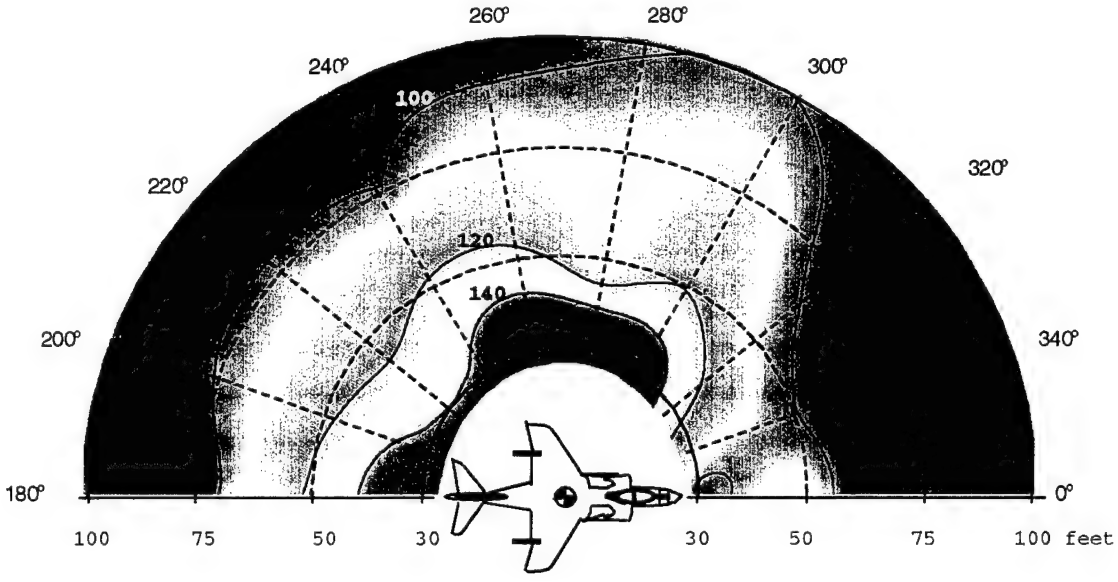

Figure D-2: 6 in.-AGL Mean Temperature Contour during a 50 ft-AGL Hover
(Phase 0 Results, Temperature Contours are in deg F)

THIS PAGE INTENTIONALLY LEFT BLANK

APPENDIX E
TEMPERATURE AND VELOCITY HEIGHT PROFILES

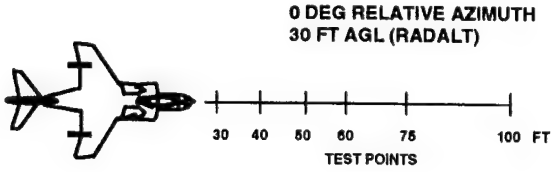

	Phase0 30/75 ft	Phase0 50/100 ft	Phase1 32 to 95 ft
Ambient Temperature (°F)	-	-	65
Winds (knots @ degrees)[1]	-	-	9@263
Aircraft Test Heading (degrees)[2]	-	-	20
Aircraft Gross Weight (lb)	-	-	18500

1. Relative to aircraft longitudinal centerline.
2. Relative to true north.

TOD 143410

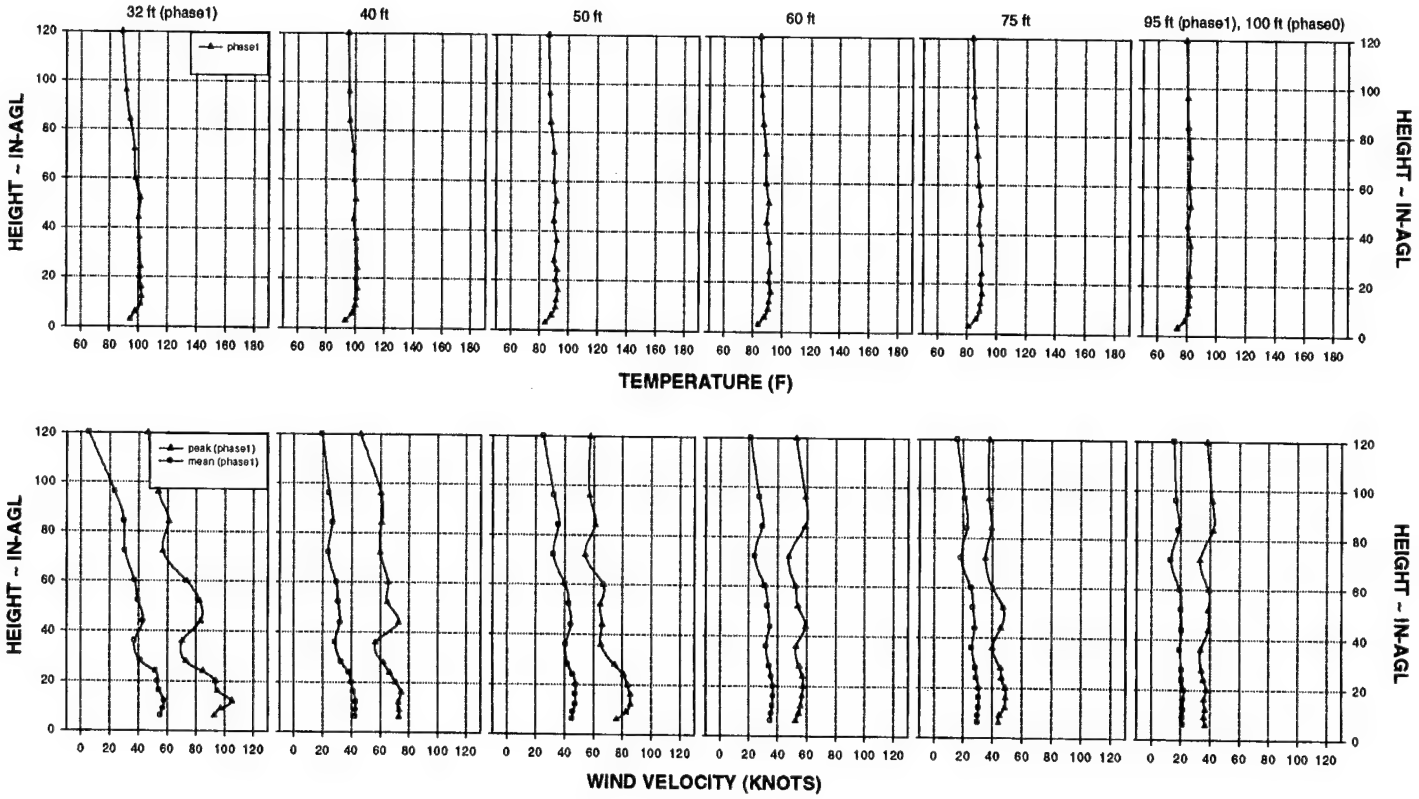

Figure E-1: Temperature and Velocity Field during a 30 ft-AGL Hover at the 0 deg Relative Test Azimuth

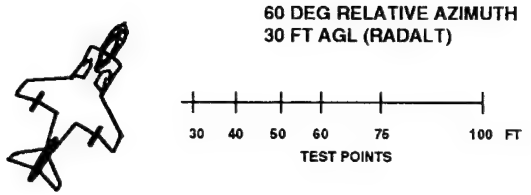

	Phase0 30/75 ft	Phase0 50/100 ft	Phase1 32 to 95 ft
Ambient Temperature (°F)	-	71	65
Winds (knots @ degrees)[1]	-	0	7@217
Aircraft Test Heading (degrees)[2]	-	76	020
Aircraft Gross Weight (lb)	-	16443	18000

1. Relative to aircraft longitudinal centerline.
2. Relative to true north.

TOD 144511

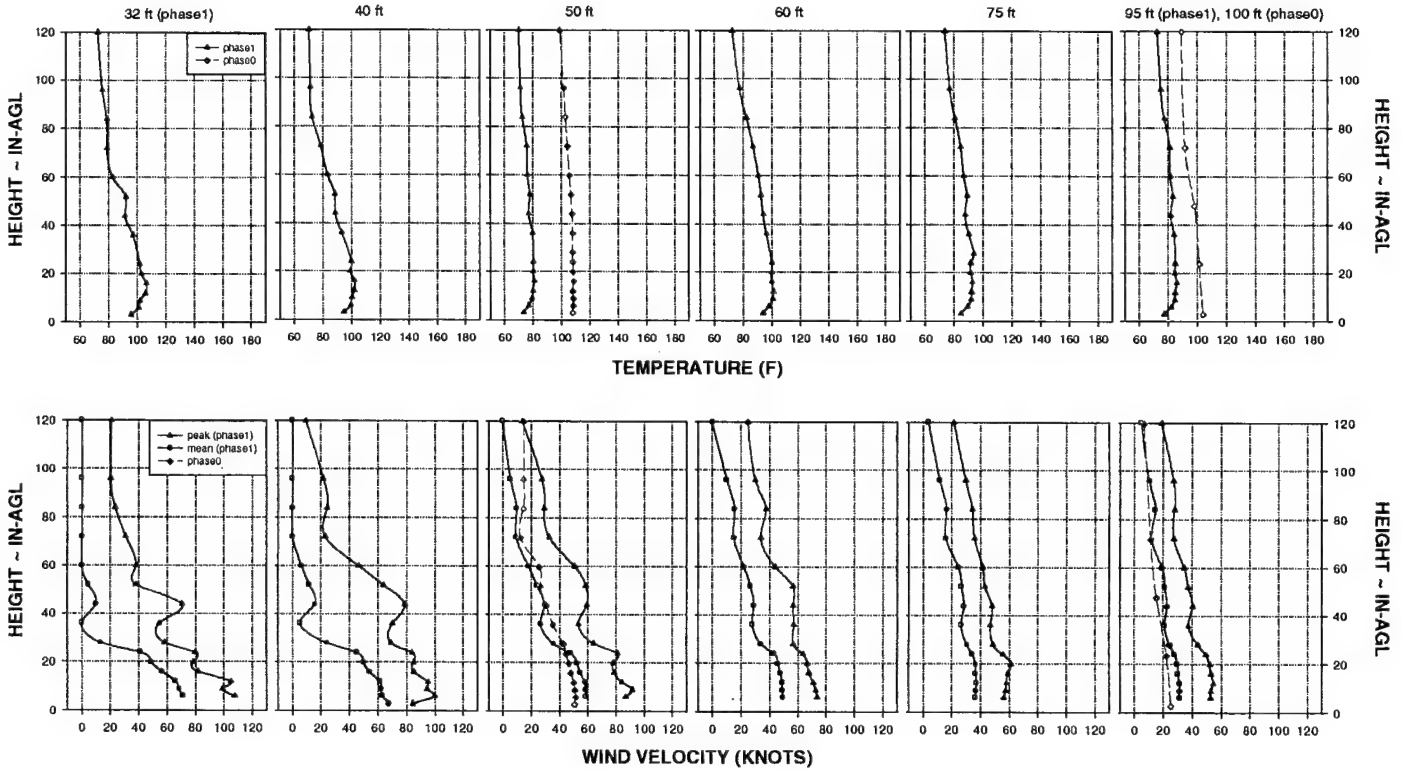

Figure E-2: Temperature and Velocity Field during a 30 ft-AGL Hover at the 60 deg Relative Test Azimuth

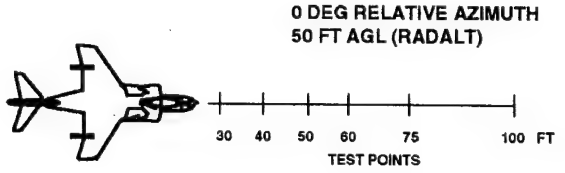

	Phase0 30/75 ft	Phase0 50/100 ft	Phase1 32 to 95 ft
Ambient Temperature (°F)	81	81	61
Winds (knots @ degrees)[1]	8@-170	3@-150	3@-248
Aircraft Test Heading (degrees)[2]	36	16	20
Aircraft Gross Weight (lb)	16723	16443	17300

1. Relative to aircraft longitudinal centerline.
2. Relative to true north.

TOD 131922

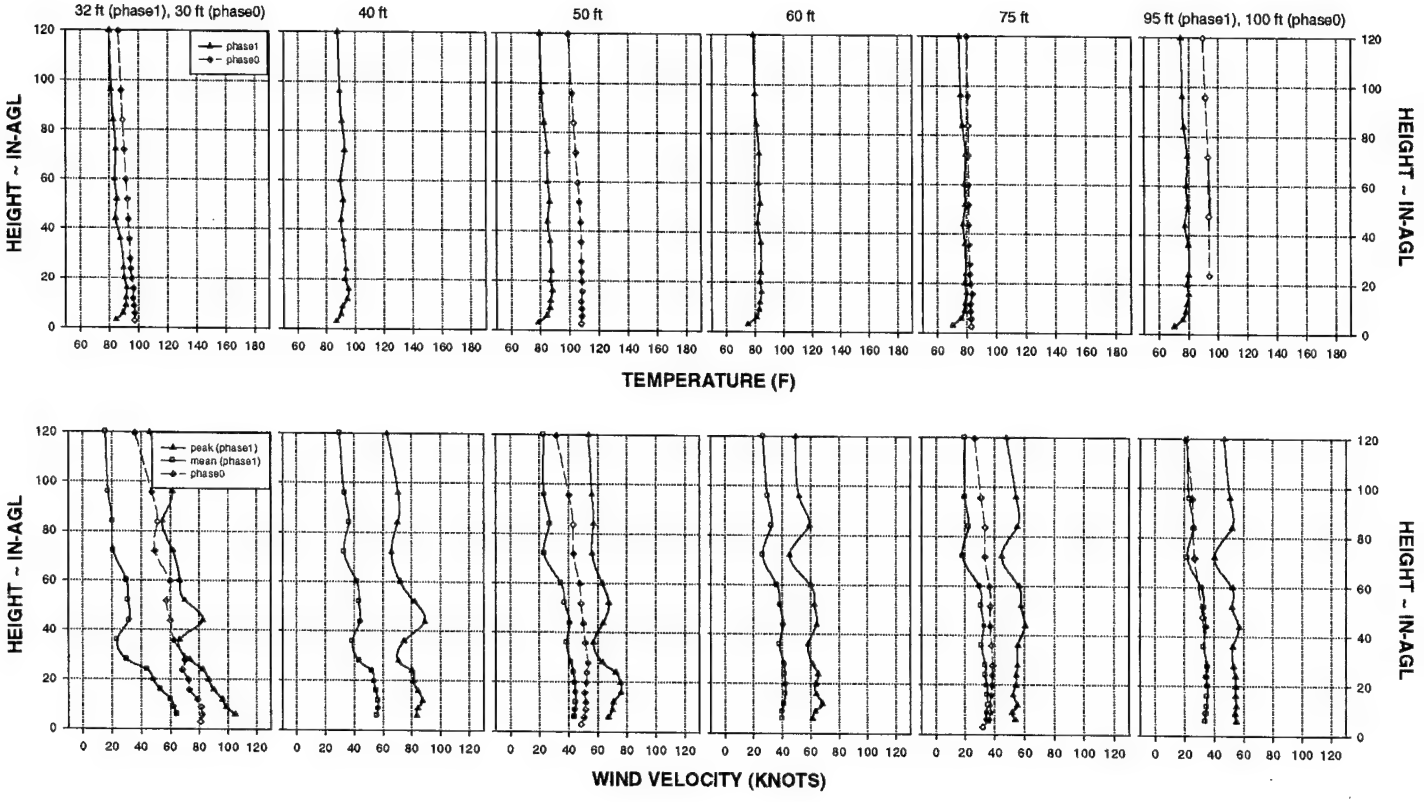

Figure E-3: Temperature and Velocity Field during a 50 ft-AGL Hover at the 0 deg Relative Test Azimuth (Lower Gross Weight)

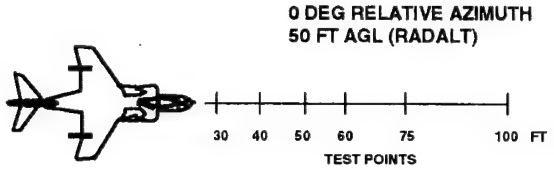

	Phase0 30/75 ft	Phase0 50/100 ft	Phase1 32 to 95 ft
Ambient Temperature (°F)	81	81	61
Winds (knots @ degrees)[1]	8@-170	3@-150	<5
Aircraft Test Heading (degrees)[2]	36	16	20
Aircraft Gross Weight (lb)	16723	16443	19500

1. Relative to aircraft longitudinal centerline.
2. Relative to true north.

TOD 134444

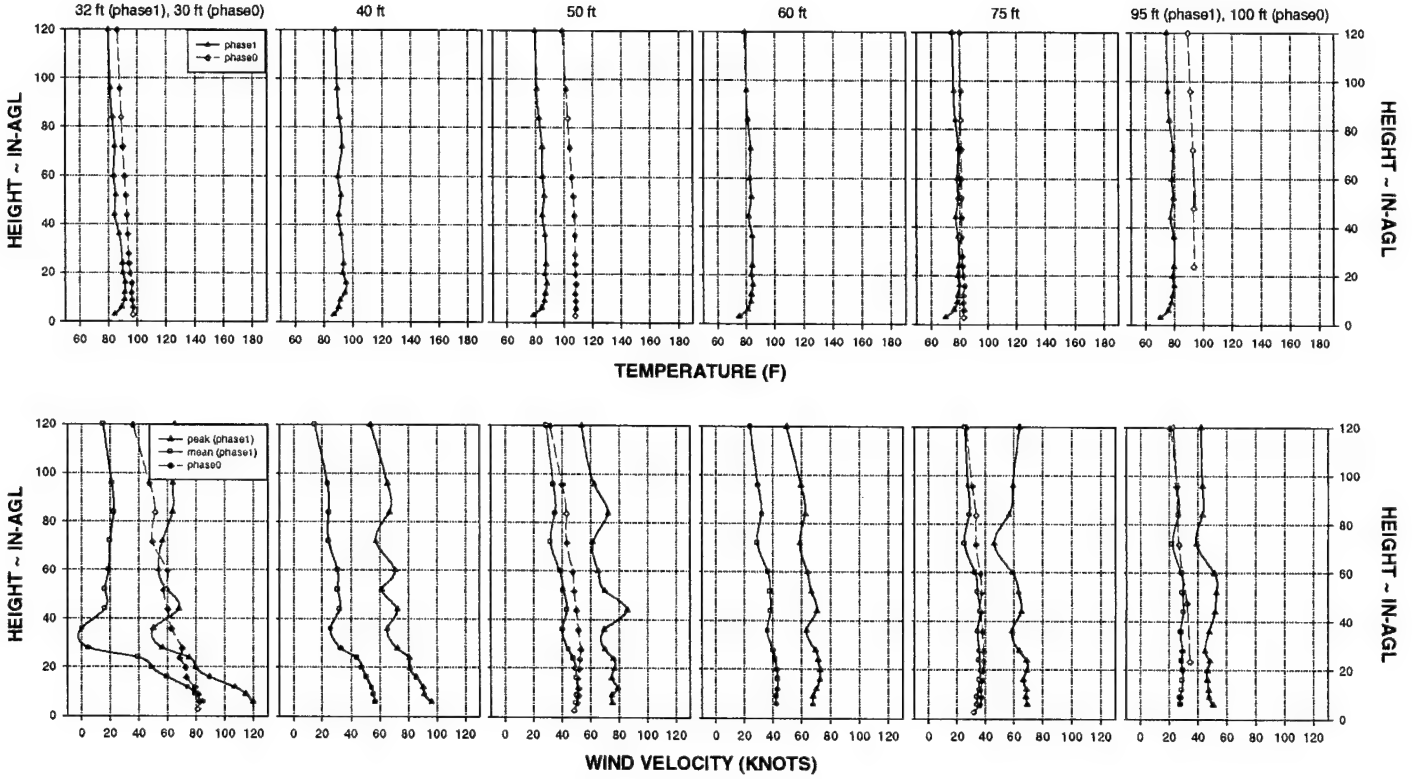

Figure E-4: Temperature and Velocity Field during a 50 ft-AGL Hover at the 0 deg Relative Test Azimuth (Higher Gross Weight)

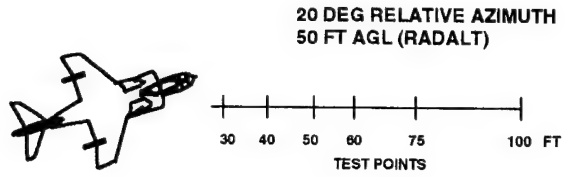

	Phase0 30/75 ft	Phase0 50/100 ft	Phase1 32 to 95 ft
Ambient Temperature (°F)	81	81	59
Winds (knots @ degrees)[1]	5@-150	5@-170	3@236
Aircraft Test Heading (degrees)[2]	56	36	40
Aircraft Gross Weight (lb)	17203	16723	18600

1. Relative to aircraft longitudinal centerline.
2. Relative to true north.

TOD 121337

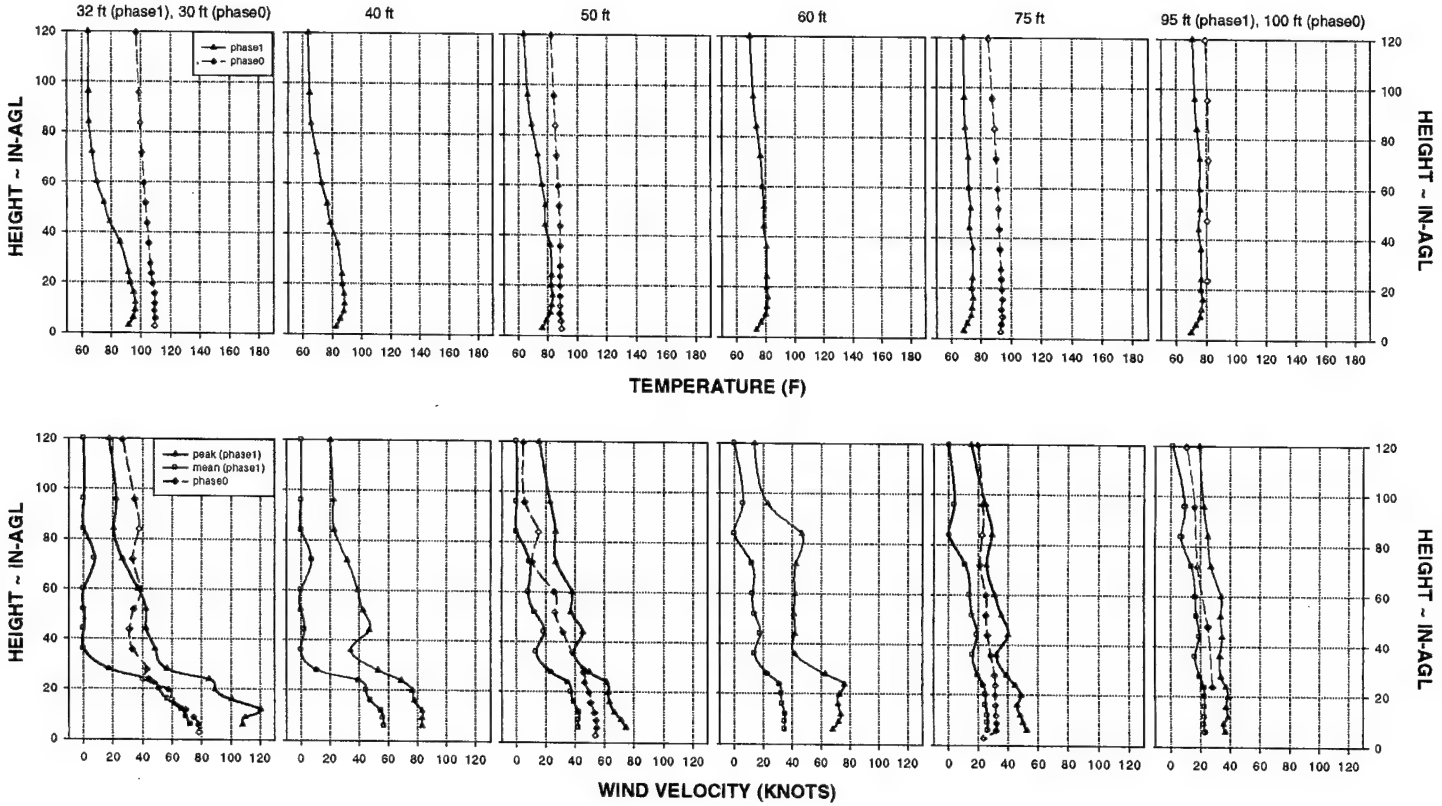

Figure E-5: Temperature and Velocity Field during a 50 ft-AGL Hover at the 20 deg Relative Test Azimuth

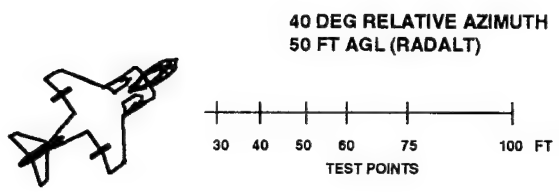

	Phase0 30/75 ft	Phase0 50/100 ft	Phase1 32 to 95 ft
Ambient Temperature (°F)	80	81	66
Winds (knots @ degrees)[1]	2@150	5@-150	4@267
Aircraft Test Heading (degrees)[2]	76	56	20
Aircraft Gross Weight (lb)	17443	17203	17200

1. Relative to aircraft longitudinal centerline.
2. Relative to true north.

TOD 145524

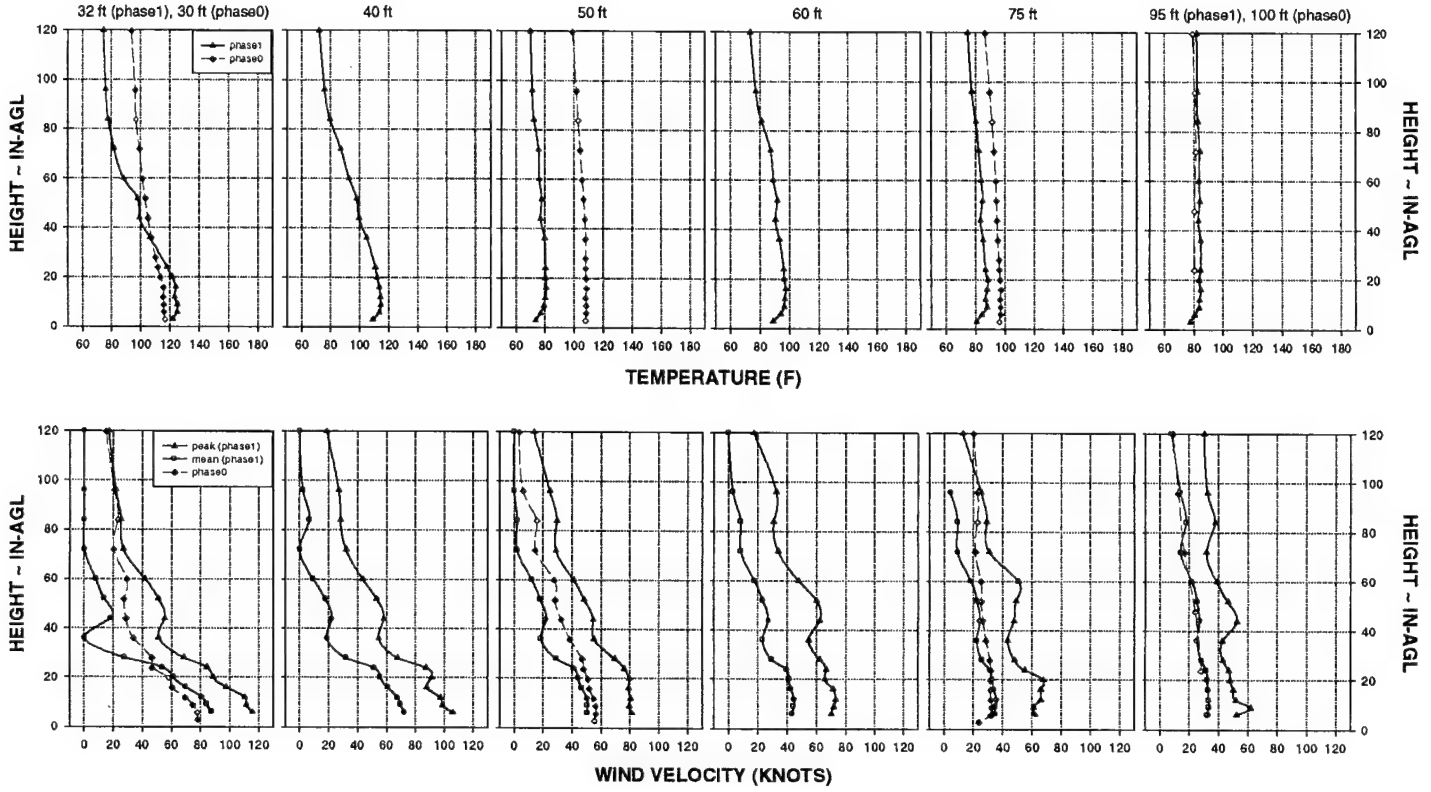

Figure E-6: Temperature and Velocity Field during a 50 ft-AGL Hover at the 40 deg Relative Test Azimuth (Lower Gross Weight)

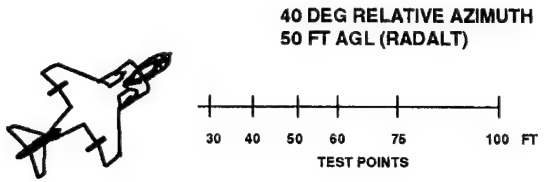

	Phase0 30/75 ft	Phase0 50/100 ft	Phase1 32 to 95 ft
Ambient Temperature (°F)	80	81	66
Winds (knots @ degrees)[1]	2@150	5@-150	<5
Aircraft Test Heading (degrees)[2]	76	56	20
Aircraft Gross Weight (lb)	17443	17203	18400

1. Relative to aircraft longitudinal centerline.
2. Relative to true north.

TOD 122317

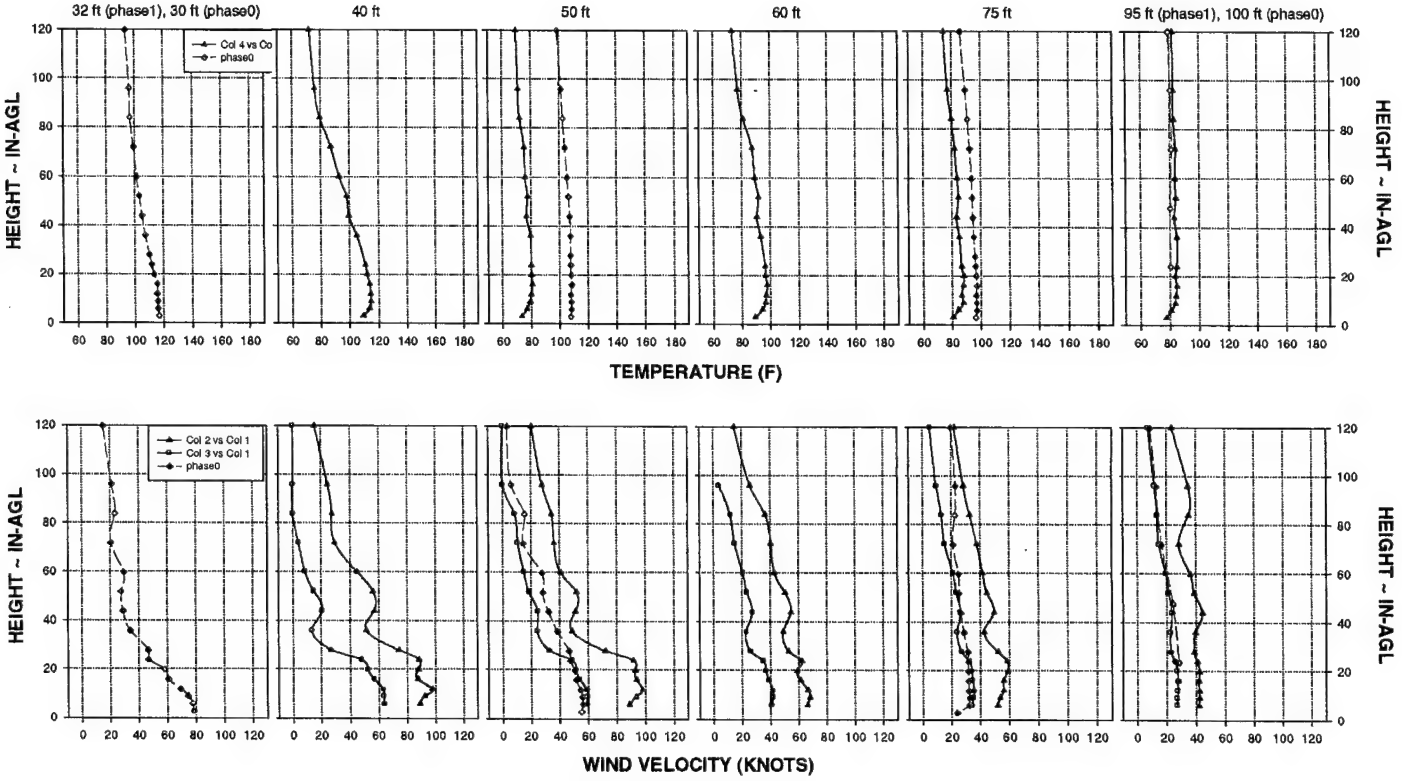

Figure E-7: Temperature and Velocity Field during a 50 ft-AGL Hover at the 40 deg Relative Test Azimuth (Higher Gross Weight)

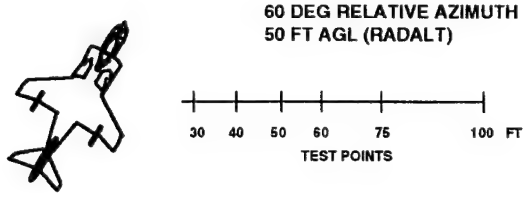

	Phase0 30/75 ft	Phase0 50/100 ft	Phase1 32 to 95 ft
Ambient Temperature (°F)	81	81	61
Winds (knots @ degrees)[1]	8@170	2@150	4@228
Aircraft Test Heading (degrees)[2]	96	76	80
Aircraft Gross Weight (lb)	15683	17443	16300

1. Relative to aircraft longitudinal centerline.
2. Relative to true north.

TOD 132005

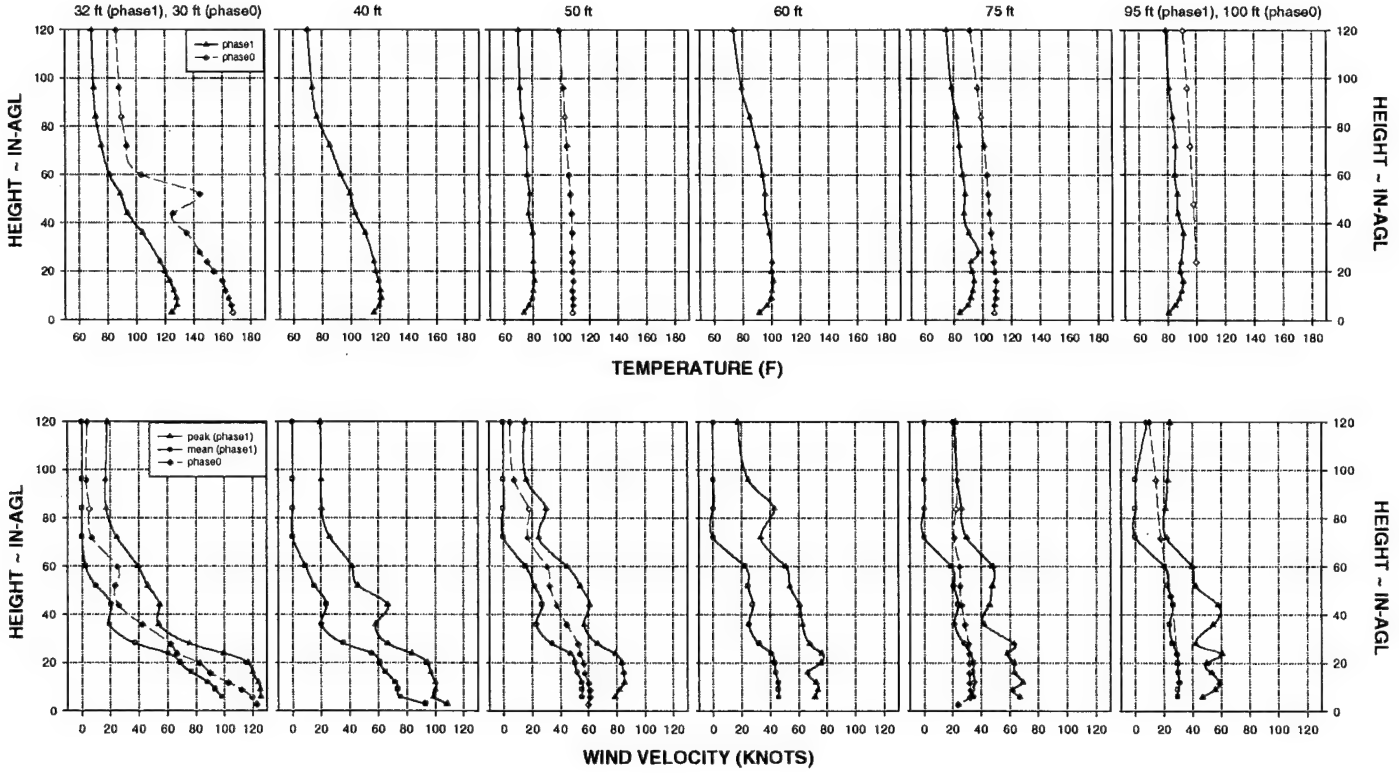

Figure E-8: Temperature and Velocity Field during a 50 ft-AGL Hover at the 60 deg Relative Test Azimuth (Lower Gross Weight)

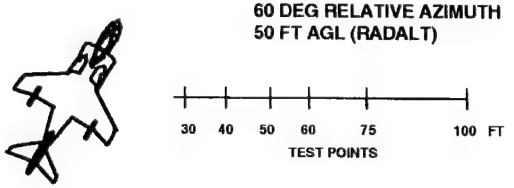

	Phase0 30/75 ft	Phase0 50/100 ft	Phase1 32 to 95 ft
Ambient Temperature (°F)	81	81	61
Winds (knots @ degrees)[1]	8@170	2@150	<5
Aircraft Test Heading (degrees)[2]	96	76	80
Aircraft Gross Weight (lb)	15683	17443	19600

1. Relative to aircraft longitudinal centerline.
2. Relative to true north.

TOD 125741

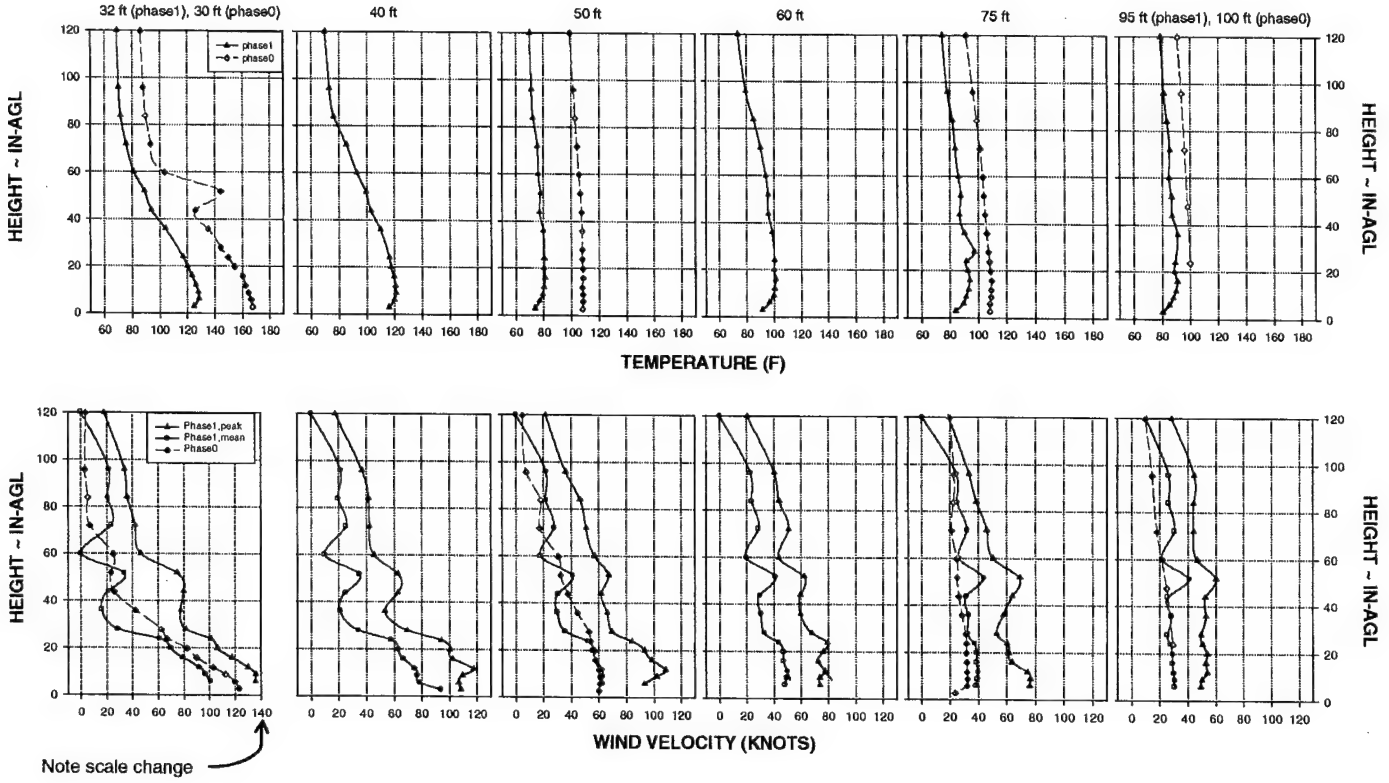

Figure E-9: Temperature and Velocity Field during a 50 ft-AGL Hover at the 60 deg Relative Test Azimuth (Higher Gross Weight)

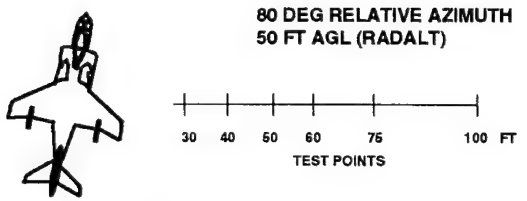

	Phase0 30/75 ft	Phase0 50/100 ft	Phase1 32 to 95 ft
Ambient Temperature (°F)	81	81	66
Winds (knots @ degrees)[1]	3@110	8@170	8@202
Aircraft Test Heading (degrees)[2]	116	96	100
Aircraft Gross Weight (lb)	15683	16203	16200

1. Relative to aircraft longitudinal centerline.
2. Relative to true north.

TOD 145605

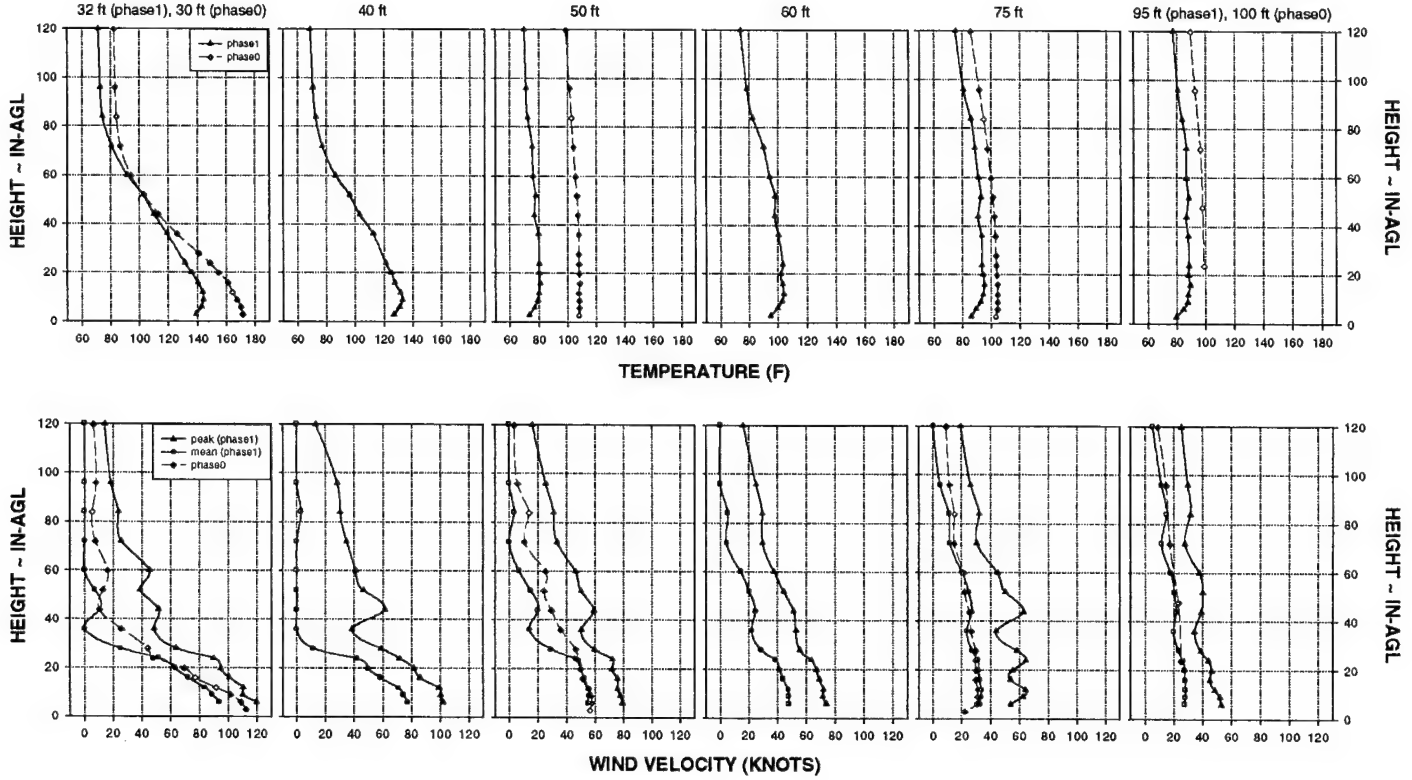

Figure E-10: Temperature and Velocity Field during a 50 ft-AGL Hover at the 80 deg Relative Test Azimuth (Lower Gross Weight)

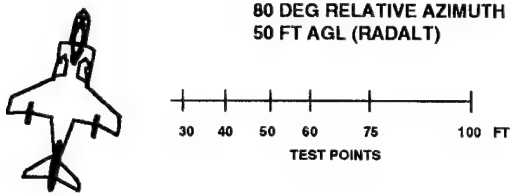

	Phase0 30/75 ft	Phase0 50/100 ft	Phase1 32 to 95 ft
Ambient Temperature (°F)	81	81	66
Winds (knots @ degrees)[1]	3@110	8@170	<5
Aircraft Test Heading (degrees)[2]	116	96	100
Aircraft Gross Weight (lb)	15683	16203	17400

1. Relative to aircraft longitudinal centerline.
2. Relative to true north.

TOD 122412

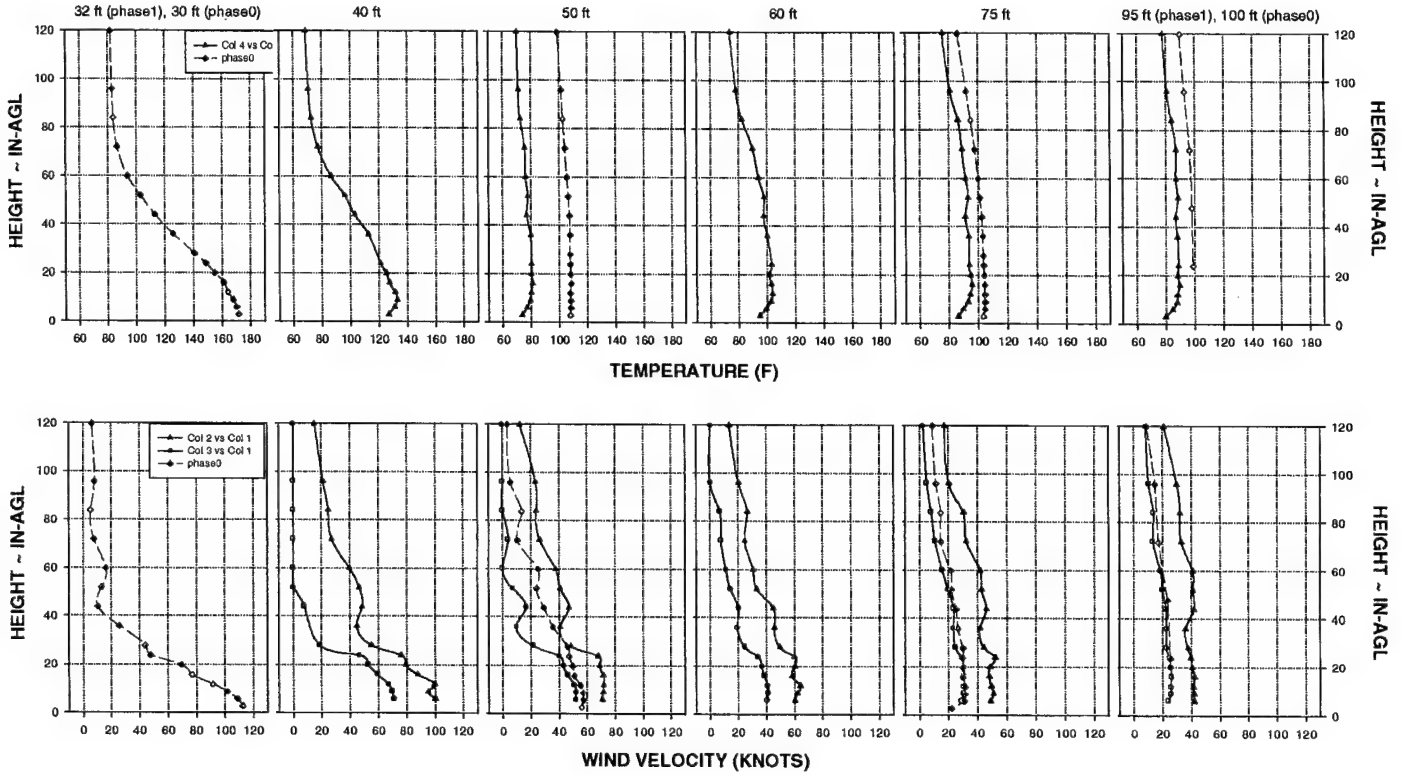

Figure E-11: Temperature and Velocity Field during a 50 ft-AGL Hover at the 80 deg Relative Test Azimuth (Higher Gross Weight)

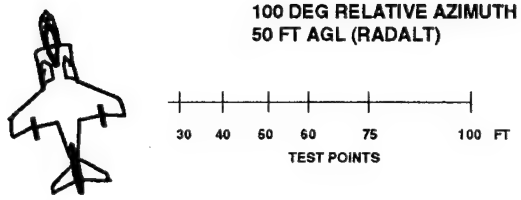

	Phase0 30/75 ft	Phase0 50/100 ft	Phase1 32 to 95 ft
Ambient Temperature (°F)	81	81	59
Winds (knots @ degrees)[1]	3@89	3@110	2@210
Aircraft Test Heading (degrees)[2]	136	116	120
Aircraft Gross Weight (lb)	15483	15683	17300

1. Relative to aircraft longitudinal centerline.
2. Relative to true north.

TOD 123315

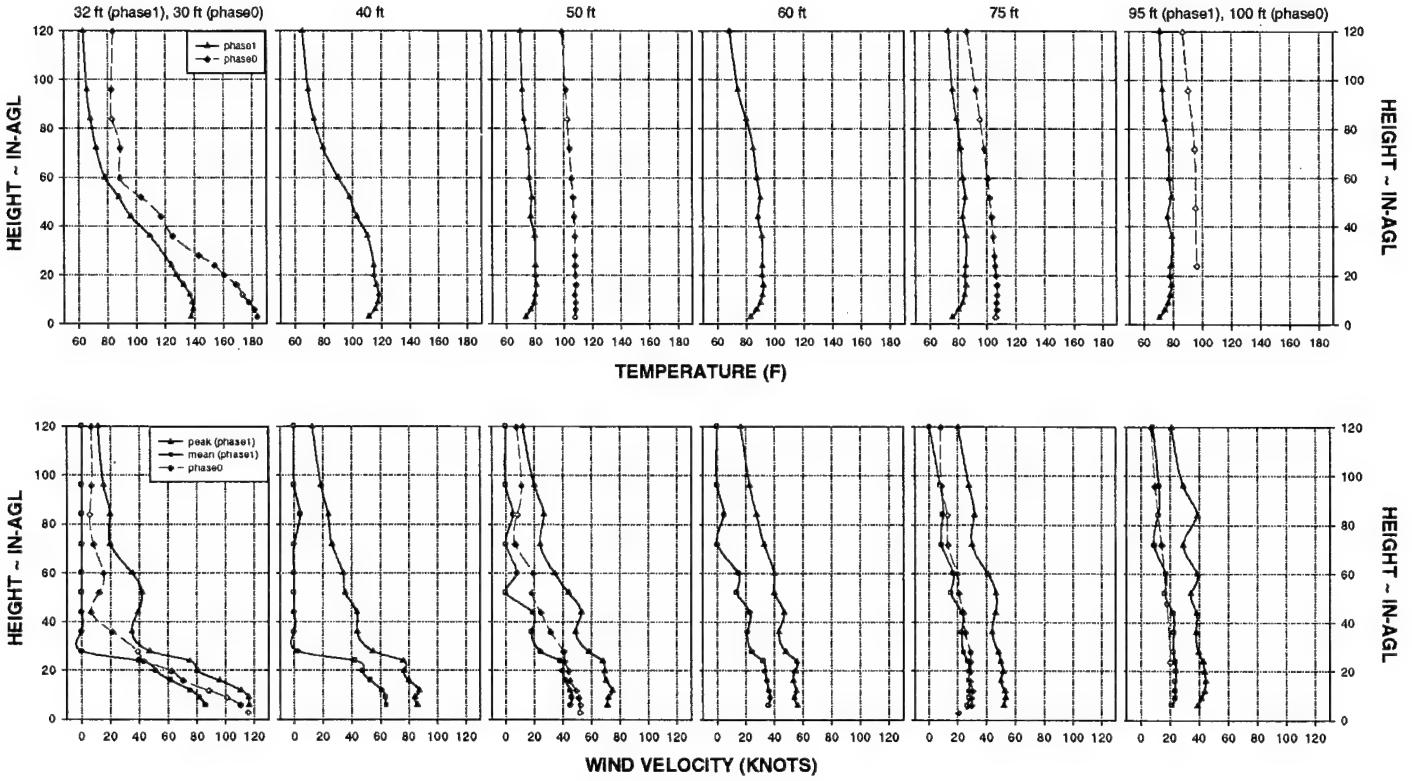

Figure E-12: Temperature and Velocity Field during a 50 ft-AGL Hover at the 100 deg Relative Test Azimuth

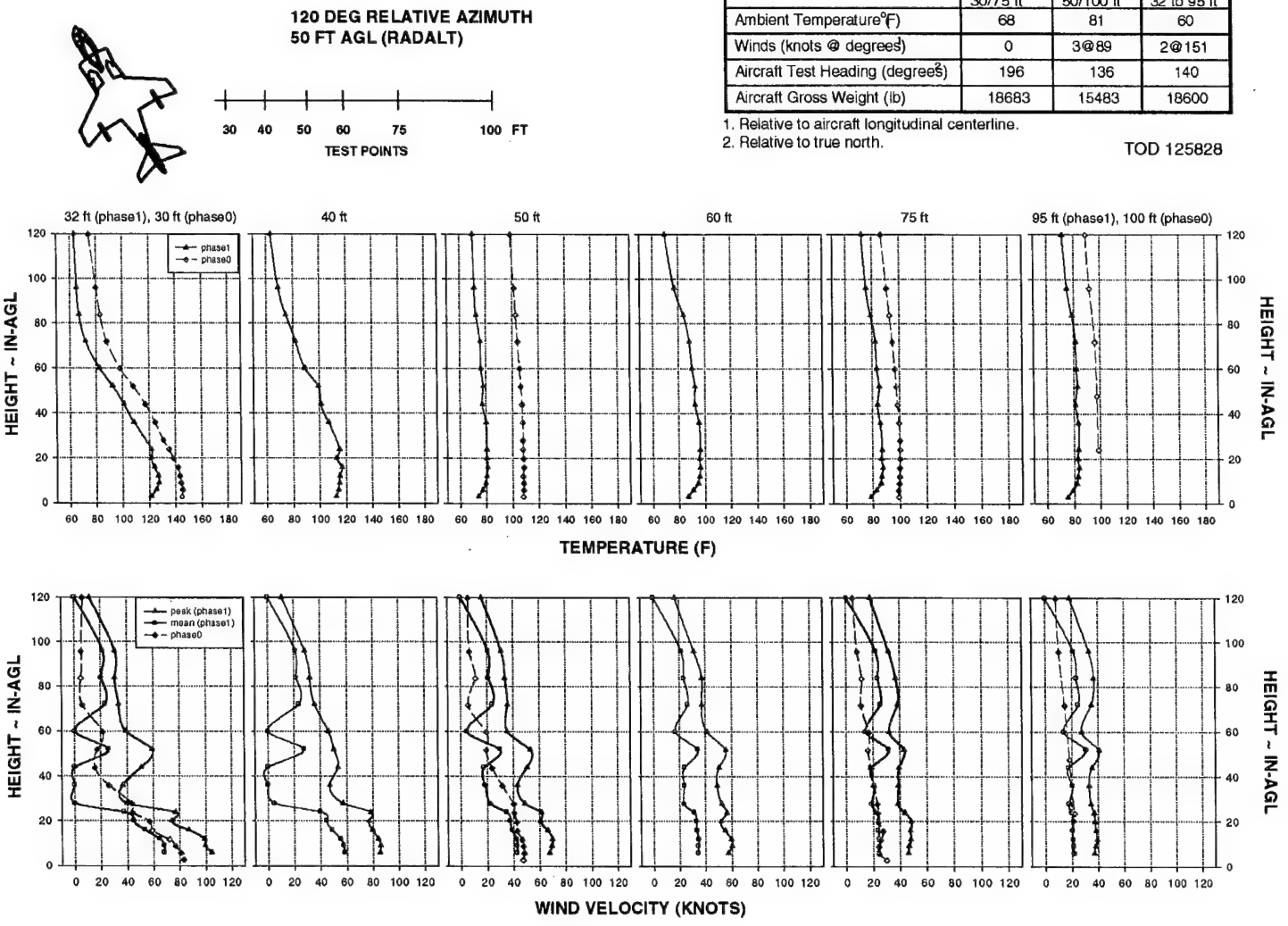

	Phase0 30/75 ft	Phase0 50/100 ft	Phase1 32 to 95 ft
Ambient Temperature(°F)	68	81	60
Winds (knots @ degrees[1])	0	3@89	2@151
Aircraft Test Heading (degrees[2])	196	136	140
Aircraft Gross Weight (lb)	18683	15483	18600

1. Relative to aircraft longitudinal centerline.
2. Relative to true north.

TOD 125828

Figure E-13: Temperature and Velocity Field during a 50 ft-AGL Hover at the 120 deg Relative Test Azimuth

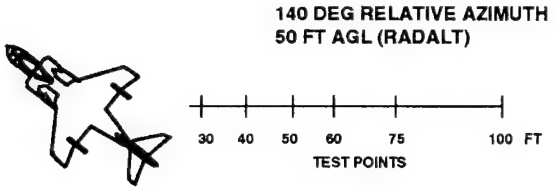

	Phase0 30/75 ft	Phase0 50/100 ft	Phase1 32 to 95 ft
Ambient Temperature (°F)	68	68	60
Winds (knots @ degrees)[1]	0	0	3@131
Aircraft Test Heading (degrees)[2]	176	156	160
Aircraft Gross Weight (lb)	18363	18683	18500

1. Relative to aircraft longitudinal centerline.
2. Relative to true north.

TOD 130836

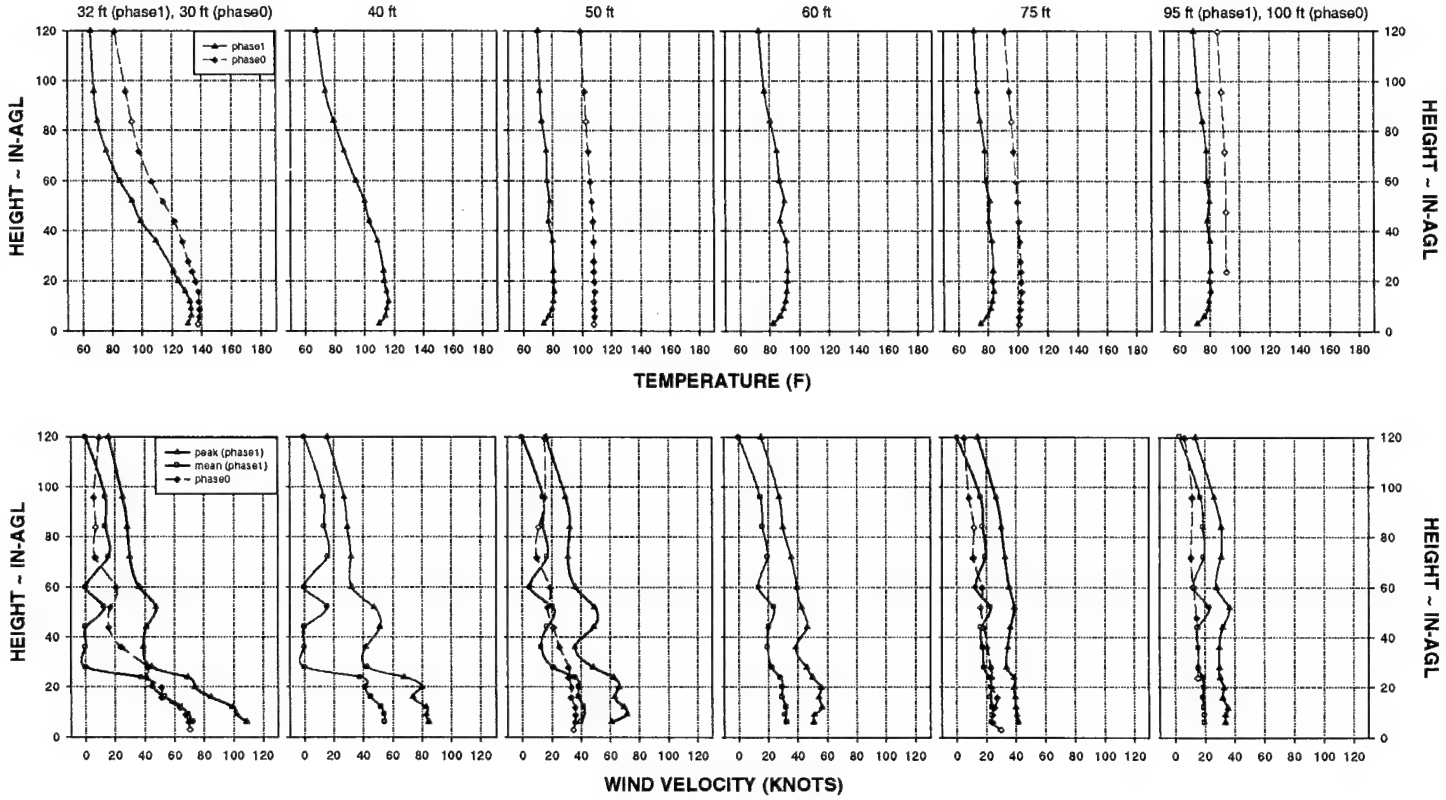

Figure E-14: Temperature and Velocity Field during a 50 ft-AGL Hover at the 140 deg Relative Test Azimuth

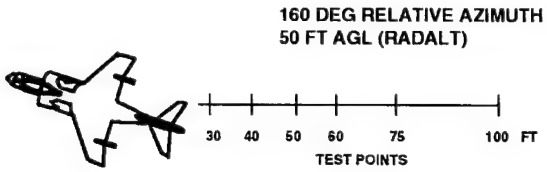

	Phase0 30/75 ft	Phase0 50/100 ft	Phase1 32 to 95 ft
Ambient Temperature (°F)	82	68	59
Winds (knots @ degrees)[1]	0	0	2@149
Aircraft Test Heading (degrees)[2]	196	176	180
Aircraft Gross Weight (lb)	18673	18363	16300

1. Relative to aircraft longitudinal centerline.
2. Relative to true north.

TOD 123354

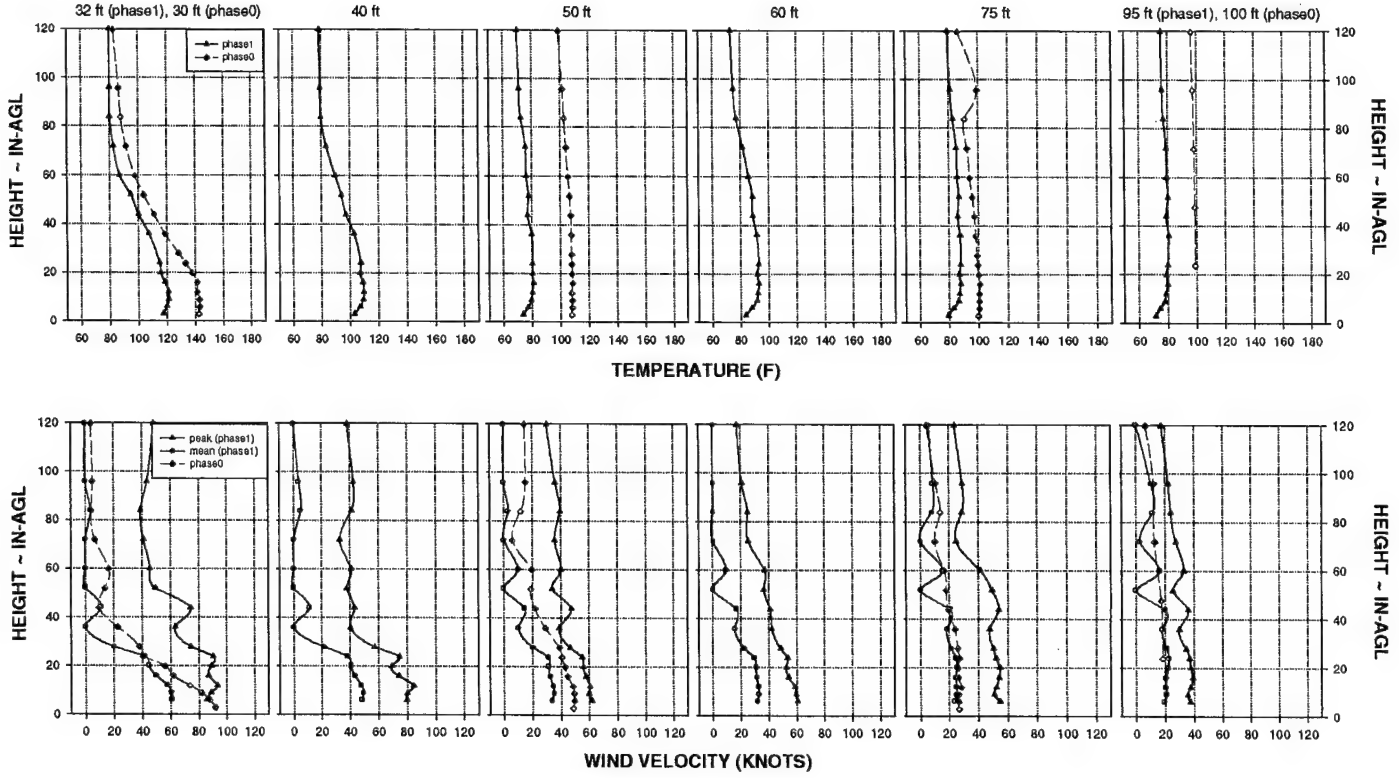

Figure E-15: Temperature and Velocity Field during a 50 ft-AGL Hover at the 160 deg Relative Test Azimuth (Lower Gross Weight)

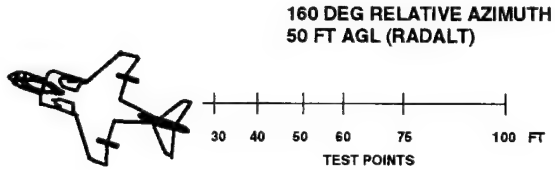

	Phase0 30/75 ft	Phase0 50/100 ft	Phase1 32 to 95 ft
Ambient Temperature (°F)	82	68	59
Winds (knots @ degrees)[1]	0	0	<5
Aircraft Test Heading (degrees)[2]	196	176	180
Aircraft Gross Weight (lb)	18673	18363	19600

1. Relative to aircraft longitudinal centerline.
2. Relative to true north.

TOD 134358

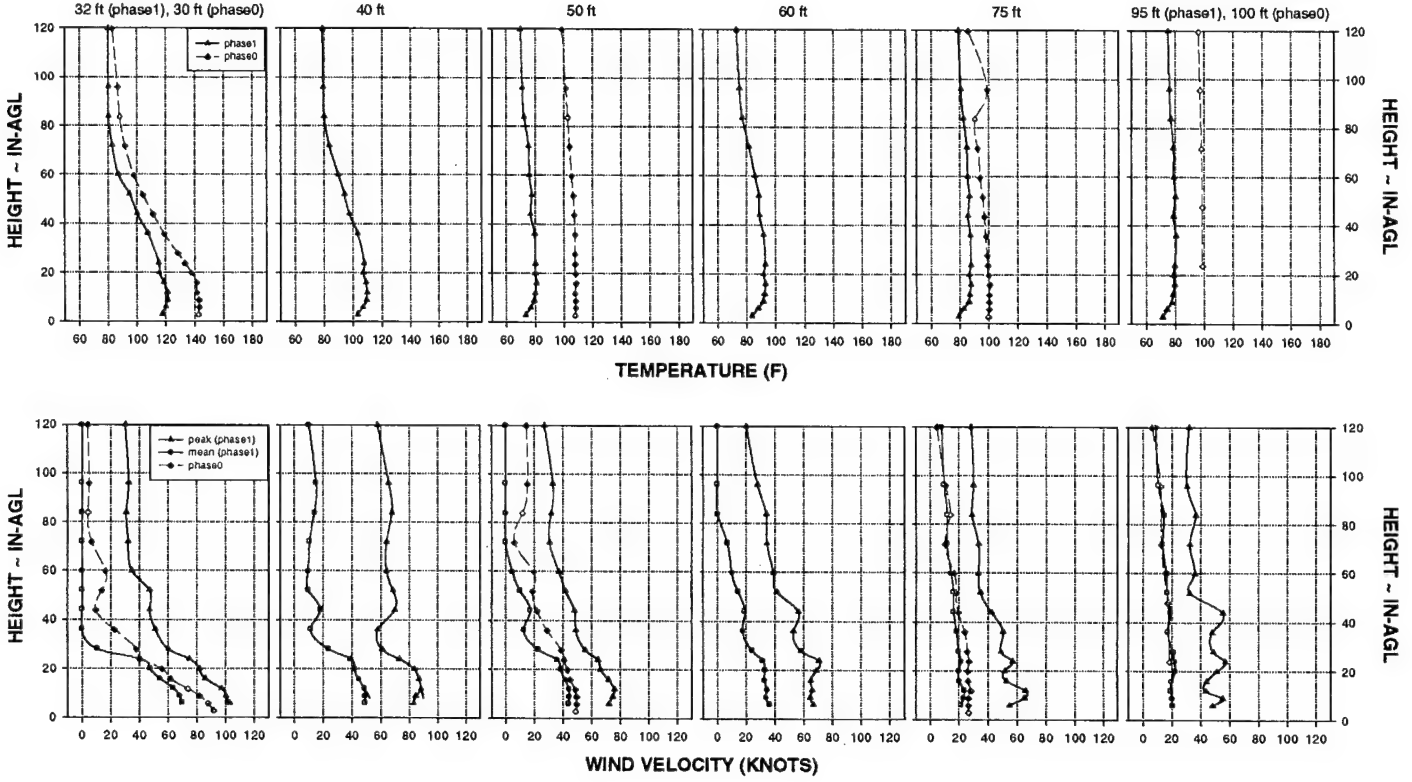

Figure E-16: Temperature and Velocity Field during a 50 ft-AGL Hover at the 160 deg Relative Test Azimuth (Higher Gross Weight)

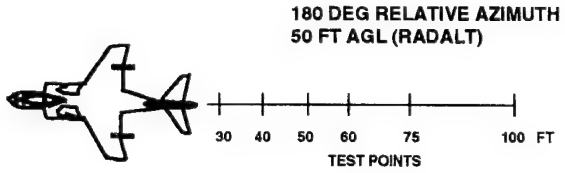

	Phase0 30/75 ft	Phase0 50/100 ft	Phase1 32 to 95 ft
Ambient Temperature (°F)	82	82	60
Winds (knots @ degrees)[1]	7@-10	0	3@097
Aircraft Test Heading (degrees)[2]	216	196	200
Aircraft Gross Weight (lb)	18483	18673	15700

1. Relative to aircraft longitudinal centerline.
2. Relative to true north.

TOD 130911

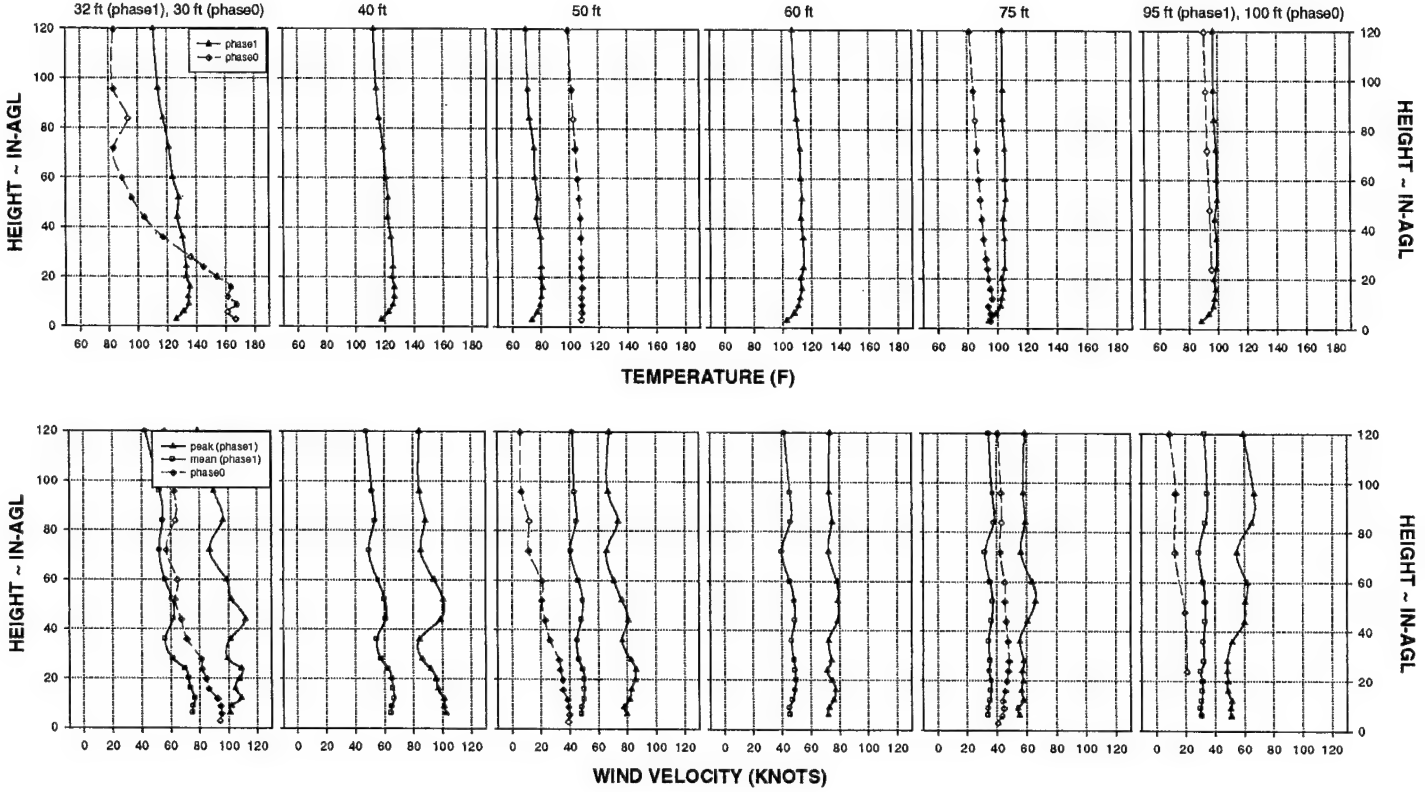

Figure E-17: Temperature and Velocity Field during a 50 ft-AGL Hover at the 180 deg Relative Test Azimuth

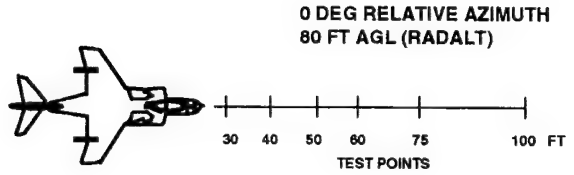

	Phase0 30/75 ft	Phase0 50/100 ft	Phase1 32 to 95 ft
Ambient Temperature (°F)	-	-	65
Winds (knots @ degrees)[1]	-	-	6@213
Aircraft Test Heading (degrees)[2]	-	-	020
Aircraft Gross Weight (lb)	-	-	19500

1. Relative to aircraft longitudinal centerline.
2. Relative to true north.

TOD 143326

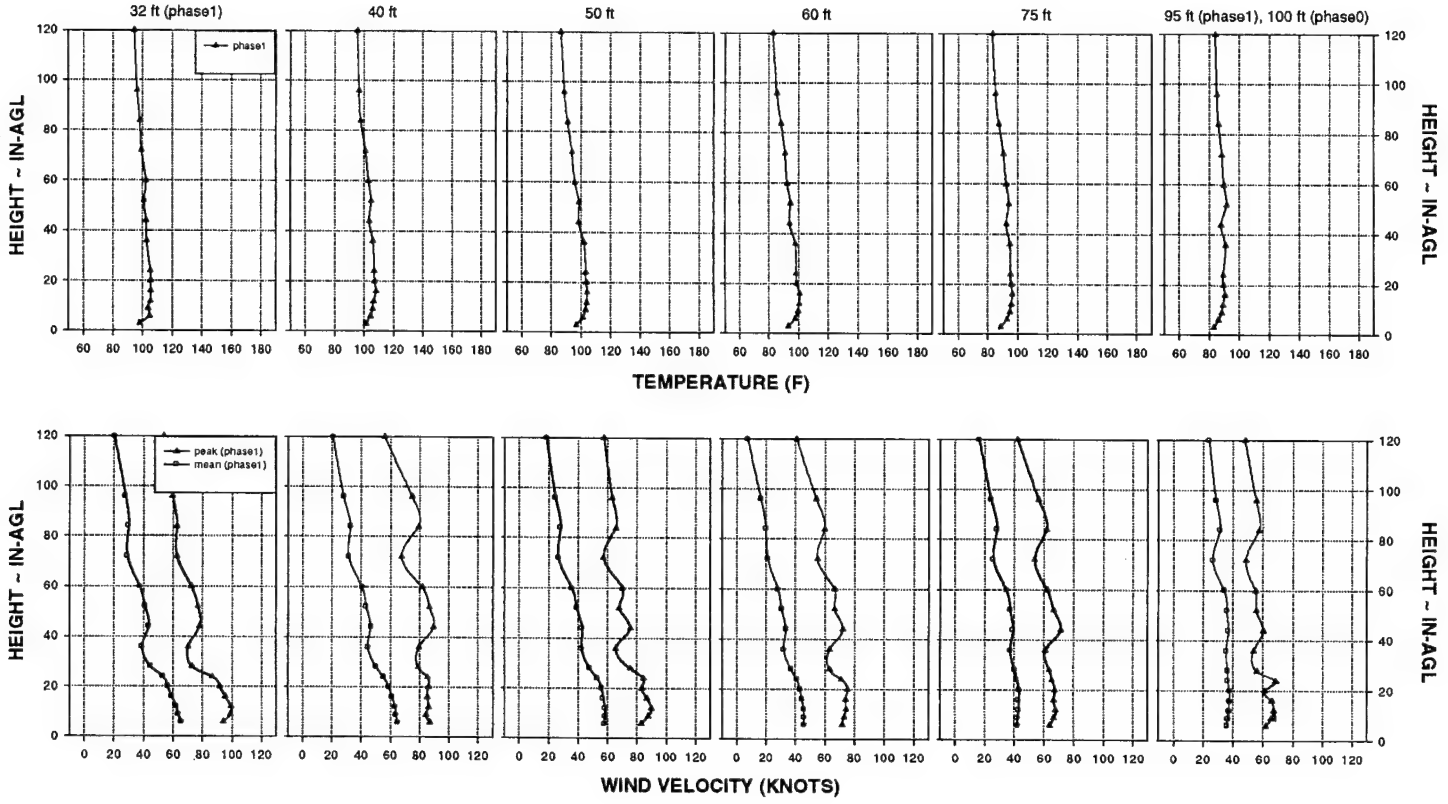

Figure E-18: Temperature and Velocity Field during a 80 ft-AGL Hover at the 0 deg Relative Test Azimuth

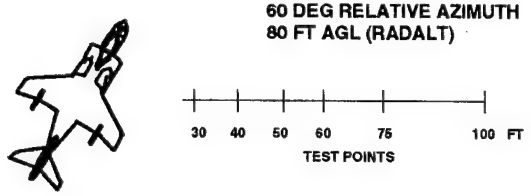

	Phase0 30/75 ft	Phase0 50/100 ft	Phase1 32 to 95 ft
Ambient Temperature (°F)	-	71	65
Winds (knots @ degrees)[1]	-	0	7@261
Aircraft Test Heading (degrees)[2]	-	76	020
Aircraft Gross Weight (lb)	-	16803	18400

1. Relative to aircraft longitudinal centerline.
2. Relative to true north.

TOD 144431

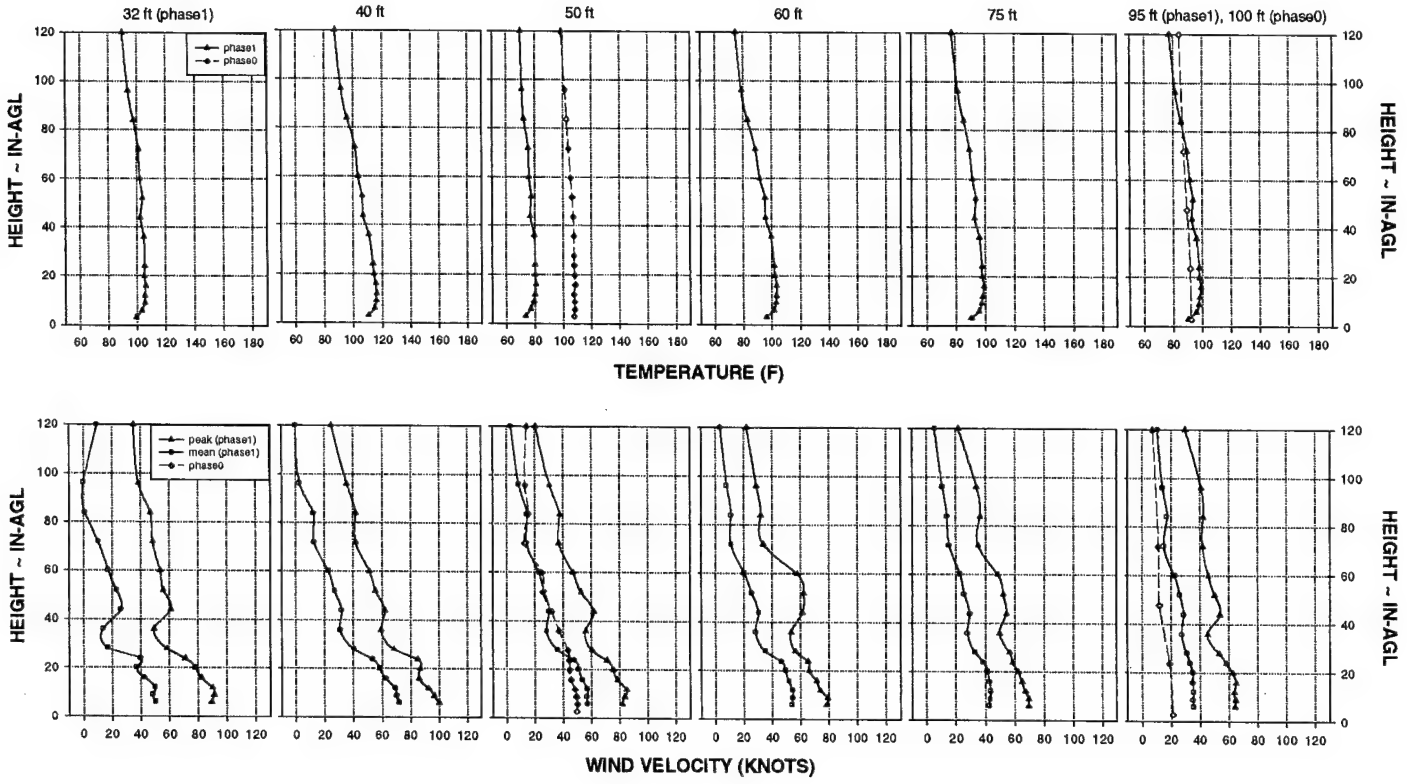

Figure E-19: Temperature and Velocity Field during a 80 ft-AGL Hover at the 60 deg Relative Test Azimuth

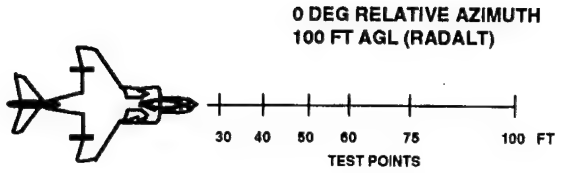

	Phase0 30/75 ft	Phase0 50/100 ft	Phase1 32 to 95 ft
Ambient Temperature (°F)	-	-	64
Winds (knots @ degrees)[1]	-	-	6@253
Aircraft Test Heading (degrees)[2]	-	-	020
Aircraft Gross Weight (lb)	-	-	17100

1. Relative to aircraft longitudinal centerline.
2. Relative to true north.

TOD 140614

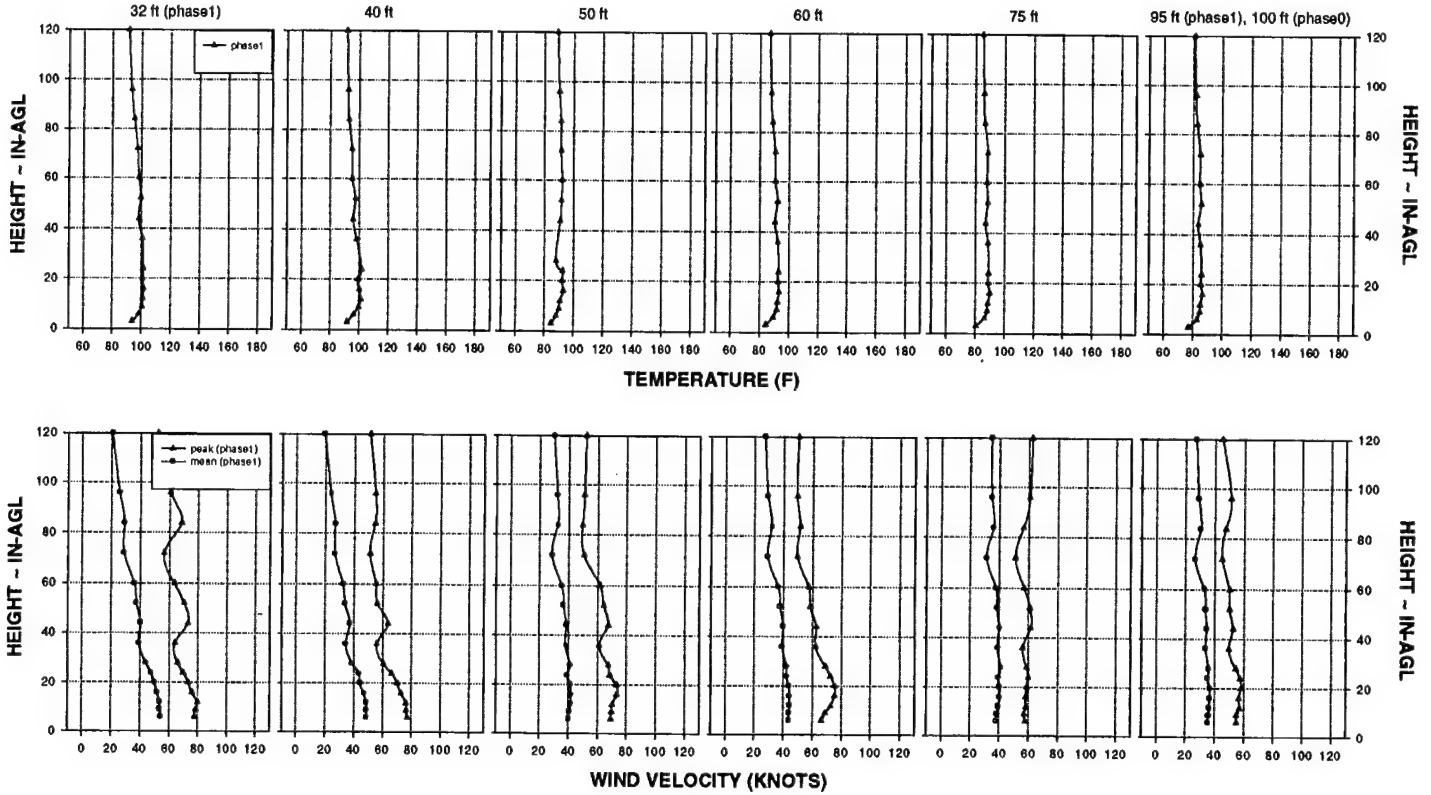

Figure E-20: Temperature and Velocity Field during a 100 ft-AGL Hover at the 0 deg Relative Test Azimuth

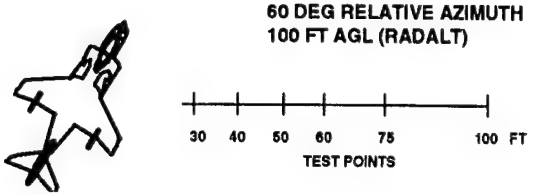

60 DEG RELATIVE AZIMUTH
100 FT AGL (RADALT)

30 40 50 60 75 100 FT
TEST POINTS

	Phase0 30/75 ft	Phase0 50/100 ft	Phase1 32 to 95 ft
Ambient Temperature (°F)	-	-	64
Winds (knots @ degrees)[1]	-	-	5@180
Aircraft Test Heading (degrees)[2]	-	-	020
Aircraft Gross Weight (lb)	-	-	16100

1. Relative to aircraft longitudinal centerline.
2. Relative to true north.

TOD 140659

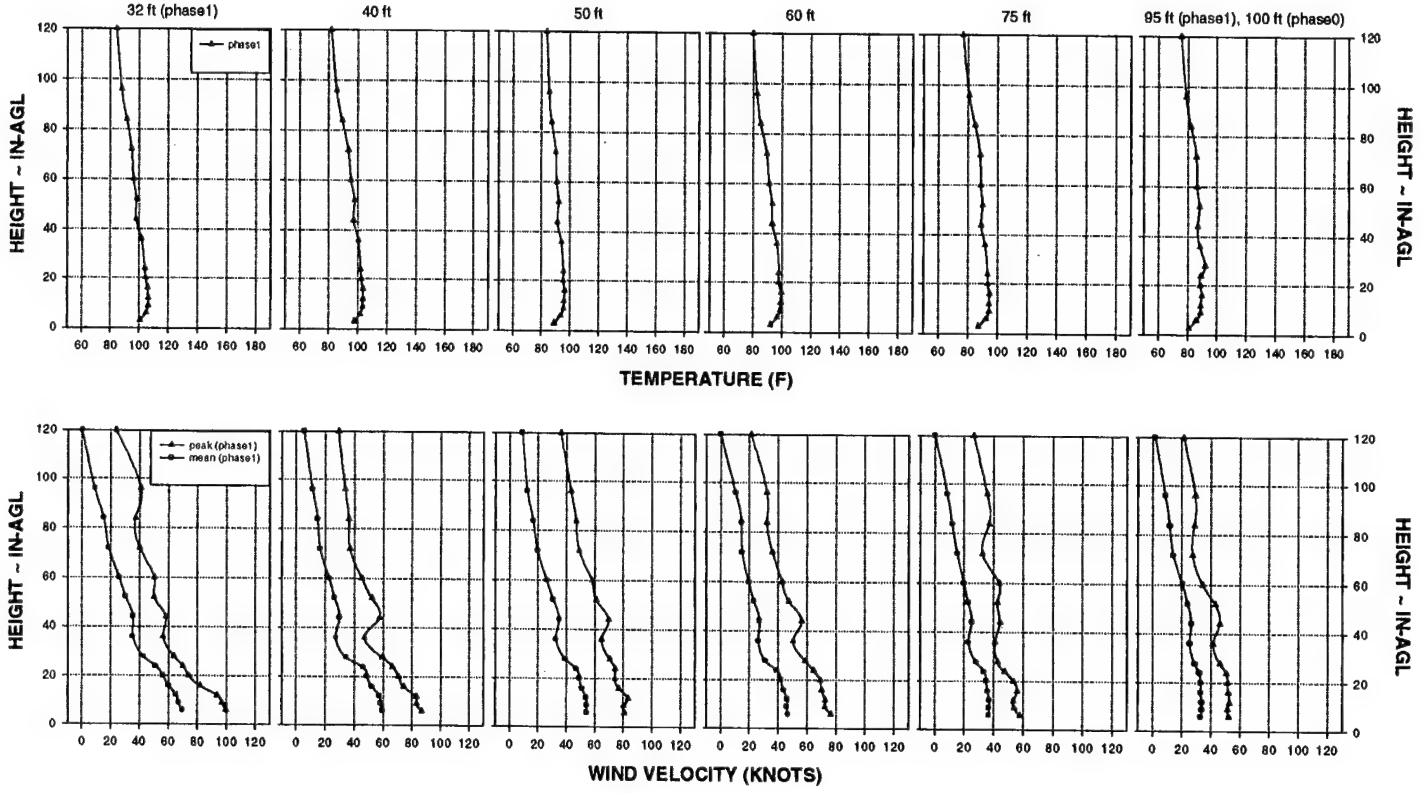

Figure E-21: Temperature and Velocity Field during a 100 ft-AGL Hover at the 60 deg Relative Test Azimuth

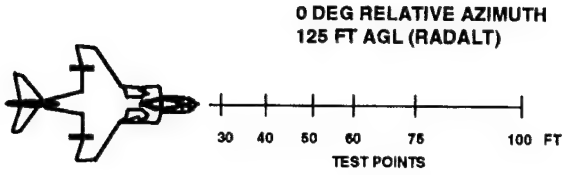

	Phase0 30/75 ft	Phase0 50/100 ft	Phase1 32 to 95 ft
Ambient Temperature (°F)	-	-	63
Winds (knots @ degrees)[1]	-	-	6@242
Aircraft Test Heading (degrees)[2]	-	-	020
Aircraft Gross Weight (lb)	-	-	18400

1. Relative to aircraft longitudinal centerline.
2. Relative to true north.

TOD 135424

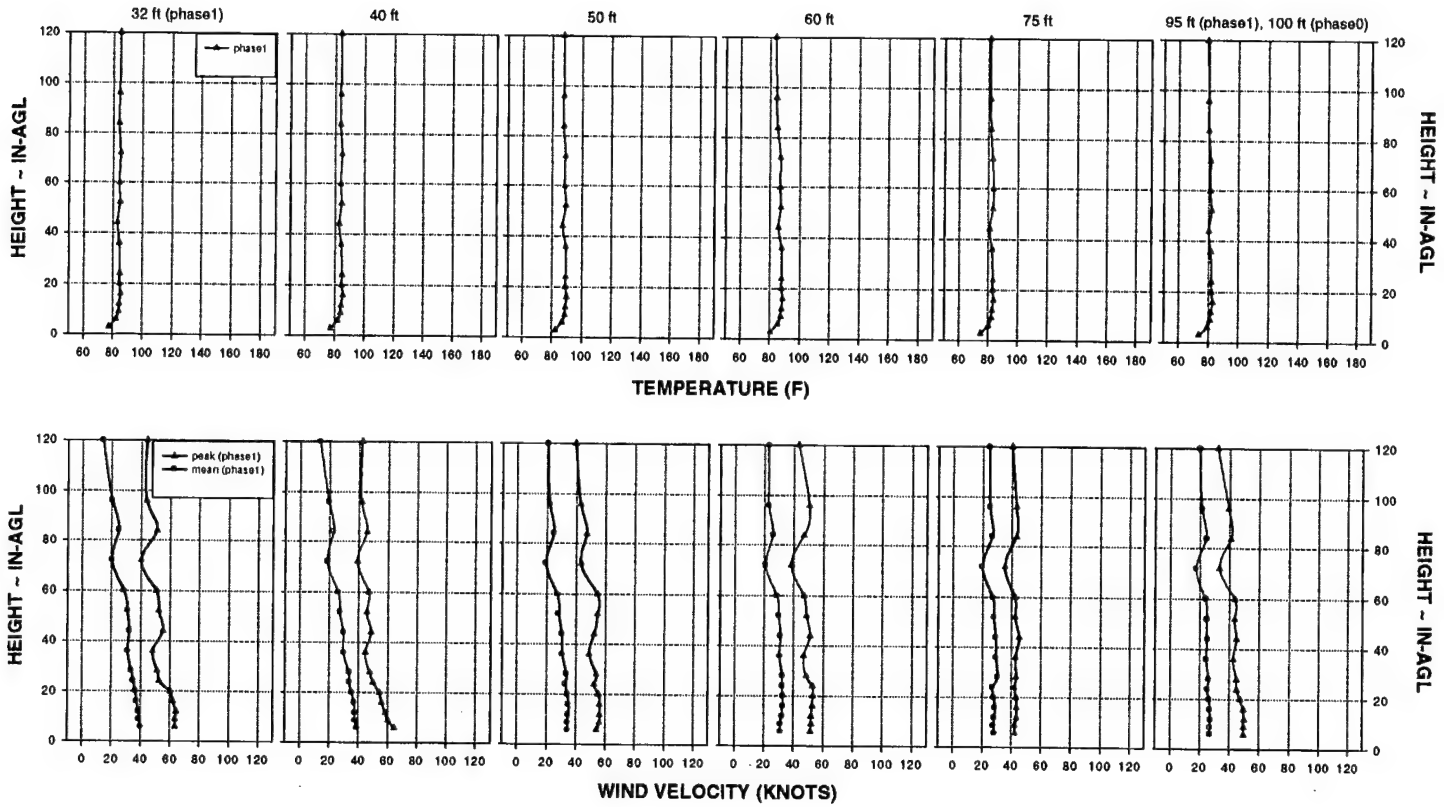

Figure E-22: Temperature and Velocity Field during a 125 ft-AGL Hover at the 0 deg Relative Test Azimuth

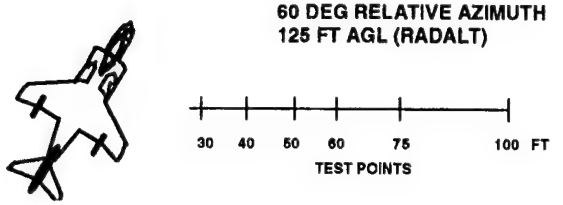

	Phase0 30/75 ft	Phase0 50/100 ft	Phase1 32 to 95 ft
Ambient Temperature (°F)	-	-	63
Winds (knots @ degrees)[1]	-	-	6@245
Aircraft Test Heading (degrees)[2]	-	-	020
Aircraft Gross Weight (lb)	-	-	17400

1. Relative to aircraft longitudinal centerline.
2. Relative to true north.

TOD 085601

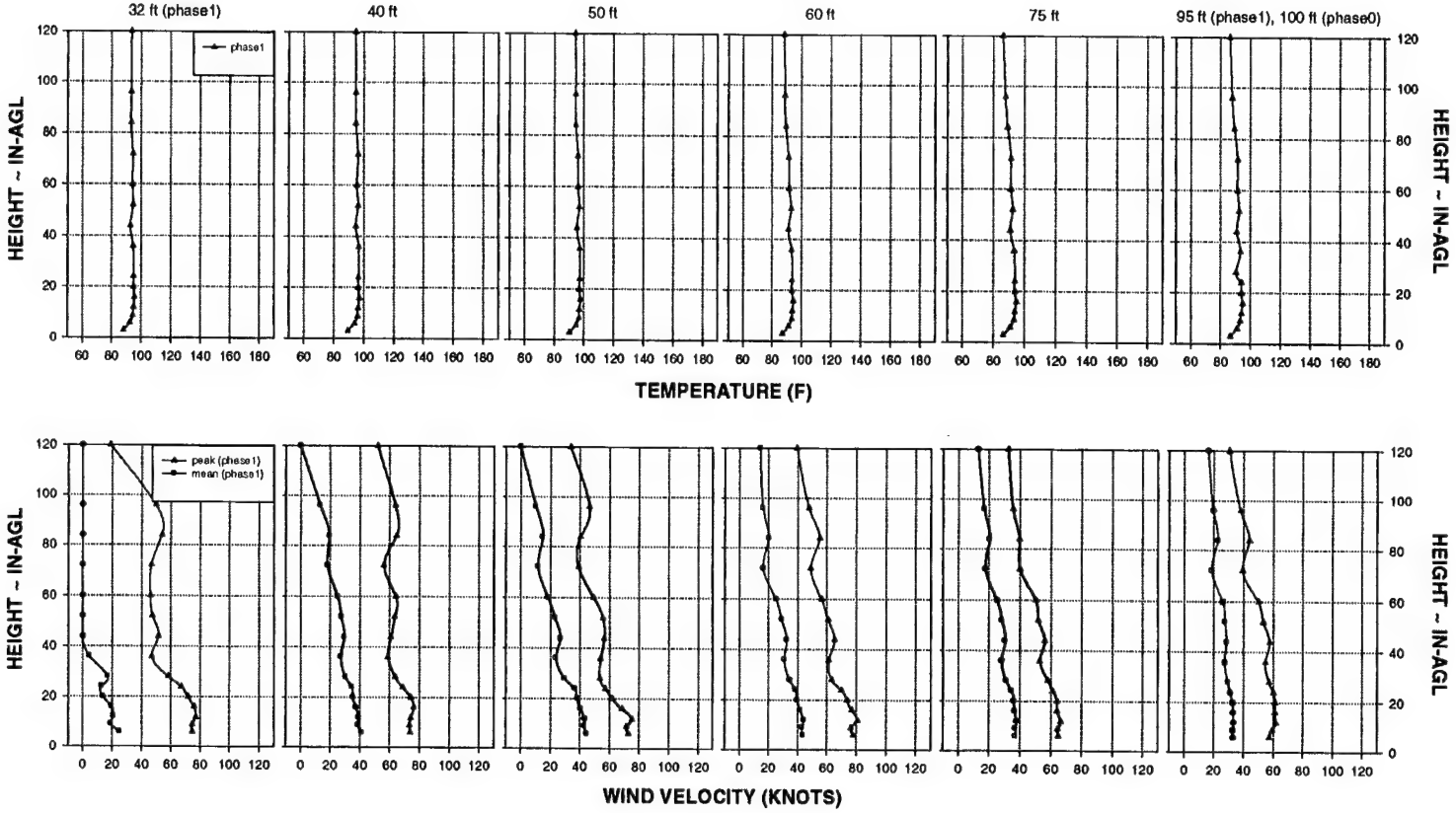

Figure E-23: Temperature and Velocity Field during a 125 ft-AGL Hover at the 60 deg Relative Test Azimuth

APPENDIX F
FLOW FIELD STREAMLINES

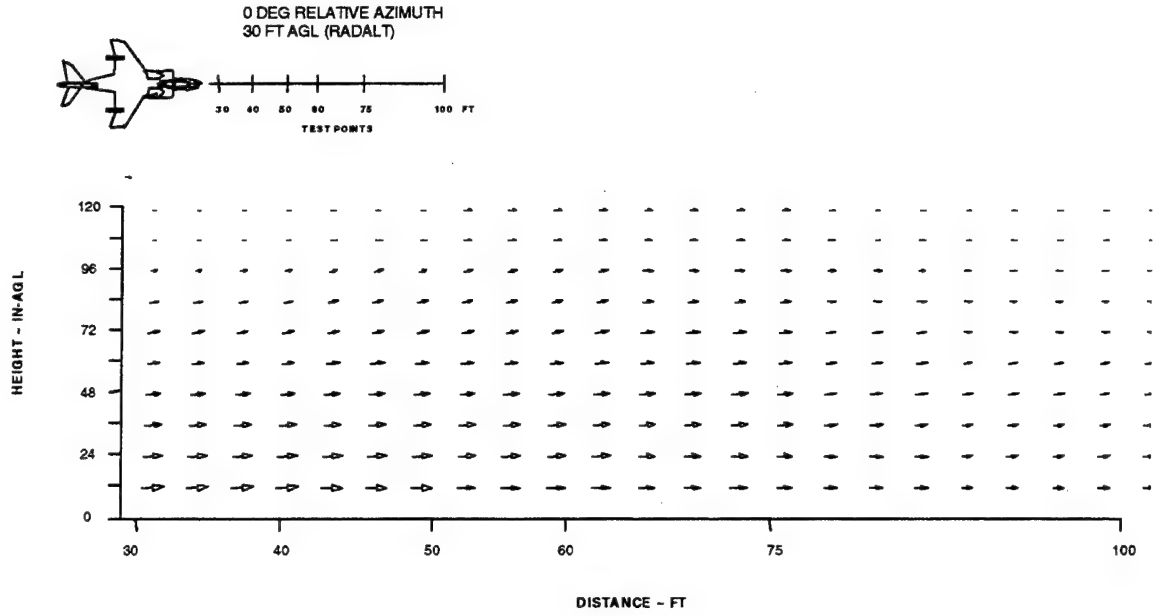

Figure F-1: Flow Field Streamlines during a 30 ft-AGL Hover at the 0 deg Relative Test Azimuth

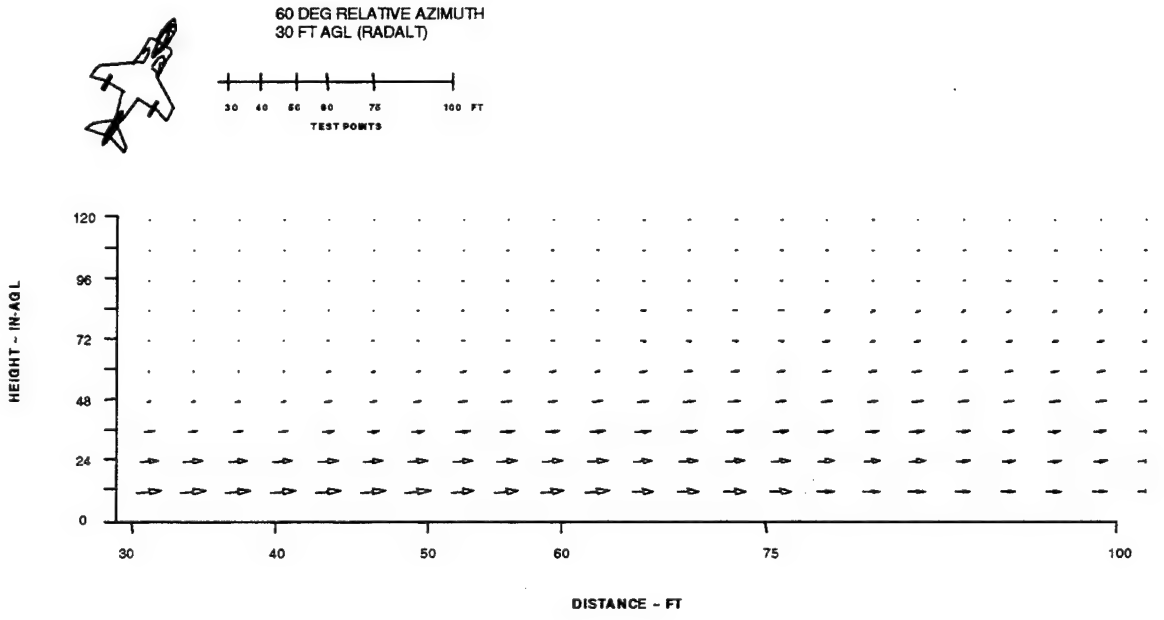

Figure F-2: Flow Field Streamlines during a 30 ft-AGL Hover at the 60 deg Relative Test Azimuth

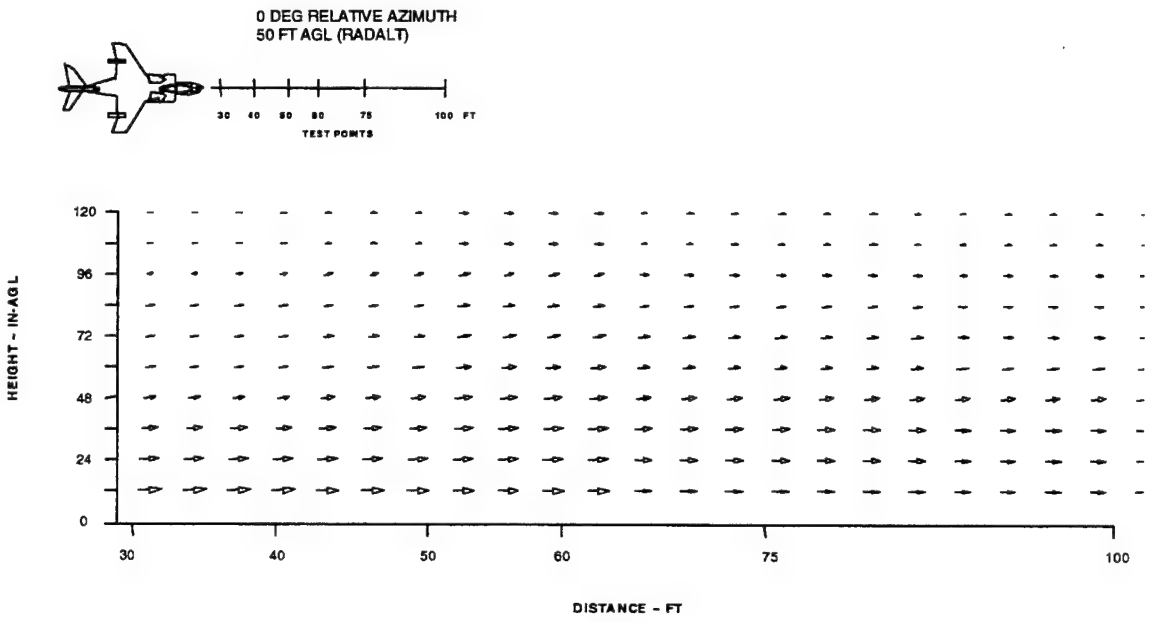

Figure F-3: Flow Field Streamlines during a 50 ft-AGL Hover at the 0 deg Relative Test Azimuth

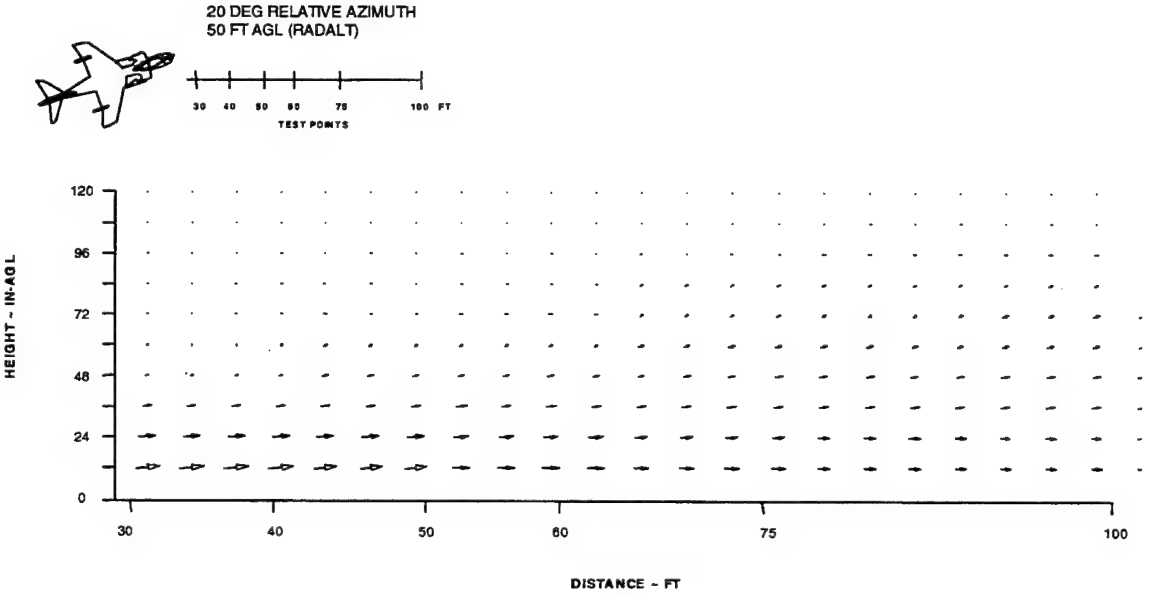

Figure F-4: Flow Field Streamlines during a 50 ft-AGL Hover at the 20 deg Relative Test Azimuth

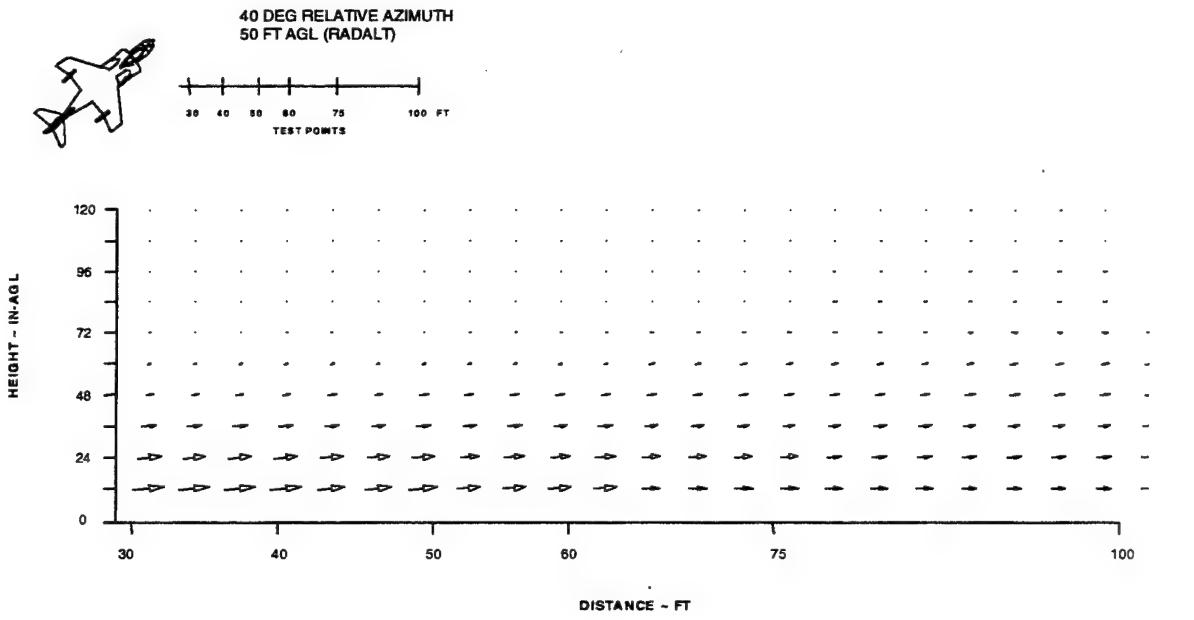

Figure F-5: Flow Field Streamlines during a 50 ft-AGL Hover at the 40 deg Relative Test Azimuth

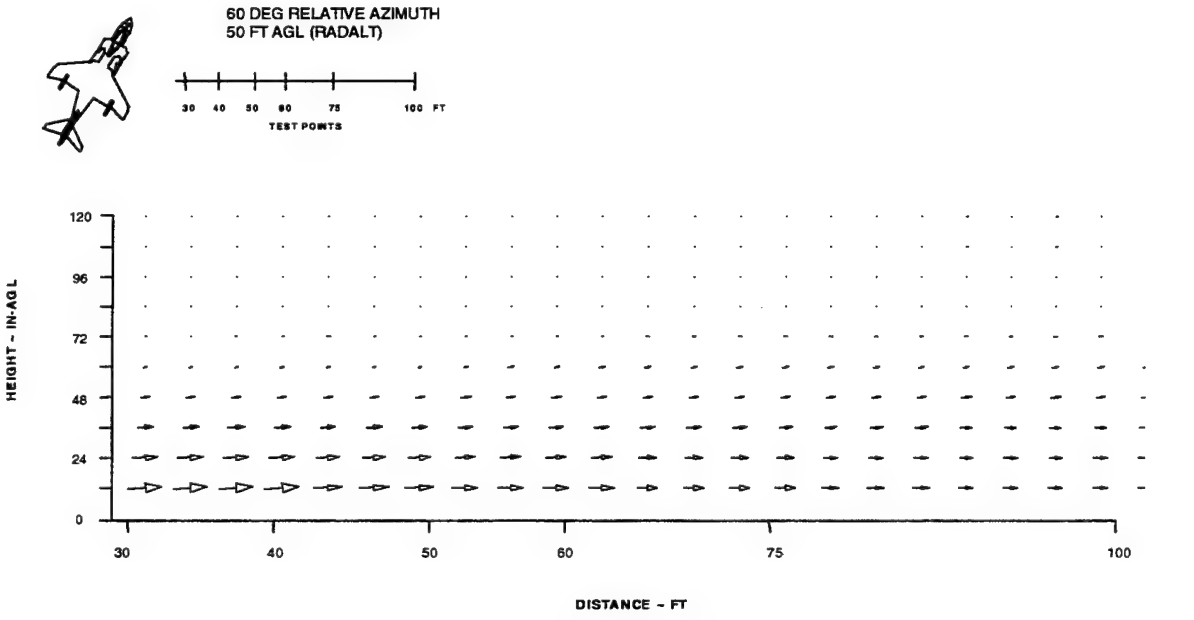

Figure F-6: Flow Field Streamlines during a 50 ft-AGL Hover at the 60 deg Relative Test Azimuth

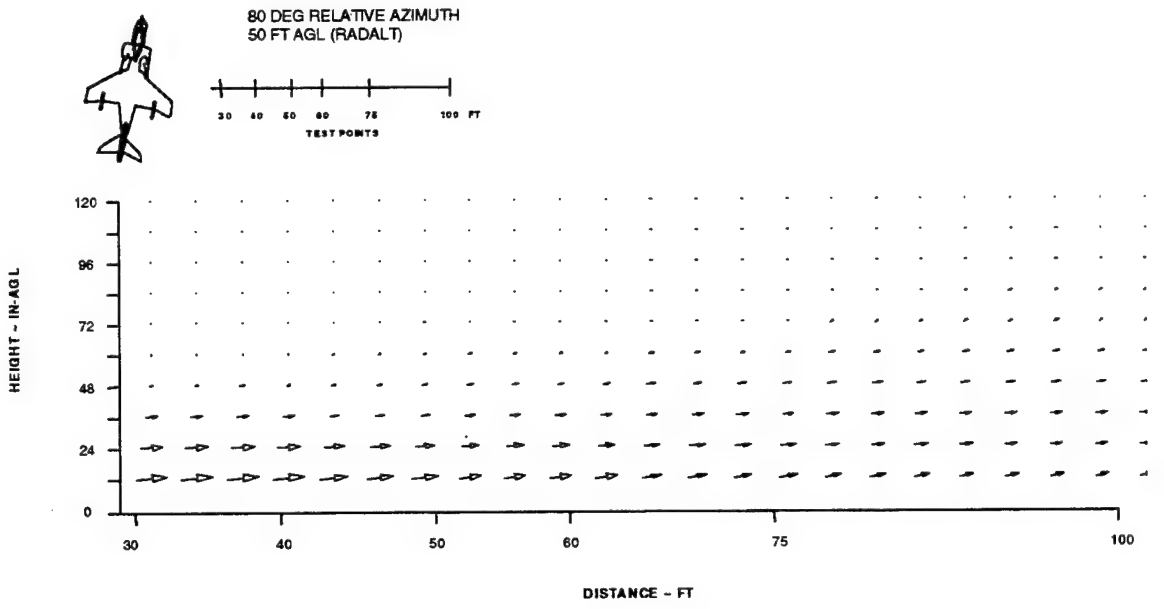

Figure F-7: Flow Field Streamlines during a 50 ft-AGL Hover at the 80 deg Relative Test Azimuth

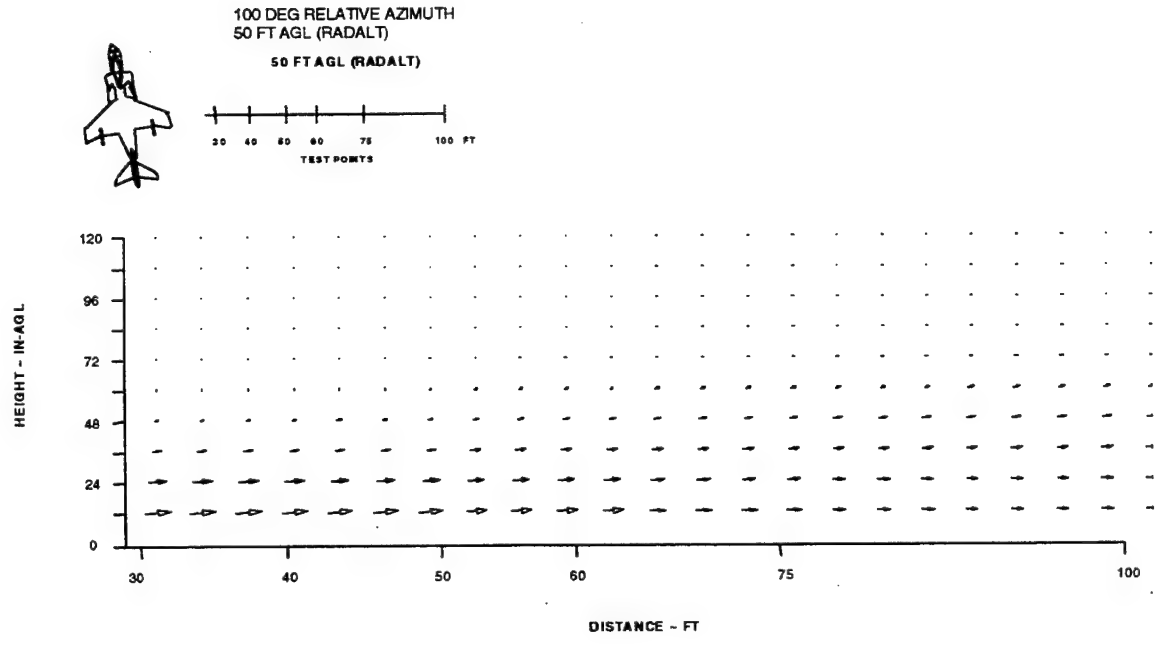

Figure F-8: Flow Field Streamlines during a 50 ft-AGL Hover at the 100 deg Relative Test Azimuth

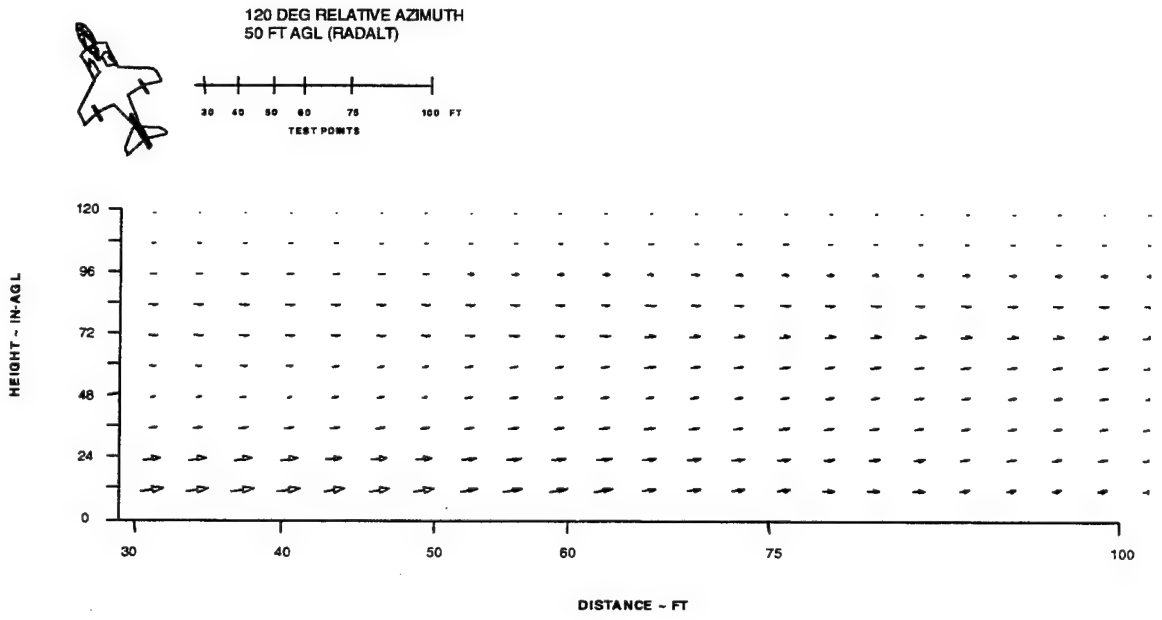

Figure F-9: Flow Field Streamlines during a 50 ft-AGL Hover at the 120 deg Relative Test Azimuth

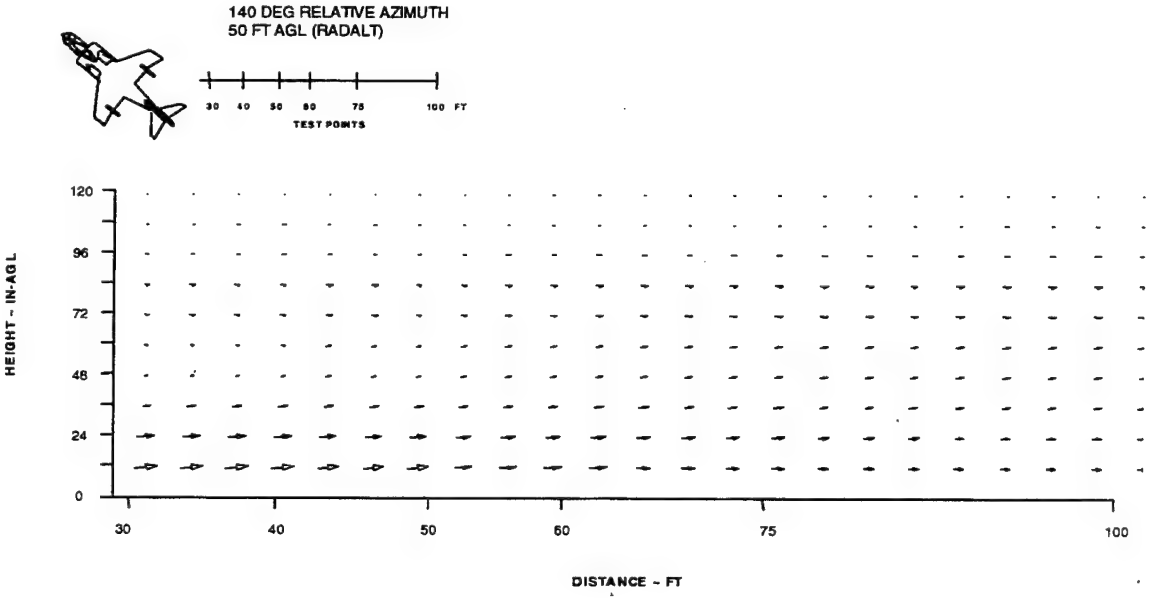

Figure F-10: Flow Field Streamlines during a 50 ft-AGL Hover at the 140 deg Relative Test Azimuth

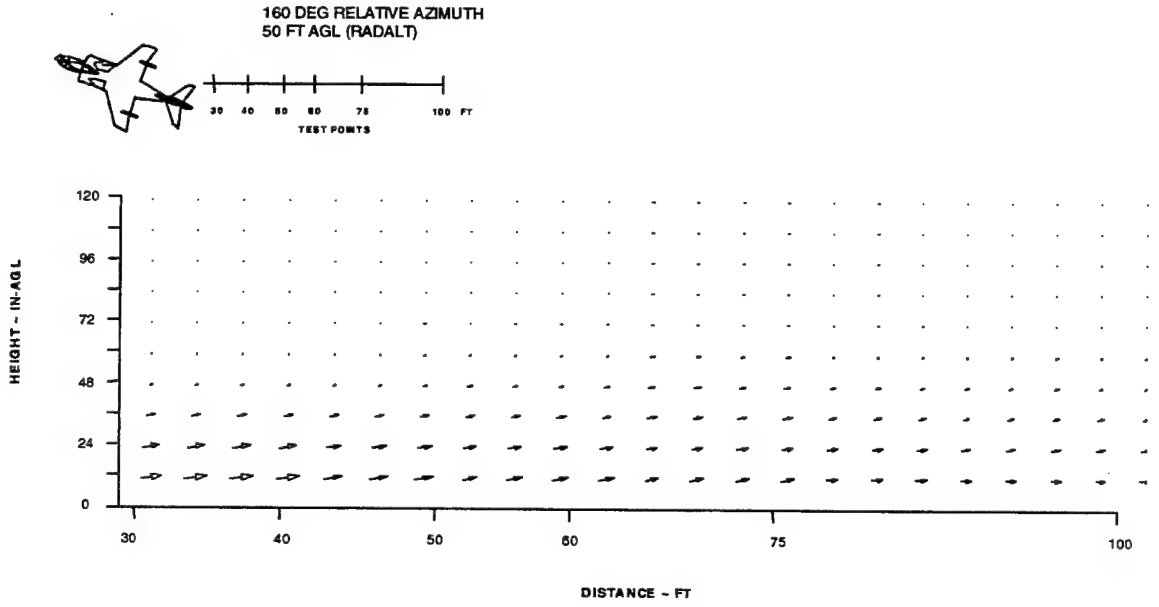

Figure F-11: Flow Field Streamlines during a 50 ft-AGL Hover at the 160 deg Relative Test Azimuth

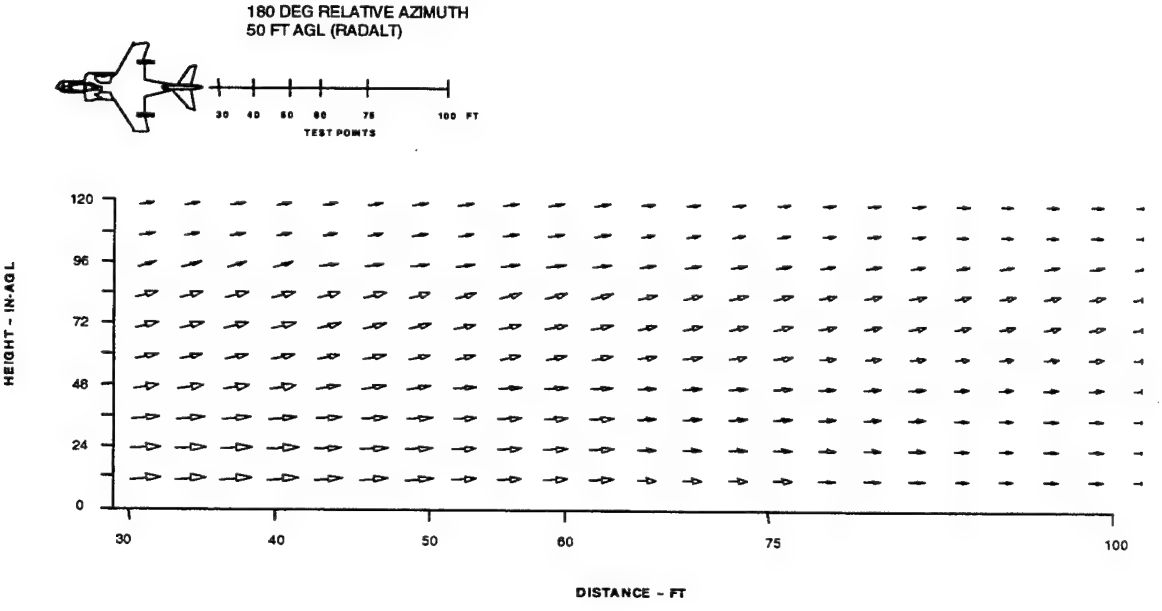

Figure F-12: Flow Field Streamlines during a 50 ft-AGL Hover at the 180 deg Relative Test Azimuth

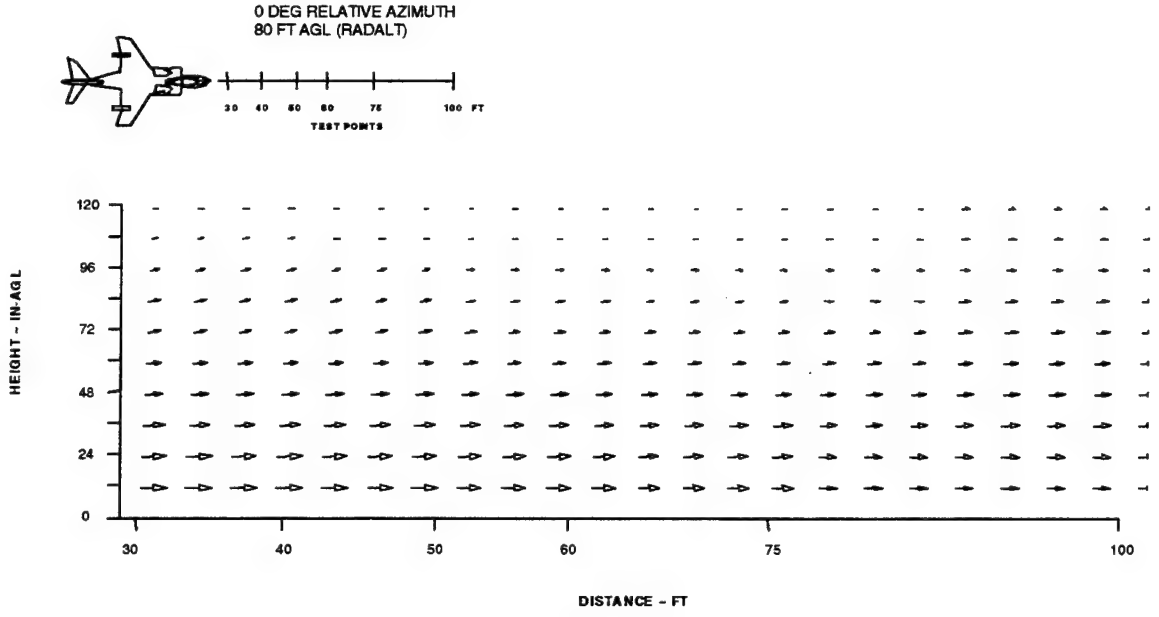

Figure F-13: Flow Field Streamlines during a 80 ft-AGL Hover at the 0 deg Relative Test Azimuth

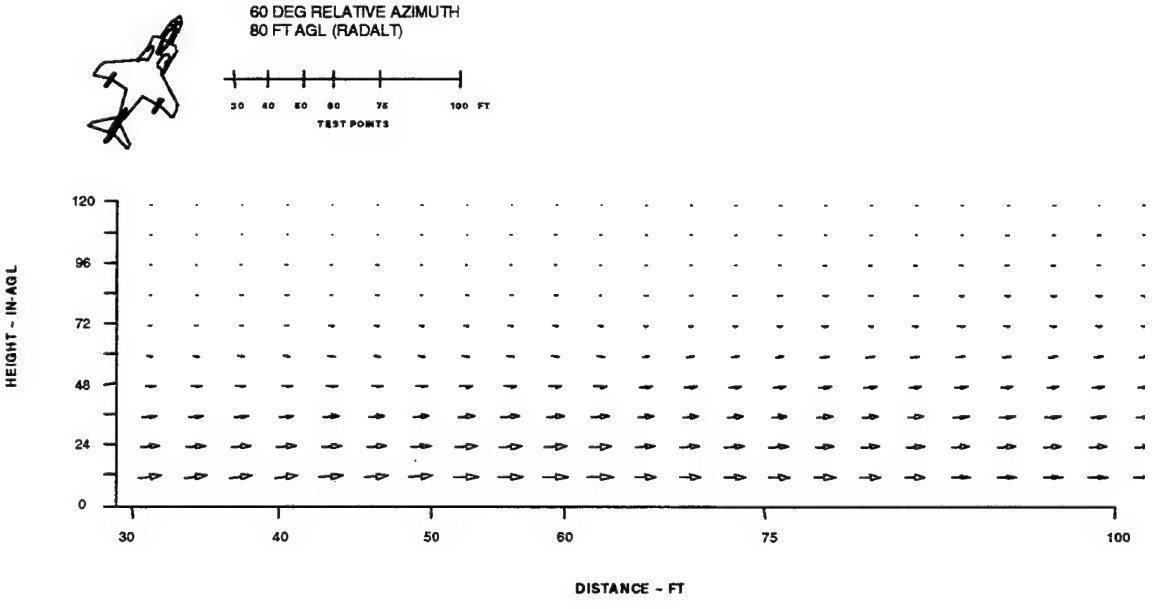

Figure F-14: Flow Field Streamlines during a 80 ft-AGL Hover at the 60 deg Relative Test Azimuth

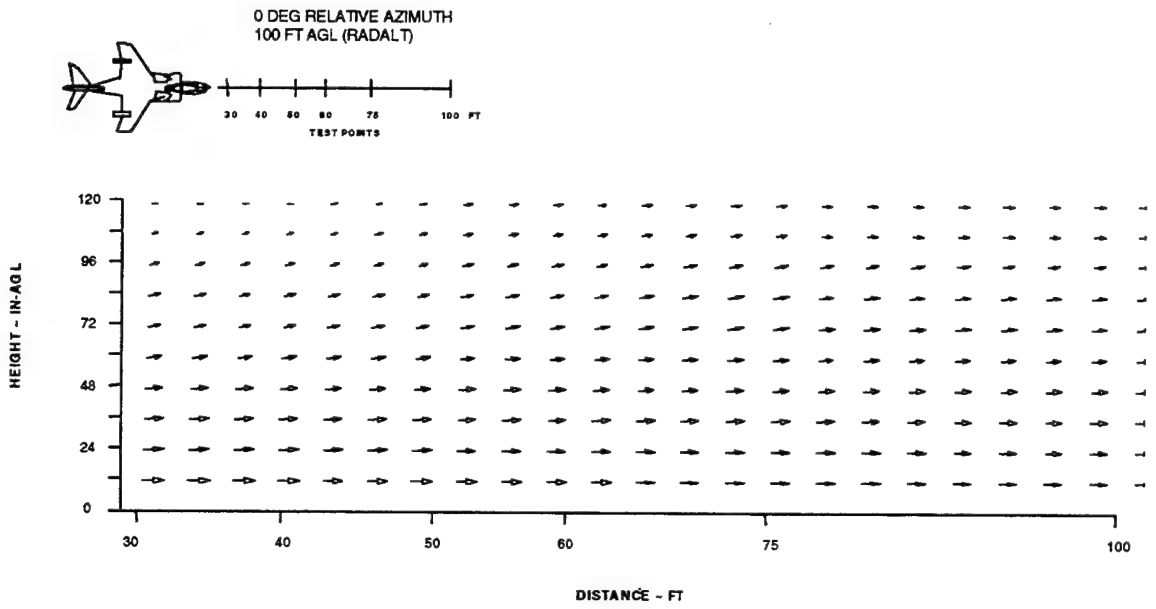

Figure F-15: Flow Field Streamlines during a 100 ft-AGL Hover at the 0 deg Relative Test Azimuth

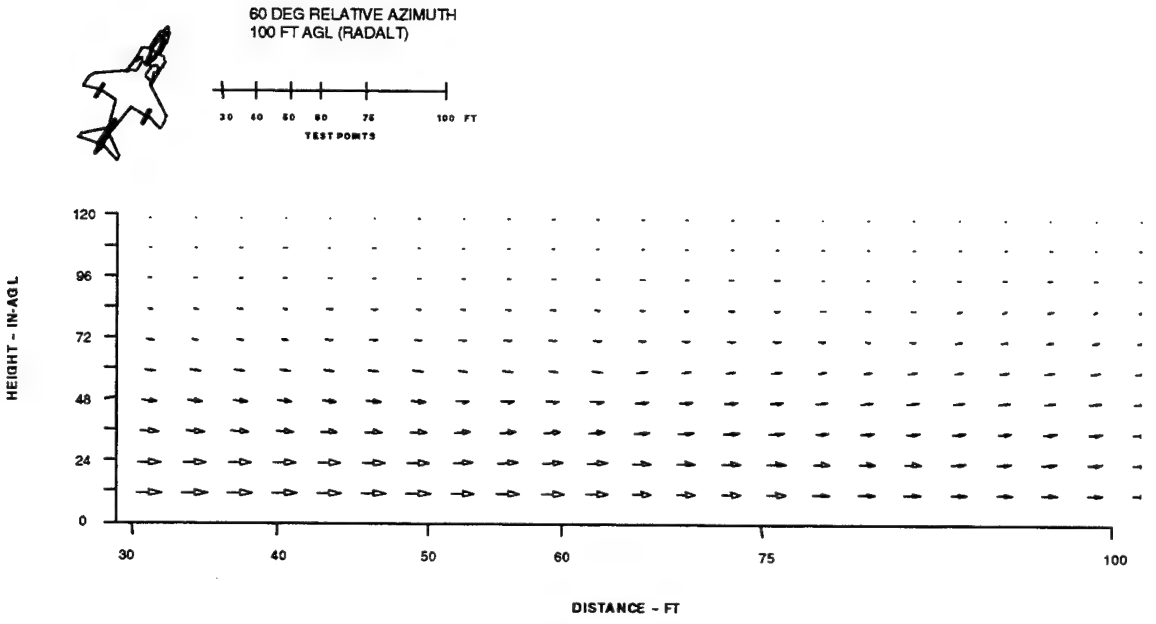

Figure F-16: Flow Field Streamlines during a 100 ft-AGL Hover at the 60 deg Relative Test Azimuth

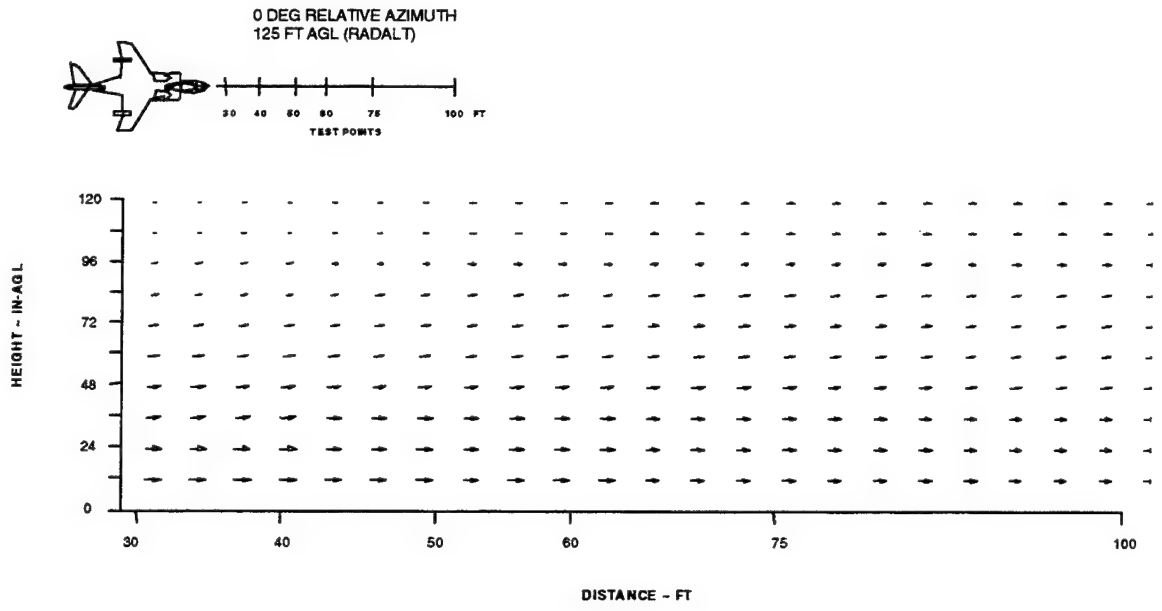

Figure F-17: Flow Field Streamlines during a 125 ft-AGL Hover at the 0 deg Relative Test Azimuth

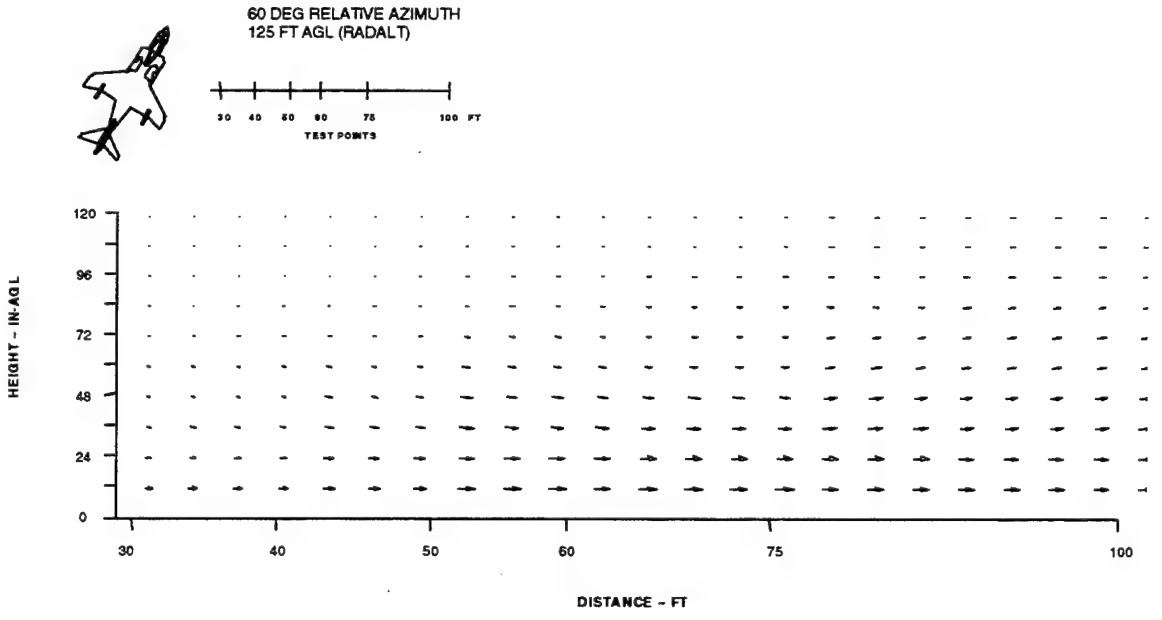

Figure F-18: Flow Field Streamlines during a 125 ft-AGL Hover at the 60 deg Relative Test Azimuth

APPENDIX G
FORCE CALCULATION AND SAFETY CENTER DATA

ANALYTIC METHODS FOR CALCULATING DOWNWASH FORCES

Personnel engulfed in the downwash flow field experience an aerodynamic drag force which is a function of the individuals size, posture, air density, the horizontal velocity field magnitudes, and its distribution with respect to height. This drag force can be calculated mathematically given the following equation:

$$D = C_D \int_0^H \left(\frac{1}{2} \rho \, V(y)^2 \right) A(y) \, dy$$

where:

D = drag force (lb)
C_D = drag coefficient (dimensionless) = 1
ρ = air density (lbm/ft^3)
$V(y)$ = peak velocity field (ft/sec), shown in figure G-1a
$A(y)$ = body frontal area (ft^2)

The velocity field $V(y)$ was found empirically through test data and is shown in figure G-1(a). The body frontal area $A(y)$ is twice the area underneath the body profile curve shown in figure G-1(b). The area can be written in terms of product of height and the body width polynomial:

$$A(y) = 2 \, y \cdot x_P(y)$$

where,

$$x_P(y) = ao + a1y + a1y^2 + \ldots + a10y^{11}$$

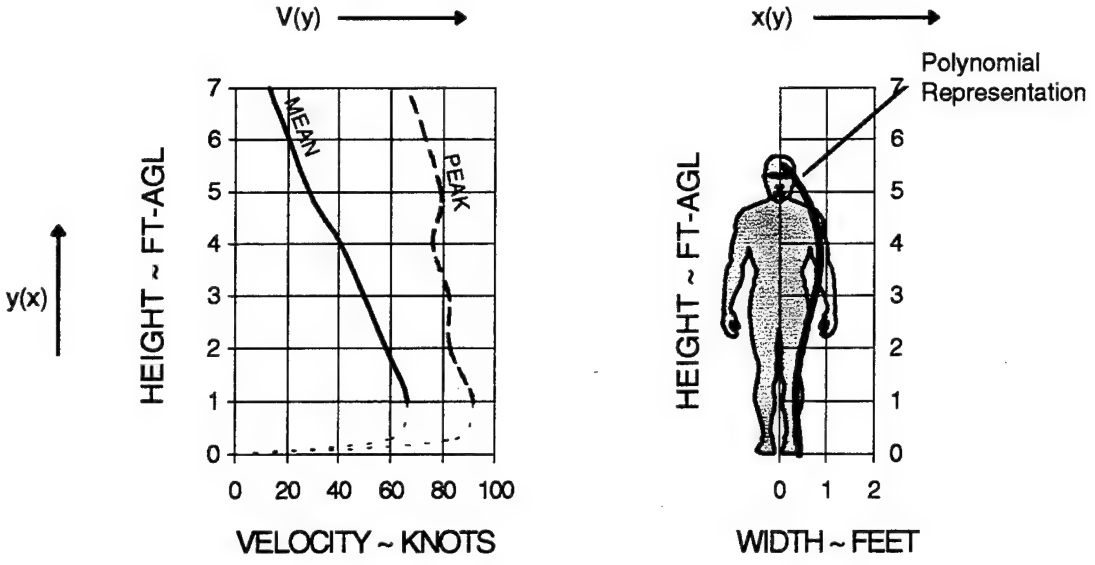

(a) (b)

Figure G-1: Velocity and Body Width as a Function of Height

Table G-1: Body Width Polynomial Coefficients used in figure G-1(b)

a0	4.31e-01	a6	2.22e-04
a1	-4.64e-02	a7	-4.18e-05
a2	-1.40e-01	a8	1.45e-05
a3	1.38e-01	a9	-7.80e-08
a4	-2.49e-02	a10	-1.90e-07
a5	-5.49e-04		

Table G-2: Navy Safety Center Outwash/Downwash Data Search AV-8B and CH-53E Specific

NAVAL SAFETY CENTER	09/01/1980 to 01/14/2000

EVENT_DATE ACFTMOD EMISCL
---------- -------- ------
03/04/1982 CH053A 3C

- - - - - - - - - - - - - - - E V E N T S U M M A R Y - - - - - - - - - - - - -

MAINT MAN WAS STANDING ON NR 2 SPONSON OF HELO REMVING ENG COWLING. A 2ND HELO TAXIED BY BLOWING REMOVED ENG COWLING OFF OF SPONSON. MAINT MAN REACHED FOR COWLING, LOST HIS BALANCE AND FELL TO GROUND, RESULTING IN A BROKEN WRIST. REMOVAL OF ENG COWLING WHERE ACFT TAXIED BY. ENG COWLING IS RELATIVELY LIGHT AND HAS A LARGE SURFACE AREA THAT IS SUSCEPTIBLE TO GUST OF WINDS. EVOLUTION OF REMOVING ENG COWLING TAKES SEVERAL MINUTES. WITH THIS TIME FACTOR INVOLVED, IT IS VERY DIFFICULT TO DETERMINE IF ANOTHER ACFT WILL TAXI BY. ALTHOUGH IT IS A CAUSE FACTOR, IT IS NOT PRIMARY CAUSE FACTOR. LACK OF NUMBER OF PERS PERFORMING MAINT ACTION. DUE TO BULKY SIZE OF ENG COWLING, SMALL WORK AREA OF SPONSON, STEPS THAT NEED TO BE PERFORMED, MINIMUM OF TWO PERS ARE REQUIRED IN REMOVAL OF ENG COWLING. WITH TWO PERS IT WOULD BE EASIER TO HANDLE COWLING WITH SUDDEN WIND GUST.

EVENT_DATE ACFTMOD EMISCL
---------- -------- ------
10/07/1985 CH053E

- - - - - - - - - - - - - - - E V E N T S U M M A R Y - - - - - - - - - - - - -

ACFT PERFORMING A POST MAINTENANCE FUNCTIONAL HOVER CHECK CREATED ROTOR WASH BLOWING OPEN AND DETACHING THE COPILOT'S COCKPIT DOOR ON SECOND ACFT, STRIKING DECK HANDLER ON THE CRANIAL. MAN WAS EXAMINED AT MEDICAL AND RELEASED FROM THAT DAY'S DUTY DUE TO A MILD CONCUSSION. HOVER CHECK WAS PRECEDED BY FOD WALKDOWN. HOVERING ACFT WAS ON LPH SPOT FIVE AND SECOND ACFT WAS ADJACENT TO THE AFT HALF OF THE ISLAND. SECOND ACFT WAS NOT SCHEDULED FOR FLIGHT AND HAD BEEN MAINTAINED THROUGHOUT THE DAY. STATUS OF DOOR NOT DETERMINED BUT, BELIEVED CLOSED, AND NOT PROPERLY LATCHED. WITHOUT CRANIAL PROTECTION, OR STRUCK IN A DIFFERENT LOCATION, DECK HANDLER MAY HAVE SUSTAINED GREATER INJURY.

EVENT_DATE ACFTMOD EMISCL
---------- -------- ------
07/14/1996 MH053E

- - - - - - - - - - - - - - - E V E N T S U M M A R Y - - - - - - - - - - - - -

FISHERMAN BLOWN INTO WATER BY ROTOR WASH FROM LANDING HELO.

HELO AT NAS USE A SEAWALL HELIPAD FOR TAKEOFFS/LANDINGS 7 DAYS A WEEK. ALONG SEAWALL ARE SEVERAL UNUSED SEAPLANE RAMPS, ONE IMMEDIATELY ADJACENT TO THE HELIPAD. AREAS ALONG SEAWALL HAVE BECOME POPULAR FOR FISHING, ESPECIALLY DURING WARM WX. THERE ARE NO WARNING SIGNS OR OTHER MEASURES TO RESTRICT ACCESS TO THESE FLIGHT LINE AREAS. IN THE PAST, BASE SECURITY HAS REMOVED UNAUTHORIZED PERSONNEL AND THEIR VEHICLES FROM SEAWALL AREAS WHEN THEY ENCROACHED ON FLIGHT LINE OPS. IN THIS INSTANCE, WHILE TRANSITIONING TO LAND AT THE HELIPAD, APPROX 50 FT AGL, ACCDR NOTICED MOVEMENT AMID LARGE BOULDERS ALONG THE SEAWALL. THE MOVEMENT WAS A FISHERMAN PARTIALLY HIDDEN BEHIND THE ADJACENT SEAPLANE RAMP. AS THE ACFT LANDED, THE INDIVIDUAL TUMBLED OVER THE BOULDERS AND INTO THE WATER. A CREWMAN WAS IMMEDIATELY DISEMBARKED TO RENDER ASSISTANCE. THE FISHERMAN CLIMBED FROM THE WATER, INFORMED THE CREWMAN HE WAS UNHURT, DECLINED TO IDENTIFY HIMSELF, AND DEPARTED.

CAUSE FACTOR: (1) SUPERVISORY: (A) OPERATIONS OFFICER: FAILED TO ENSURE PROPER WARNING SIGNS EXISTED TO PREVENT UNAUTHORIZED PERSONNEL FROM ENTERING DANGEROUS AREAS DURING FLIGHT OPERATIONS.

EVENT_DATE	ACFTMOD	EMISCL
07/10/1998	CH053D	

- - - - - - - - - - - - - - - E V E N T S U M M A R Y - - - - - - - - - - - - -

PARKED ACFT EXHAUST BLEW OFF LID OF RTR BLADE CANISTER INJURING MARINE

DURING OPERATION BANTUM RUNNER, THERE WAS AN INCREASED NUMBER OF TRANSIENT TRANSPORT ACFT FLYING IN AND OUT OF THE MCAF. DURING THIS OPERATION, A TRANSPORT ACFT WAS PARKED WITH THE AFT END OF THE ACFT FACING TOWARDS THE OPEN HANGER. THIS WAS THE FIRST TIME THIS PROCEDURE WAS EXPERIENCED AND THEREFORE MAINT PERS WERE UNAWARE OF THE POTENTIAL HAZARDS. IN THE PAST, WHEN A TRANSPORT ACFT TAXIED INTO THE FLT LINE FOR ACFT PACK UP FOR UNIT SDLM OR DEPLOYMENTS, IT WOULD PARK WITH THE FRONT OF THE ACFT FACING OR PARALLELING THE HANGAR. THE PROBLEM EXISTS WHEN THE EXHAUST TRANSVERSES ACROSS THE HANGAR, IT BLOWS DUST AND DEBRIS. THERE WAS A REDUCED AMOUNT OF SPACE IN THE HANGAR DUE IN PART TO ONE OF THE PARTICIPATING UNITS UTILIZING ONE THIRD OF HANGAR, AS A RESULT, THE UNSECURED BLADE CANISTER WAS STAGED OUTSIDE OF THE HANGAR. AS THE #1 ACFT TURNED INTO THE FLT LINE, THE EXHAUST BLEW THE LID OF THE CANISTER APPROX 30 TO 40 FT INTO THE AIR, IT STRUCK THE HANGAR AND PUT A SIX INCH TEAR IN THE SIDE. IT THEN PROCEEDED TO LAND NEXT TO A MARINE, AND ROLL OVER ON TO HER FOOT AND SHIN.

CAUSE FACTOR: (1) MAINT PERS: (A) ORG MAINT ROTORS: MAINT PERS FAILED TO SECURE CANISTERS BY FASTENING THE CAMLOCKS AT THE FOUR CORNERS BEFORE THE MAINT ACTION WAS COMPLETE. (B) ORG MAINT ROTORS: MAINT PERS STORED ROTOR BLADE CANISTER IMPROPERLY. (C) ORG MAINT ROTORS: MAINT PERS FAILED TO CLOSE HANGAR DOOR DURING HEAVY TRANSPORT TAXIING INTO AND OUT OF THE FLT LINE.

EVENT_DATE	ACFTMOD	EMISCL
09/20/1999	CH053E	

- - - - - - - - - - - - - - - E V E N T S U M M A R Y - - - - - - - - - - - - -

WHILE IN TRANSIT TO LDG, ROCK WAS THROWN BY RTR DWNWASH INTO PARKD CAR

TWO HELO'S WERE TRANSITIONING TO LAND HALF-WAY DOWN THE RWY ON THE EAF WHEN A ROCK WAS THROWN BY THE ROTOR DOWNWASH OF DASH 2, THROUGH A CAR WINDOW INJURING THE DRIVER. THE DRIVER SAW THE HELO APPROACHING TO LAND, WITNESSED THE DUST CREATED BY THE ROTOR DOWNWASH, AND TRIED TO SEEK COVER BEHIND A HILL NEAR THE RWY. THE RWY IS 1002 FT 8 INCHES BY 78 FT WIDE MADE OF AM2 MATTING SURROUNDED BY LOOSE DIRT AND ROCKS, RANGING FROM SMALL PEBBLES TO BOULDERS. ON THE SOUTH SIDE THERE IS A HGWY 65 FT FROM THE RWY. ON THE NORTH SIDE THERE IS A DIRT ROAD 30 FT FROM THE RWY. BOTH THE HGWY AND THE ROAD PARALLEL THE RWY. THERE IS A WINDSOCK ON A SMALL HILL 96 FT ROM THE RWY WHERE THE DRIVER, ATTEMPTED TO SHIELD THE CAR FROM THE ROTOR DOWNWASH. THERE ARE ALSO BUILDINGS IN CLOSE PROXIMITY OF THE RWY. ONE IS 122 FT FROM THE RWY. TO REDUCE POSSIBLE HAZARDS THE SECTION BRIEFED TO LAND ON THE LAST ONE THIRD OF THE RWY BY THE RAMP AND TO WAVEOFF ANYTIME A VEHICLE WAS SEEN ON THE HGWY OR DIRT ROAD. THE VEHICLE CAME AROUND THE BUILDING UNOBSERVED BY ANY ACRW DURING THE FINAL TRANSITION TO LDG AT A POINT WERE THE ROTOR DOWNWASH WAS THE GREATEST.

CAUSE FACTOR: (1) SUPV; FACILITIES: (A) FACILITY CO: FAILED TO RECOGNIZE HAZARDOUS/UNSAFE EAF CONDITIONS.

THIS PAGE INTENTIONALLY LEFT BLANK

DISTRIBUTION:

Joint Strike Fighter Program Office (SE)	(1)
Joint Strike Fighter Program Office (SEAV)	(1)
ASN RD&A (PEO(A) (PMA-257))	(1)
COMOPTEVFOR	(1)
NAVTESTWINGLANT Patuxent River, MD (55TW01A)	(1)
NAVAIRWARCENACDIV Patuxent River, MD (4.10.4)	(1)
NAVAIRWARCENACDIV Patuxent River, MD (4.11)	(1)
NAVAIRWARCENACDIV Patuxent River, MD (4.11.1.2)	(1)
NAVAIRWARCENACDIV Patuxent River, MD (4.3.2.1)	(1)
NAVAIRWARCENACDIV Patuxent River, MD (4.6.4.7)	(4)
NAVAIRWARCENACDIV Patuxent River, MD (Technical Publishing Team)	(1)
NASA Ames Research Center	(1)
USAF Armstrong Lab	(1)
Boeing (via JSF PO X-32 Program Staff)	(1)
Lockheed Martin (via JSF PO X-35 Program Staff)	(1)
BAE Systems	(1)
Rolls Royce	(1)
UK Ministry of Defense	(1)
Ministry of Defense of Italy	(1)
DTIC	(1)